THESIS

On

Filter Selection for Speckle Noise Reduction

Submitted in the partial fulfillment of the requirements for the award of degree of

Master of Engineering

in

Electronic Instrumentation & Control Engineering

to

Thapar University

Patiala

Submitted by

Venkata Rukmini . Ch

Roll No: 80651023

Under Esteemed Guidance of

MR. M. D. Singh

Lecturer

Electrical and Instrumentation Engineering Department

THAPAR UNIVERSITY

PATIALA (PUNJAB) -147004

JUNE 2008

CERTIFICATE

This is to certify that my work presented in this thesis entitled **"Filter Selection for Speckle Noise Reduction"** in partial fulfillment of the requirements for the award of the degree of **Master of Engineering** in **Electronic Instrumentation and Control Engineering** at **Thapar University, Patiala,** is an original record under supervision and guidance of **Mr. M. D. Singh**. The matter embodied in this report has not been submitted anywhere for the award of any other degree of this or any other university.

Ch. V. Rukmini

Date: 01/07/08

Venkata Rukmini . Ch
Roll No 80651023

It is certified that the above statement made by the student is correct to the best of my knowledge.

1/7/08

Mr. M. D. Singh
Lecturer, EIED,
Supervisor,
Thapar University, Patiala

12/9/08

Dr Dilbag Singh
External Examiner.

S. Ghosh

Dr. SmarajitGhosh
Professor & Head, EIED
Thapar University, Patiala

R K Sharma

Dr. R K Sharma
Dean of Academic Affairs
Thapar University, Patiala

ACKNOWLEDGEMENT

First of all I would like to thank the Almighty, who has always guided me to work on the right path of the life. My greatest thanks are to my parents who bestowed ability and strength in me to complete this work. I am deeply indebted to my parents and friends for their inspiration and ever encouraging moral support, which enabled me to pursue my studies.

I am very thankful to the Head of the Department of Electronic & Instrumentation Engineering, Thapar University, Patiala, Dr. Smarajit Ghosh, for his encouragement, support and for providing the facilities for the completion of this thesis.

This work would not have been possible without the encouragement and able guidance of my supervisor Mr. M.D. Singh lecturer and Mr. Mandeep Singh Assistant Professor, EIED Dept. Their enthusiasm and optimism made this experience both rewarding and enjoyable. Most of the novel ideas and solutions found in this thesis are the result of our numerous stimulating discussions. Their feedback and editorial comments were also valuable for writing this thesis.

I am also very thankful to the entire faculty and staff members of Electronic & Instrumentation Engineering Department for their direct–indirect help and cooperation.

A special thanks to Scott T. Acton, (author of Speckle Reducing Anisotropic Diffusion Filter) for providing the SRAD MATLAB files for comparison work.

Place: Thapar University, Patiala *Venkata Rukmini . Ch*

Date: 1/07/08

(ROLL NO. 80651023)

ABSTRACT

This work provides the knowledge about adaptive and anisotropic diffusion techniques for speckle noise removal from different types of images like synthetic, photographic, ultrasound and Synthetic Aperture Radar images and the various filters based on anisotropic diffusion for the removal of speckle are also being discussed. A comparative study is made on the performance of the Lee filter, Kuan filter, Frost filter, SRAD1 filter, AD filter, and SRAD2 filter in removing the speckle from the image and in preserving the edges. Finally an algorithm is developed which performs all the filtering techniques on the input image and the statistical parameters are calculated for the output images obtained from all the filters. These statistical parameters are weighted on the scale of 10 and compared, the images corresponding to the best statistical value are displayed along with the filter name and corresponding value of the statistical parameters.

For the evaluation of the performance of above mentioned filters statistical parameters like Signal to Noise Ratio, Root Mean Square Error, Peak Signal to Noise Ratio, Correlation of Coefficient, and Mean Structural Similarity Index Measure are used and the MATLAB codes required in calculating these parameters are developed. These parameters are used to calculate the image quality of the output image obtained from above mentioned filters, based on the values of these parameters the performance of the filters in terms of speckle removal and edge preservation is discussed.

Usually each filter gives optimal result for a particular type of image at a particular parametric value like SRAD1 gives good results for ultrasonic images and AD gives good results for synthetic images. Hence the proposed algorithm relieves the human from taking the decision regarding which filter is to be used for an image type since this algorithm selects the best output among the different filter outputs and displays the optimal results among the different results produced by different filtering techniques.

TABLE OF CONTENTS

Contents	*PAGE NO.*
Certificate	**i**
Acknowledgement	**ii**
Abstract	**iii**
Table of Contents	**iv**
List of Figures	**viii**
List of Graphs	**x**
List of Tables	**xi**
List of Abbreviations	**xv**
Chapter 1: Introduction	**1**
1.1 Background	1
1.2 Scope of this report	2
1.3Usefulness of this report	3
1.4 Overview of the chapters	3
Chapter 2: Review of Literature	5
Chapter 3: Background	**20**
3.1 Image Basics	20
3.1.1 Definition of an Image	20

3.1.2 Digital Image 20
3.1.3 Types of Imaging 20
3.1.3.1 X-rays 20
3.1.3.2 Ultrasound Scan 21
3.1.3.3 Computerized Tomography Scan 22
3.1.3.4 Magnetic Resonance Imaging Scan 22
3.1.3.5 Optical Imaging 23
3.1.3.6 Infrared Imaging 23
3.2 Noise in an Image 23
3.2.1 Types of Spatial Filters 24
3.3 Speckle Noise 25
3.4 Speckle Reduction Techniques 31
3.4.1 Adaptive Filtering 31
3.4.1.1 Computation of local statistics 31
3.4.1.2 Region Growing Procedure 32
3.4.1.3 Application of Smoothening Operator 33
3.4.2 Anisotropic Diffusion 33
3.4.2.1 Anisotropic Diffusion for Speckle Reduction 35
3.5 Estimation of Statistical Parameters 37
3.5.1 Estimation of Signal to Noise Ratio 37
3.5.2 Estimation of Root Mean Square Error 38
3.5.3 Estimation of Peak Signal to Noise Ratio 38
3.5.4 Estimation of Correlation of Coefficient 38
3.5.5 Estimation of Mean Structural Similarity Index 39
3.6 Ultrasound imaging 39
3.6.1 Introduction 39
3.6.2 Transducer Probe 40
3.6.3 Applications of Ultrasound Imaging 42

3.7 Synthetic Aperture Radar Imaging 43
3.7.1 Introduction 43
3.7.2 Applications of Synthetic Aperture Radar Imaging 45
3.7.3 Radar Filters 47

Chapter 4: Methodology 51

4.1 Digital Image Processing 51

4.2 MATLAB Software 51

4.3 Simulate Noise 51

4.4 Performance Evaluation of different Speckle Reducing Filters 52

4.4.1 Algorithm of SRAD1 52

4.4.2 Algorithm of AD 53

4.4.3 Algorithm of SRAD2 54

4.4.4 Algorithm for Signal to Noise Ratio 56

4.4.5 Algorithm for Correlation of Coefficient 56

4.4.6 Algorithm for Mean Structural Similarity Index Measure 57

4.4.7 Algorithm for Root Mean Square Error and Peak Signal to noise ratio 58

4.5 Algorithm for Filter Selection 58

Chapter 5: Results & Discussions 59

5.1 Synthetic Image 59

5.1.1 Filtering Results of Lee, Kuan and Frost Filters on Synthetic Image 60

5.1.2 Filtering Results of SRAD1 for Synthetic Image 61

5.1.3 Filtering Results of AD for Synthetic Image 66

5.1.3.1 Results of AD for different iterations 66

5.1.3.2 Results of AD for different values of kappa 72
5.1.3.3 Results of AD for different values of delta 74
5.1.4 Filtering Results of SRAD2 for Synthetic Image 76
5.2 Photographic Image 80
5.2.1 Filtering Results of Lee, Kuan and Frost Filters on Photographic mage 81
5.2.2 Filtering Results of SRAD1 for Photographic Image 83
5.2.3 Filtering Results of AD for photographic Image 86
5.2.4 Filtering Results of SRAD2 for Photographic Image 87
5.3 Ultrasonic image 89
5.3.1 Filtering Results of Ultrasound Image by Lee, Kuan, Frost, SRAD1, AD and SRAD2 90
5.4 Synthetic Aperture Radar image 92
5.4.1 Filtering Results of Lee, Kuan and Frost Filters on Synthetic Aperture Radar Image 93
5.4.2 Filtering Results of SRAD1 for SAR Image 94
5.4.3 Filtering Results of AD for SAR Image 95
5.4.4 Filtering Results of SRAD2 for SAR Image 96

Conclusion **98**

Scope for Future Work **99**

References 100

Bibliography 105

LIST OF FIGURES

Figure	Figure Name	Page No.
3.1	Chest x-ray image	**21**
3.2	Ultrasound scan of normal prostate gland	**21**
3.3	Computerized Tomography Scan	**22**
3.4	MRI of the spine	**22**
3.5	The linear relation between the local variance and mean of the speckle	**28**
3.6	Images corrupted with speckle noise having different standard	**30**
3.7	Real ultrasound image	**31**
3.8	Ultrasonic transducer	**41**
3.9	The parts of an ultrasound machine	**42**
3.10	Synthetic Aperture Radar Imaging Concept	**44**
3.11	Radar image and result of Frost filter	**50**
4.1	The quantitative shape of the nonlinearity	**54**
5.1	Noise free image and noisy image with different levels of standard deviations of noise	**59**
5.2	Filtering Results of synthetic image obtained from SRAD1 with T=3	**65**
5.3	Filtering Results of synthetic image obtained from SRAD1 with T=5	**65**
5.4	Filtering Results of synthetic image obtained from SRAD1 with T=10	**66**
5.5	Filtering Results of synthetic image obtained from SRAD1 with T=15	**66**
5.6	Filtering Results for AD with noi = 15, kappa = 27, delta = 1/6 and option = 1	**76**
5.7	Filtering results of SRAD2 with rect = [10 10 80 10].	**80**
5.8	Noise free image and noisy image with different levels of standard deviations of noise	**80**
5.9	Filtering Results on SRAD1 on l7 image with T=3	**84**

5.10 Filtering Results on SRAD1 on l7 image with T=5 **85**
5.11 Filtering Results on SRAD1 on l7 image with T=10 **85**
5.12 Filtering Results on SRAD1 on l7 image with T=15 **85**
5.13 Filtering Results on AD on l7 with noi = 15, kappa = 27, delta = 1/7 and option = 1 **87**
5.14 Filtering results of SRAD2 on l7 with rect = [75 14 34 227]. **89**
5.15 Real ultrasonic image and noise induced ultrasonic **90**
5.16 Filtering Results of us3.7 image from SRAD1 on us3.7 image with T=2 **91**
5.17 Filtering Results of us3.7 image from AD for l7 with noi = 15, kappa = 4, delta = 1/7 and option = 1 **91**
5.18 Filtering results of us3.7 image from SRAD2 with rect = [224 239 6 3]. **91**
5.19 Real Synthetic Aperture Radar Image and noise induced image **92**
5.20 Real image and noisy induced images with different levels of standard deviations of noise **92**
5.21 Filtering Results for SRAD1 on sar2 image with T=1 **95**
5.22 Filtering Results for AD on sar2 image with noi = 1, delta = 1/7, kappa = 17 and option = 1 **96**
5.23 Filtering results of SRAD2 with rect = [140 96 5 7]. **97**

LIST OF GRAPHS

Graph	Title	Page No.
5.1	Representation of the result obtained by applying SRAD1 on s7	**61**
5.2	Representation of the result obtained by applying SRAD1 on s75	**62**
5.3	Representation of the result obtained by applying SRAD1 on s8	**63**
5.4	Representation of the result obtained by applying SRAD1 on s85	**63**
5.5	Representation of the result obtained by applying SRAD1 on s9	**64**
5.6	Representation of the result obtained by applying SRAD1 on s95	**65**
5.7	Representation of the result obtained by applying AD on s7	**67**
5.8	Representation of the result obtained by applying AD on s75	**67**
5.9	Representation of the result obtained by applying AD on s8	**68**
5.10	Representation of the result obtained by applying AD on s85	**69**
5.11	Representation of the result obtained by applying AD on s9	**69**
5.12	Representation of the result obtained by applying AD on s95	**70**

LIST OF TABLES

Table	Title	Page No.
5.1	Statistical Results of the images before filtering	**60**
5.2	Statistical Results of the images filtered by Lee filter	**60**
5.3	Statistical Results of the images filtered by Kuan filter	**60**
5.4	Statistical Results of the images filtered by Frost filter	**60**
5.5	Statistical Results of the image s7 filtered by SRAD1 for different iterations	**61**
5.6	Statistical Results of the image s75 filtered by SRAD1 for different iterations	**62**
5.7	Statistical Results of the image s8 filtered by SRAD1 for different iterations	**62**
5.8	Statistical Results of the image s85 filtered by SRAD1 for different iterations	**63**
5.9	Statistical Results of the image s9 filtered by SRAD1 for different iterations	**64**
5.10	Statistical Results of the image s95 filtered by SRAD1 for different iterations	**64**
5.11	Statistical Results of the image s7 filtered by AD for different iterations	**66**
5.12	Statistical Results of the image s75 filtered by AD for different iterations	**67**
5.13	Statistical Results of the image s8 filtered by AD for different iterations	**68**
5.14	Statistical Results of the image s85 filtered by AD for different iterations	**68**
5.15	Statistical Results of the image s9 filtered by AD for different iterations	**69**
5.16	Statistical Results of the image s95 filtered by AD for different iterations	**70**
5.17	Statistical Results of the image s7 filtered by AD for different iterations and option = 2	**70**
5.18	Statistical Results of the image s75 filtered by AD for different iterations and option = 2	**71**
5.19	Statistical Results of the image s8 filtered by AD for different iterations and option = 2	**71**
5.20	Statistical Results of the image s85 filtered by AD for different iterations and option = 2	**71**

5.21 Statistical Results of the image s9 filtered by AD for different iterations and option = 2 **71**

5.22 Statistical Results of the image s95 filtered by AD for different iterations and option = 2 **72**

5.23 Statistical Results of the image s7 filtered by AD for different values of kappa **72**

5.24 Statistical Results of the image s75 filtered by AD for different values of kappa **73**

5.25 Statistical Results of the image s8 filtered by AD for different values of kappa **73**

5.26 Statistical Results of the image s85 filtered by AD for different values of kappa **73**

5.27 Statistical Results of the image s9 filtered by AD for different values of kappa **73**

5.28 Statistical Results of the image s95 filtered by AD for different values of kappa **74**

5.29 Statistical Results of the image s7 filtered by AD for different values of delta **74**

5.30 Statistical Results of the image s75 filtered by AD for different values of delta **74**

5.31 Statistical Results of the image s8 filtered by AD for different values of delta **75**

5.32 Statistical Results of the image s85 filtered by AD for different values of delta **75**

5.33 Statistical Results of the image s9 filtered by AD for different values of delta **75**

5.34 Statistical Results of the image s95 filtered by AD for different values of delta **75**

5.35 Statistical Results of the image s7 filtered by SRAD2 filter with the selection of different homogenous regions **76**

5.36 Statistical Results of the image s75 filtered by SRAD2 filter with the selection of different homogenous regions **77**

5.37 Statistical Results of the image s8 filtered by SRAD2 filter with the selection of different homogenous regions **78**
5.38 Statistical Results of the image s85 filtered by SRAD2 filter with the selection of different homogenous regions **78**
5.39 Statistical Results of the image s9 filtered by SRAD2 filter with the selection of different homogenous regions **79**
5.40 Statistical Results of the image s95 filtered by SRAD2 filter with the selection of different homogenous regions **79**
5.41 Statistical Results of the photographic images before filtering **81**
5.42 Statistical Results of the images filtered by Lee filter **82**
5.43 Statistical Results of the images filtered by Kuan filter **82**
5.44 Statistical Results of the images filtered by Frost filter **82**
5.45 Statistical Results of the image l7 filtered by SRAD1 for different iterations **83**
5.46 Statistical Results of the image l75 filtered by SRAD1 for different iterations **83**
5.47 Statistical Results of the image l8 filtered by SRAD1 for different iterations **83**
5.48 Statistical Results of the image l85 filtered by SRAD1 for different iterations **83**
5.49 Statistical Results of the image l9 filtered by SRAD1 for different iterations **84**
5.50 Statistical Results of the image l95 filtered by SRAD1 for different iterations **84**
5.51 Statistical Results of the image l7 filtered by AD for **86**
5.52 Statistical Results of the image l75 filtered by AD **86**
5.53 Statistical Results of the image l8 filtered by AD **86**
5.54 Statistical Results of the image l85 filtered by AD **86**
5.55 Statistical Results of the image l9 filtered by AD **87**
5.56 Statistical Results of the image l7 filtered by SRAD2 filter with the selection of different homogenous regions **87**
5.57 Statistical Results of the image l75 filtered by SRAD2 filter with the selection of different homogenous regions **88**
5.58 Statistical Results of the image l8 filtered by SRAD2 filter with the selection

of different homogenous regions **88**
5.59 Statistical Results of the image l85 filtered by SRAD2 filter with the selection of different homogenous regions **88**
5.60 Statistical Results of the image l9 filtered by SRAD2 filter with the selection of different homogenous regions **88**
5.61 Statistical Results of the image l95 filtered by SRAD2 filter with the selection of different homogenous regions **89**
5.62 Statistical Results of the ultrasonic images for unfiltered images, Lee filtered images, Kuan filtered images and Frost filtered images **90**
5.63 Best results obtained from different filters for ultrasonic image **90**
5.64 Statistical Results of SAR images before filtering **93**
5.65 Statistical Results of the SAR images filtered by Lee filter **93**
5.66 Statistical Results of the SAR images filtered by Kuan filter **93**
5.67 Statistical Results of the SAR images filtered by Frost filter **93**
5.68 Statistical Results of the image SAR2 filtered by SRAD1 for different iterations **94**
5.69 Statistical Results of the image SAR4 filtered by AD for different iterations **94**
5.70 Statistical Results of the image SAR6 filtered by SRAD1 for different iterations **94**
5.71 Statistical Results of the image SAR8 filtered by SRAD1 for different iterations **94**
5.72 Statistical Results of the image SAR2 filtered by AD **95**
5.73 Statistical Results of the image SAR4 filtered by AD **95**
5.74 Statistical Results of the image SAR6 filtered by AD **95**
5.75 Statistical Results of the image SAR8 filtered by AD **96**
5.76 Statistical Results of the image SAR2 filtered by SRAD2 **96**
5.77 Statistical Results of the image SAR4 filtered by SRAD2 **96**
5.78 Statistical Results of the image SAR6 filtered by SRAD2 **97**
5.79 Statistical Results of the image SAR8 filtered by SRAD2 **97**

LIST OF ABBREVIATIONS

• 2D	Two-Dimensional
• 3D	Three-Dimensional
• AD	Anisotropic Diffusion
• ASSF	Adaptive Speckle Suppression Filter
• ASSR	Adaptive Smoothening Speckle Reduction
• AWMF	Adaptive Weighted Median Filter
• DeSpeRADo	Deconvolution Speckle Reducing Anisotropic Diffusion
• DF	Directive Filters
• EDS	Enhanced Directional Smoothing
• ENL	Equivalent Numbers of Looks
• HRGMF	Homogenous Region Growing Mean Filter
• ICOV	Instantaneous Coefficient Of Variation
• LASER	Light Amplification by Stimulated Emission of Radiation
• LPND	Laplacian Pyramid based Nonlinear Diffusion Filter
• LPNDSF	Laplacian Pyramid Nonlinear Diffusion and Shock filter
• MAD	Median Absolute Deviation
• MAP	Maximum A Posteriori
• MATLAB	MATrix LABoratory
• MNWD	Multiscale Nonlinear Wavelet Diffusion
• MRI	Magnetic Resonance Imaging
• MSSIM	Mean Structural Similarity Index Measure
• NCD	Nonlinear Anisotropic Diffusion
• ND	Nonlinear Diffusion

• NMWD	Nonlinear Multiscale Wavelet Diffusion
• PDE	Partial Derivative Equation
• PET	Positron Emission Tomography
• PSNR	Peak Signal to Noise Ratio
• RMSE	Root Mean Square Error
• SAR	Synthetic Aperture Radar
• SBF	Squeeze Box Filter
• SBF-DVM	Squeeze Box Filter using dynamically varying window
• SNR	Signal to Noise Ratio
• SRAD	Speckle Reducing Anisotropic Diffusion
• SSIM	Structural Similarity Index Measure
• SSP	Split Spectrum Processing
• US	Ultra Sound
• USDSAI	UltraSound DeSpeckling Assessment Index
• WSRAD	Windowed Speckle Reducing Anisotropic Diffusion
• ZAP	Zero Adjustment Procedure

Chapter-1
Introduction

1.1 Background

Each imaging system suffers with a common problem of "Noise". Unwanted data which may reduce the contrast deteriorating the shape or size of objects in the image and blurring of edges or dilution of fine details in the image may be termed as noise. It may be due to one or more of the following reasons

- Physical nature of the system
- Shortcomings of image acquisition devices
- Image developing mechanism
- Due to environment.

Mathematically there are two basic models of Noise; additive and multiplicative. Additive noise is systematic in nature and can be easily modeled and hence removed or reduced easily. Whereas multiplicative noise is image dependent, complex to model and hence difficult to reduce. When multiplicative noise caused by the de-phased echoes from the scatterers appears, it is called "Speckle Noise". Although it appears as noise but it contains useful information because it is due to surroundings of the target. Speckle may appear distinct in different imaging systems but it is always manifested in a granular pattern due to image formation under coherent waves.

Speckle is the result of the diffuse scattering, which occurs when a sound wave (RFsound or Ultrasound) pulse randomly interferes with the small particles or objects on a scale comparable to the sound wavelength. Speckle is an inherent property of SAR and Ultrasound images, and is modeled as spatial correlated multiplicative noise. In most cases, it is considered a contaminating factor that severely degrades image quality. To improve image analysis, speckle reduction is generally used for two applications:

- Visualization enhancement
- Auto-segmentation improvement.

Most speckle filters are developed for enhancing visualization of speckle images. Their main applications are in two areas SAR and Ultrasound.

Medical imaging like Ultrasound is very popular due to its low cost, least harmful to human body, real time view and small size. But this imaging has major disadvantage of having Speckle. Synthetic aperture radar (SAR) imagery used for air-born images of earth which are further helpful in study of environment and vegetation on that piece of earth, also suffers with same type of noise-like feature that is Speckle.

This thesis work is carried out to study the speckle characteristics through its mathematical model and then analysis of some prominent speckle reduction filters specific to SAR imagery. Since SAR images contains specific shapes and edges, a synthetic model of true picture has been taken to study the speckle and analysis of filters on Speckled synthetic images. Synthetic images have been taken from Dr. Alexandra Pizurica. She has many international publications and known for her contribution towards wavelets based speckle reduction filters. We used her synthetic images for testing of spatial filters. To generate speckles we have used the algorithm of Gent University, Belgium because it has been recognized by many researchers as most real-look speckle producing algorithm. Spatial filters are analysed because less work has been done in this domain as compare to the wavelets. Filter analysis has been done to select the best filter for a given image on the basis of some statistical parameters. Finally we try to present an automatic modular approach to filter a speckled image using a "filter bank" on the basis of speckle analysis and filter performance.

1.2 Scope of this report:

- The presence of random speckle noises, caused by the interference of reflected ultrasound wave fronts makes computer-aided image processing and interpretation difficult task.
- Thus speckle noise filtering is very much important for improving suitable conditions of post processing of the image

- In this work three filters are discussed SRAD1, AD and SRAD2, these filters have the combined property of edge preservation and noise removal. Each filter is different from the other in terms of partial differentiation equation used. Edge preservation is obtained by the use of partial differential equation which is used in the respective algorithms and noise removal is obtained by using averaging or median filtering. Images are filtered by using six filters (Lee, Kuan, Frost, SRAD1, AD and SRAD2) and their results are formulated in terms of statistical parameters like SNR, Coc, MSSIM, RMSE and PSNR.

1.3 usefulness of this report:

This report covers the information regarding the nature of specke, its causes, and possible methods to reduce them. Information of various filtering methods of adaptive and anisotropic diffusion techniques to denoise the image and preserve edges are discussed. Statistical parameters like SNR, Coc, MSSIM, RMSE and PSNR for image quality assessment are also discussed.

1.4 Overview of the chapters

This thesis report has been divided in to the following chapters

- Chapter-1 "**Introduction**", it includes the background information and overview of thesis report.
- Chapter-2 "**Review of Literature**", it provides overview of the work done in this area.
- Chapter-3 "**Background**", this explains the basics of US imaging and SAR imaging, Model of speckle noise, Adaptive and Anisotropic Diffusion techniques for speckle removal, and statistical parameters for image quality assessment.
- Chapter-4 "**Methodology**", provides algorithms of SRAD1, AD, SRAD2 and also algorithms for the statistical parameters SNR, Coc, MSSIM, RMSE and PSNR are presented. Finally algorithm for the filter selection in order to obtain optimum results is discussed

- Chapter-5 "**Results & Discussion**" presents the database and graphs regarding the statistical parameters of the output images obtained by changing the parameters to the filters Lee, Kuan, Frost, SRAD1, AD and SRAD2, also pros and cons of each filter are discussed.

Conclusion.

Scope for Future Work

References

Bibliography

Chapter 2
REVIEW OF LITERATURE

This chapter provides brief overview of work done in this area.

Christoph B.Burckhardt in 1978 proposed that the speckle reduction depends on the number of independent amplitude values that are measured. In this work the author derived the condition for the independence of two amplitude values, and thus a limit is given for the possible reduction in speckle. It was especially shown that the improvement in SNR is almost as good for a “maximum amplitude writing” compound scan as for an “averaging” compound scan is considered. In view of its other advantages the first mode of operation is to be preferred. It was then shown that the transducer has to be translated by about half its width when independent amplitude values are to be obtained. This places a definite limit on the possible improvement in SNR. The possible improvement is lower for high-resolution (i.e., large aperture) transducers than for low-resolution (i.e., small aperture) transducers. **[1]**

Kiyo Tomiyas in 1983 proposed Computer Simulation of Speckle in a SAR image pixel. A computer program is described in this paper. It was written to simulate the radar return from a single pixel containing numerous scatterers. The phase and amplitude of the signal reflected from the pixel generally varies from pulse to pulse due to intrapixel interference. After integration, the pixel response usually differs with each "azimuth look," and author says that this speckle variation between azimuth looks may be as much as 20 dB or more. Speckle variation can be significantly reduced by averaging or median filtering multiple azimuth looks per pixels. **[2]**

Matthewo Donnell. et.al in 1988 made incoherent averaging of measurements made at different look directions is used to reduce speckle noise in medical ultrasound images. In this work an analytic expression for the correlation between two measurements made at different spatial positions is derived. Using this expression the optimum aperture

displacement for efficient incoherent averaging (i.e., compounding) is computed and found to be equal to approximately one-half the aperture length. **[3]**

Armand Lopes et.al in 1990 proposed Adaptive Speckle Filters and Scene Heterigenity. The presence of speckle in radar images makes the radiometric and textural aspects less efficient for class discrimination. Many adaptive filters have been developed for speckle reduction. In this paper, the most well-known filters are analyzed. It is shown in this paper that they are only reliable in a bounded field. Author tried to modify their behavior by introducing two thresholds on the coefficient of variation. The lower one is easily established as a function of the image parameters. The second upper threshold is fixed approximately, however author says that a study should be done to determine it more precisely. Author says that when real or simulated synthetic Aperture Radar images are tested, the proposed modified filters adequately average homogeneous areas and better preserve, at the same time, edges and textural information. **[4]**

Pietro Perona et.al in 1990 developed anisotropic diffusion to overcome the problems involved in standard scale space technique. In this diffusion process the removal of noise and preservation of edges are simultaneously achieved by choosing the conduction coefficient as a function of the magnitude of brightness function. Thus this conduction coefficient function encourages the smoothening across the edges and inhibits the smoothening across the boundaries. **[5]**

A.J. Healey et.al in 1991 proposed different filtering techniques for the removal of speckle. These techniques can be broadly classified as:

- Processing entire image either in one step or via partitioning in to number of images e.g. - adaptive filtering.
- Implementation of spatial or frequency compounding.
- Application of phase acknowledgment methods alternative of phase acknowledgement is 'The Zero Adjustment Procedure'(ZAP)

Discussion made by the author in this paper concludes that with the advent of the new generation of DSP (Digital Signal Processing) technology the phase acknowledging techniques are now feasible on a real time basis.
Advantage features with these methods are

- Correction processing is localized;
- Overall image resolution is retained;
- Performance is robust to noise;
- No specific statistical distribution is assumed and all algorithmic parameters can be calculated from the A-line data. **[6]**

Erik Steen et.al in 1993 explored the application of nonlinear filtering techniques in volume rendering of medical ultrasound data Volume rendering methods based on an initial probabilistic classification have been used with success on Computed Tomography and Magnetic Resonance data, but have shown to fail in ultrasonic studies because of substantial noise content and other limitations in the ultrasonic imaging system.
Boundaries can be detected by computing local gradients in the volume, but these computations will generally be very noise sensitive.

Noise can be reduced by applying linear filtering schemes such as the moving average filter, but this will blur the boundaries. Hence nonlinear filtering schemes are proposed.

Author concludes that modified nonlinear filtering scheme smoothes within homogeneous regions while leaving significant monotone transitions unaltered also avoids introduction of artificially sharp boundaries. **[7]**

Richard N. Czerwinska et.al in 1995 presented a novel adaptation of the median filter to the problem of boundary-preserving, speckle reduction in ultrasonic imaging. The technique involves applying a bank of oriented one-dimensional median filters to the image, and retaining at each point the largest value among all the filter bank outputs. The result is an operator which suppresses speckle noise while retaining the structure of the

image, particularly the thin bright streaks, which tend to occur along boundaries between tissue layers. **[8]**

Mustafa Karaman et.al in 1995 proposed an adaptive smoothing technique for speckle suppression in medical B-scan ultrasonic imaging. The technique is based on filtering with appropriately shaped and sized local kernels. For each image pixel, a filtering kernel, which fits to the local homogeneous region containing the processed pixel, is obtained through a local statistics based region growing technique. The filter used in this technique makes use of local image content to eliminate speckle effectively while preserving resolvable details. Here trade-off between smoothing and signal preservation is controllable by the look-up table consisting of statistical similarity bounds for different values of local statistics.

An adaptive smoothening speckle reduction (ASSR) technique involves 3 main steps:

- Computation of local statistics.
- Region growing procedure.
- Application of smoothening operator.

If median operator is used in smoothening step then that filtering technique is called as ASSF-MEDIAN.

If mean operator is used in the smoothening step then that filtering technique is called as ASSF-MEAN

In this paper the performance of ASSF is investigated on the phantom and tissue images together. Comparison of performances of adaptive weighted filter (AWMF) and homogenous region growing filter (HRGMF) states that ASSF is better in preserving the resolvable details. This is because window size in ASSF is calculated in such a manner so that its size must be large enough for accurate measurement of local statistics. On the other hand, it must be kept sufficiently small for accurate detection of resolvable structures. The region merging procedure in ASSF is employed to avoid high-frequency artifacts. The similarity of mean intensities of the neighboring regions and their sizes are used as the merging criteria. **[9]**

Sofia Ben Jebara et.al in 1999 proposed speckle reduction in radar images using predictive, multiresolution and thresholding techniques. The schemes adopted are based

on a "judicious" combination of these techniques. In fact, by analyzing the performances of each technique separately, it is possible to compensate the limitations imposed by the predictive technique and the multiresolution/thresholding technique. In this work the author developed two method based on multiresolution, thresholding and prediction combination. Author says that by taking advantage of each method, Contour conservation for multiresolution, texture conservation for prediction and noise cancellation for thresholding, it is possible to reduce properly the speckle in SAR images. **[10]**

Mark P. Wachowiak et.al in 2000 proposed a neural-based approach to classify and estimate the statistical parameters of speckle noise found in biomedical ultrasound images.

The parameter like Contrast, Angular second moment, Entropy, Correlation, Mean, Standard deviation, kurtosis and features from discrete wavelet transform (DWT) are used by the neural networks to solve the classification problem.

These features provide texture and contrast measures. At the same time parameter for classification is also estimated in this work.

In this study two sets of tests were performed

- Consisted of test images contaminated with the same noise model parameters that were used in training
- Consisted of images that were contaminated with random model parameters, that were continuously distributed over the allowable ranges **[11]**

Chedsada Chinrungrueng et.al in 2001 developed an edge preserving noise reduction filter called as Savitzky–Golay filter. This paper describes a novel filter which is a two-dimensional (2-D) extension of the one-dimensional (1-D) Savitzky–Golay filter. The new filter, referred to as the 2-D weighted Savitzky–Golay filter is based on the least squares fitting of a polynomial function to image intensities. The performance of the proposed filter has been compared with that of the commonly used median filter in reducing speckle noise on a synthetic image and an ultrasound thyroid image. Experimental results indicate that on these particular examples, the new filter can achieve at least the same level of noise reduction and edge preservation as that of the median

filter, but with far less computation time. Since its complexity scales linearly with the problem size, the new filter is suitable for filtering problems with large windows. In addition, its performance also shows to be less sensitive to the size of the filtering window compared to the median filter. Because of these properties, author suggest that the 2-D weighted Savitzky–Golay filter is a promising substitute for the median filter in reducing speckle noise of medical ultrasound images. **[12]**

Alin Achim et.al in 2001 presented a novel speckle suppression method for medical ultrasound images. In this paper it is shown that the sub-band decompositions of ultrasound images have significantly non-Gaussian statistics that are best described by families of heavy-tailed distributions such as the alpha-stable. Then, author design a Bayesian estimator that exploits these statistics. Alpha-stable model is used develop a blind noise-removal processor that performs a nonlinear operation on the data. Here firstly, the logarithmic transform of the original image is analyzed into the multiscale wavelet domain.

Three main steps involved in this algorithm are:

- The logarithm of the image is decomposed into several scales through a multiresolution analysis employing the 2-D wavelet transform. This step guarantees that the speckle is transformed from multiplicative into additive and its characteristics are differentiated from the signal characteristics in each decomposition level.
- After decomposing the original image, the signal and noise components in various scales are modeled as and Gaussian processes, respectively. The parameters of the distributions are estimated from the measurements by means of a LS (least square) fitting in the characteristic function domain.
- Bayesian processor based on a signal prior is built at each scale for statistically optimal signal feature extraction and speckle suppression.

Results show that the processor developed is more effective than thresholding methods, and it processor performs like a feature detector but this approach is computationally expensive due to the fact that the prior distribution parameters need to be estimated at each scale of interest. However it can be used in off-line processing. **[13]**

Debasis Mazumdar et.al in 2002 presented adaptive weighted median filter (AWMF) for reducing speckle noise in medical ultrasonic images because conventional noise cleaning algorithms fail to reduce noise in ultrasound images because these images are heavily corrupted by the noise and they possess sharp contrast which could be retained.
Statistics show that speckle can be modeled as a multiplicative noise. However the signal processing stages inside the scanner modifies the original statistics of the noise.
AWMF is based on the weighted median, which originates from the well-known median filter through the introduction of weight coefficients.
By adjusting the weight coefficients and consequently the smoothing characteristics of the filter according to the local statistics around each point of the image, it is possible to suppress noise while edges and other important features are preserved.
In this paper it is shown that application of the filter for the processing of several ultrasonic scans have improved the detect ability of small structures and subtle grey-scale variations without affecting the sharpness or anatomical information of the original image this is because at the region of edges it selects the frequency of weights in such a manner that the central pixel of the scanning window is more assured. This property confirms the edge preservation and the sharpness of the image at the cost of a little bit of less noise suppression. **[14]**

C. Loizou, et.al in 2002 developed six speckle reduction-filtering techniques in this work. The filters developed were:

- *speckle* and *amnoise* using first order local statistics such as the mean and the variance,
- *anisodiff* utilizing speckle anisotropic diffusion,
- *momente using* local statistics with higher statistical moments such as the skewness and kurtosis of the histogram,
- *rtd* utilizing anisotropic diffusion
- *speck* using geomentric filter

Results show that *amnoise* and *momente* performed better over other filters mentioned above hence these filters can be used as preprocessing step in a system for the automated segmentation of ultrasound images. **[15]**

Yongjian Yu et.al., in 2002 provided the derivation of speckle reducing anisotropic diffusion (SRAD) by showing that lee and frost filters can be caste as partial differential equations and then SRAD is derived by allowing edge-sensitive anisotropic diffusion within this context. SRAD is a diffusion method tailored to ultrasonic and radar imaging applications.

As the conventional anisotropic diffusion is the edge-sensitive diffusion for images corrupted with additive noise, SRAD is the edge-sensitive diffusion for speckled images.

Just as the Lee and Frost filters utilize the coefficient of variation in adaptive filtering, SRAD exploits the *instantaneous* coefficient of variation, which is shown to be a function of the local gradient magnitude and Laplacian operators. **[16]**

Scott T. Acton in 2003 generalized the 2D SRAD algorithm developed for despeckling ultrasound images to obtain a SRAD algorithm capable of enhancing volumetric ultrasound data. In this work Firstly, an instantaneous coefficient of variation edge detector (3D ICOV) appropriate for three-dimensional data set is presented then, the 2D SRAD partial differential equation is formulated by replacing the gradient operator in the traditional diffusion mechanism with the derived 3D ICOV operator.

Experiments are conducted firstly by using 3D SRAD algorithm tested on a synthetic 3D dataset as acquired from an ellipsoid using a hypothetical 2D B-scan imager.

2D and 3D algorithms are compared quantitatively by using average edge sharpness, average intensity in a band encircling that object, and coefficient of variation. **[17]**

Aleksandra Pizurica et.al in 2003 proposed a robust wavelet domain method for noise filtering in medical images. The proposed method adapts itself to various types of image noise as well as to the preference of the medical expert; a single parameter can be used to balance the preservation of (expert-dependent) relevant details against the degree of noise reduction. The algorithm exploits generally valid knowledge about the correlation of

significant image features across the resolution scales to perform a preliminary coefficient classification. This preliminary coefficient classification is used to empirically estimate the statistical distributions of the coefficients that represent useful image features on the one hand and mainly noise on the other. The adaptation to the spatial context in the image is achieved by using a wavelet domain indicator of the local spatial activity. The results demonstrate its usefulness for noise suppression in medical ultrasound and magnetic resonance imaging. **[18]**

Yongjian Yu et.al in 2004 derived a partial differential equation (PDE) for speckle reduction from minimizing a cost functional of the instantaneous coefficient of variation. Then, it is shown that the piecewise exponential function is the solution of the derived PDE. Finally this derived PDE is expressed using log-compressed ultrasound data, followed by a numerical implementation scheme.
Comparison between SRAD and generalized SRAD shows that the generalized SRAD is complementary to the conventional SRAD, in the sense that the former one emphasizes feature preservation and the latter emphasizes edge enhancement, while both remove speckle in the observed images. **[19]**

Zhou Wang et.al in 2004 proposed framework for quality assessment based on the degradation of structural information SSIM index exhibit input-dependent behavior in measuring signal distortions. Its indexing approach is a particular implementation of the philosophy of structural similarity, from an image formation point of view. Image quality metrics can be classified according to the availability of an original (distortion-free) image with which the distorted image is to be compared. Most existing approaches are known as *full-reference*, meaning that a complete reference image is assumed to be known. In many practical applications, however the reference image is not available, and a *no-reference* or "blind" quality assessment approach is desirable. In a third type of method, the reference image is only partially available, in the form of a set of extracted features made available as side information to help evaluate the quality of the distorted image. This is referred to as *reduced-reference* quality assessment. This paper focuses on full-reference image quality assessment. SSIM compares local patterns of pixel

intensities that have been normalized for luminance and contrast. It was proposed, based on the assumption that the human visual system is highly adapted to extract structural information from the viewing field. It follows that a measure of structural information change can provide a good approximation to perceived image distortion. The similarity measure is a function of three independent components they are luminance, contrast, structural similarity. This work show that since SSIM is a symmetric measure, it can be thought of as a similarity measure for comparing any two signals or any two images. **[20]**

M. Mastriani et.al in 2004 proposed Enhanced Directional Smoothing (EDS) Algorithm for Edge-Preserving Smoothing of Synthetic-Aperture Radar Images. Most of the filters described in the literature are based on the fact that ratio of the standard deviation to the signal value, the "coefficient of variation," is theoretically constant at every point in a SAR image. However this fact is irrelevant for directional and enhanced directional smoothening. The EDS filter has a speckle reduction approach that performs spatial filtering in a square-moving window know as kernel, window size is selected to be odd. The EDS filtering is based on the statistical relationship between the central pixel and its surround-ding pixels. To protect the edges from blurring while smoothing, a directional averaging filter is used by the author. EDS performs the filtering based on either local statistical data given in the filter window to determine the noise variance within the filter window, or estimating the local noise variance using the effective equivalent number of looks (ENL) of a SAR image. The estimated noise variance is then used to determine the amount of smoothing needed for each speckle image. The noise variance determined from the local filter window is more applicable if the intensity of an area is constant or flat whilst ENL is suitable if there are difficulties determining if an area of the image is flat. **[21]**

Scott T. Acton in 2005 proposed a new PDE that combines the enhancement of speckle reducing anisotropic diffusion (SRAD) with the mechanism of deconvolution. The resulting method, called deconvolutional speckle reducing anisotropic diffusion (DeSpeRADo), surpasses the edge localization ability of SRAD while yielding lower error in terms of area estimation and improved detection of fine features.

Comparative study is made among Lee filter, Wiener filter, basic SRAD and DeSpeRADo in terms of pratt figure of merit, linear feature detection, deformation in area. **[22]**

Yong Yue et.al in 2005 introduced a novel Multiscale Nonlinear Wavelet Diffusion (MNWD) method for ultrasound speckle suppression and edge enhancement. It is considered that wavelet diffusion as an approximation to nonlinear diffusion within the framework of the dyadic wavelet transform; this knowledge is exploited in the design of a speckle suppression filter with an edge enhancement feature. MNWD takes advantage of the sparsity and multiresolution properties of wavelet, and the iterative edge preservation and enhancement feature of nonlinear diffusion. In this algorithm, speckle is suppressed by employing the iterative multiscale diffusion on the wavelet coefficients, while the edges of the image are enhanced by using an iterative signal compensation process. The proposed method is validated using synthetic and real echocardiographic images. Denoising results show that MNWD reduce speckle in the regions where intensity is intermediate. **[23]**

Khalifa Djemal in 2005 proposed speckle deduction in ultrasound images by minimization of total variation. To limit the noise in an image, some techniques are based on the calculation of an average intensity in each pixel of the image by considering some neighborhood. However, these techniques tend to attenuate contours present in the image. This affect edge and particularly penalizing for the segmentation algorithms whose finality is to find contours.

The restoration method by minimization of total variation, consists in minimizing under constraints of the great variations present in the image while preserving contours. An ultrasound image restoration method based on the resolution of non linear partial derivative equation (PDE) is presented in this work.
Results of the work show that speckle is practically removed by this method, discontinuities are practically preserved, and the regions of the restored image are more homogeneous and improve the result of segmentation. **[24]**

Fan zhang et.al [IEEE 2006] proposed laplacian pyramid nonlinear diffusion and shock filter (LPNDSF). Proposed LPNDSF coupled nonlinear diffusion and shock filter process and is applied in Laplacian pyramid domain of an image, to remove speckle and enhance edges simultaneously.**[25]**

Ahmed M. Badawi et.al in 2006 proposed a novel algorithm for speckle reduction in medical ultrasound imaging while preserving the edges with the added advantages of adaptive noise filtering and speed. Nonlinear image diffusion algorithm discussed in this paper incorporates two local parameters of image quality, namely, scatterer density, image gradient and texture-based contrast, to weight the nonlinear diffusion process. This novel diffusion filter was then implemented using back propagation neural network for fast parallel processing of volumetric images. The experimental results show that weighting the image diffusion with these parameters produces better noise reduction and better edge detection quality with reasonable computational cost. From the experiments conducted by the author we can confirm that introduction of the contrast and the scatterer density into the diffusion process increases the good performance of the nonlinear diffusion algorithm in removing the speckle noise and preserving the important structures and edges of the image. As the proposed method showed a better quality of diffusion and better edge map, this method can be used further as a preprocessing phase before applying any segmentation or active contour model processes. **[26]**

Yong Yue et.al in 2006 proposed nonlinear multiscale wavelet diffusion (NMWD) algorithm for speckle suppression, this algorithm is designed to utilize the favorable denoising properties of two frequently used techniques: the sparsity, multiresolution properties of the wavelet and the iterative edge enhancement feature of nonlinear diffusion. The strategy used here removes the signal mean during the edge estimation, and edge related components can be easily separated from the noise related components by magnitude difference. Results of the tests of SRAD and NMWD on both synthetic and real ultrasonic images reveal that only NMWD can significantly reduce speckle in both high and low contrast edges. **[27]**

Peter C. Tay et.al in 2006 presented a novel stochastically driven filtering method to despeckle B mode ultrasound images. It is an iterative filtering method that considers local extrema of the Bmode image as outliers and applies local smoothing to these outliers. Each iteration produce a sequence with locally reduced variance. The local extrema of the new sequence are considered as outliers and the process is iterated. This method produces a convergent sequence of images by squeezing the stochastically distributed pixel values to a limiting value. This is called as squeeze box filter (SBF). By dynamically varying the window which is used to find the local mean, results can be obtained with fewer- iterations. SBF with despeckling method using dynamically varying window (SBF-DVM) replaces each outlier values with the mean determined from this dynamically varying window. Studies show that SBF and SBF-DVM show better despeckling when compared to the Nagan, Lee, Frost, Kuan, AWMF, and SRAD, also ultrasound despeckling assessment index (USDSAI) is high for SBF and SBF-DVM. **[28]**

Alla Aksel et.al in 2007 investigates extensions to speckle reducing anisotropic diffusion (SRAD) for the purpose of improving automated segmentation in echocardiographic imagery.

Firstly, windowed SRAD (WSRAD) which considers a larger local neighborhood for the instantaneous coefficient of variation (ICOV) operator thus eliminating erroneous smoothing of diffuse feature edges hence it attempts to increase edge contrast while preserving object size via the addition of neighborhood statistics to the SRAD diffusion coefficient.

Secondly, author consider de-convolution SRAD (DeSpeRADo), which attempts to eliminate blurring artifact inherent to the ultrasound imaging system.

Segmentation was performed on myocardial images, filtered with SRAD, WSRAD, and DeSpeRADo for quantifying the performance of the techniques. Results of WSRAD show high segmentation accuracy. **[29]**

Yang Mo Yoo et.al in 2007 proposed laplacian pyramid-based nonlinear diffusion (LPND), for medical ultrasound images. With this method, speckle is removed by nonlinear diffusion filtering of band-pass ultrasound images in Laplacian pyramid

domain. For nonlinear diffusion in each pyramid layer, a gradient threshold is automatically determined by a variation of median absolute deviation (MAD) estimator.
For the comparison the experiments are carried on commercial gray scale phantom image. Results of comparison of the filters laplacian pyramid based nonlinear diffusion filter (LPND), Gaussian regularized nonlinear diffusion(ND), speckle reduced anisotropic diffusion (SRAD), nonlinear anisotropic diffusion(NCD) is as follows:

- LPND preserves edges and small structures while maximally removing speckle thus resulting increased contrast and improved visibility of small structures in each image.
- ND shows sharper but jagged edges and gives relatively low contrast.
- SRAD broadens the boundaries of bright regions and shrinks those of dark regions.
- NCD enhances the coherence of organ surface, it also causes blurring of small structures and reduces the contrast

Of the above mentioned filters the performance of LPND is good. **[30]**

Ricardo G. Dantas et.al in 2007 proposed a novel method for speckle reduction in ultrasound medical imaging, which uses a bank of wideband 2-D directive filters, based on modified Gabor functions.
One widely used method for ultrasound speckle reduction is the split spectrum processing (SSP), but the use of one-dimensional (1-D), narrow-band filters makes the resultant image experience a significant resolution loss, hence there is a wide trade off between the level of speckle reduction and the acceptance loss of resolution in SSP. In order to overcome this critical drawback author proposed the above mentioned method.

This paper presents a single-image method for ultrasound speckle reduction, based on modified Gabor functions, henceforth called directive filters (DF). These two dimensional (2-D) filters have the ability to split the spectrum of the RF image in different frequency directions. When a whole set of filters is used, covering the spectrum in all directions, the input RF image can be split in different B-mode images, each one with the original structure information in a specific orientation. When these partial

outputs are compounded, it results in an image in which the structure information is enhanced and speckle is drastically reduced. Difference between SSP and DF is that SSP uses narrow band pass filter blurring effect where as DF uses wide-band filter.

Selection of number of filters also play an important role in DF because with an increasing number of filters, the overlapping area among them also increases, resulting in redundant information that has small contribution in the quality of the final image. On the contrary with a small number of filters the overlapping area is reduced, and some spectral information can be lost.

In this paper DF was tested with both simulated and real data. Results with simulated data indicate a high level of speckle reduction, as shown by the improvement in the SNR of the three different regions. It also can be noticed a contrast enhancement shown by the PDE curves. The result with real data if visually inspected, indicates that, after DF processing, the bright regions are more homogeneous but without having lost the fine details.

Thus DF can be used as a stand-alone method or as a preprocessing stage, prior to the use of other techniques, such as adaptive filtering or spatial compound, improving the overall result. **[31]**

Chapter 3

Background

3.1 Image Basics

3.1.1 Definition of an Image

The term image refers to a two-dimensional light intensity f(x, y). Where *x* and *y* denote spatial coordinates and the value of f at any point (x, y) is propotional to the brightness (or gray level) of the image at that point.

3.1.2 Digital Image

The term digital image refers to an image f(x, y) that has been discretized both in spatial coordinates and brightness. A digital image can be considered a matrix whose row and column indices identify a point in the image and the corresponding matrix element value identifies the gray level at that point. The elements of such a digital array are called pels (picture elements), or more commonly pixels. Images are built up of pixels that contain color information and are aligned with the cartesian coordinate system. The zero point is found at the top-left corner of the image (in PostScript, for example, the zero point is found at the bottom-left corner of the page). The image's width is represented by the variable N the image's height with the variable M as shown below.

$$f(x, y) = \begin{pmatrix} f(0, 0) & f(0, 1) & . & f(0, N-1) \\ f(1, 0) & f(1, 1) & . & f(1, N-1) \\ . & . & . & . \\ f(M-1, 0) & f(M-1, 1) & . & f(M-1, N-1) \end{pmatrix}$$

3.1.3 Types of Imaging

Some of the imaging techniques are described below

3.1.3.1 X-rays

X-rays use beams of ionizing radiation to expose photographic film. Placing the human body between the beam and the film leaves an image of the body on the film. When

radiation penetrates in to the tissues easily black areas are seen, for example air in the lungs on a chest x-ray. Bones appear white because they are hardest to penetrate. X-rays are a good way of looking at bones and air inside the human body but they do not show up soft tissues well.

Fig 3.1 Chest x-ray image

3.1.3.2 Ultrasound Scans

These scans use high frequency sound waves which are emitted from a probe. The echoes that bounce back from structures in the body are shown on a screen. The structures can be much more clearly seen when moving the probe over the body and watching the image on the screen. The main problem in these scans is the presence of speckle noise which reduces the diagnosis ability.

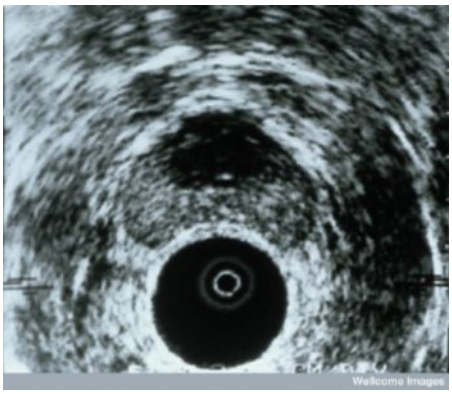

Fig 3.2 Ultrasound scan of normal prostate gland

3.1.3.3 Computerized Tomography (CT) Scan

It uses multiple x-rays (ionizing radiation) to create a slice by slice image of the body. The slices (scans) are viewed as if you are looking up through the feet of the person to see the cross section. Therefore, a right sided organ such as the liver appears on the left of the image. These can be used to take an accurate biopsy.

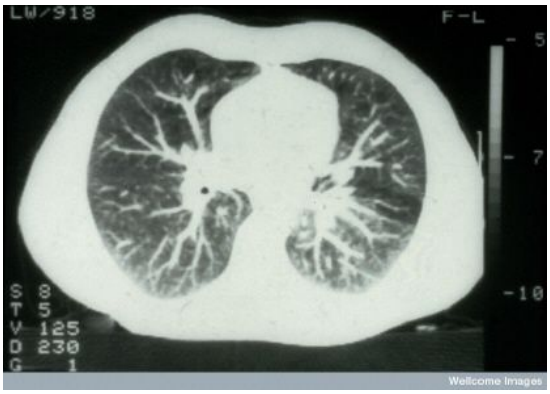

Fig 3.3 Computerized Tomography Scan

3.1.3.4 Magnetic Resonance Imaging (MRI) Scan

MRI - images are similar to CT images except they show up the details of soft tissue better. MRI scans do not use X-rays but use a strong pulsed magnetic force to polarize cells - line up the (electrons) and measure the energy given off by the electrons when they bounce back into their normal orbits in-between pulses.

Fig 3.4 MRI of the spine.

3.1.3.5 Optical Imaging

It is an imaging technique that involves inference from the deflection of light emitted from a laser or infrared source due to anatomic or chemical properties of material (e.g. cell tissue).

3.1.3.6 Infrared Imaging

This type of imaging is also called as Infrared Thermography/thermal imaging/thermal video. Thermographic cameras detect radiation in the infrared range of the electromagnetic spectrum (roughly 900–14,000 nanometers or 0.9–14 μm) and produce images of that radiation. Since infrared radiation is emitted by all objects based on their temperatures, according to the black body radiation law, thermography makes it possible to "see" one's environment with or without visible illumination. The amount of radiation emitted by an object increases with temperature, therefore thermography allows one to see variations in temperature (hence the name). When viewed by thermographic camera, warm objects stand out well against cooler backgrounds; humans and other warm-blooded animals become easily visible against the environment, day or night.

These images are used in various fields like Industrial, Military, Research, and medical for various purposes. However their use is limited because of the presence of noise hence research work is going in the field of removing the noise.

3.2 Noise in an Image

It is generally desirable for image brightness (or film density) to be uniform except where it changes to form an image. There are factors, however, that tend to produce variation in the brightness of a displayed image even when no image detail is present. This variation is usually random and has no particular pattern. In many cases, it reduces image quality and is especially significant when the objects being imaged are small and have relatively low contrast. This random variation in image brightness is designated noise. This noise can be either image dependent or image independent. All the digital images contain some visual noise. The presence of noise gives an image a mottled, grainy, textured, or snowy appearance.

There are three primary types of noise: Random, fixed pattern and banding. Random noise revolves around an increase in intensity of the picture. It occurs through color discrepancies above and below where the intensity changes. It is random, because even if the same settings are used, the noise occurs randomly throughout the image. It is generally affected by exposure length. Random noise is the hardest to get rid of because we cannot predict where it will occur. The digital camera itself cannot account for it, and it has to be lessened in an image editing program.

Fixed pattern noise surrounds hot pixels. Hot pixels are pixel bits that are more intense than others surrounding it and are much brighter than random noise fluctuations. Long exposures and high temperatures cause fixed pattern noise to appear. If pictures are taken under the same settings, the hot pixels will occur in the same place and time. Fixed pattern noise is the easiest type to fix after the fact. Once a digital camera realizes the fixed pattern, it can be adjusted to lessen the affects on the image. However, it can be more dubious to the eye than random noise if not lessened.

Banding noise depends on the camera as not all digital cameras will create it. During the digital processing steps, the digital camera takes the data being produced from the sensor and creates the noise from that. High speeds, shadows and photo brightening will create banding noise. Gaussian noise, salt & pepper noise, passion noise, and speckle noise are some of the examples of noise.

3.2.1 Types of Spatial Filters

Some of the types of spatial filters are discussed below.

General Filters

Filters in the General class are linear spatial convolution filters which calculate a weighted average of the cells in the current filter window. The filter kernel contains the array of weighting coefficients used in the calculation. The three filters in this class (Low Pass / Average, High Pass, and High Boost) use different sets of filter weights to emphasize features with different spatial frequencies in the input image. The filters in this class have no user-defined parameters.

Edge Detection Filter

Filters in the Edge Detection class are designed to detect boundaries between image areas that have distinctly different brightness. The output raster is a grayscale image of these edges; the output cell brightness is proportional to the difference in neighboring cell brightness in the original image. The filter output is a nonlinear combination of the cell values in the filter window, which results from combining the output of two separate linear filters. Each of the predefined Edge Detection filters (Gradient-Sobel, Gradient-Roberts, and Gradient-Prewitt) uses a pair of filter kernels of fixed size. The two kernels detect and reinforce local brightness gradients (edges) in two perpendicular directions within the image. The output of the two kernels is combined to produce a measure of the overall magnitude of the local gradient at each cell in the input raster.

Noise Reduction Filter

The filters in the Noise Reduction class are designed to remove extreme or outlier values from image areas that should have relatively uniform values. These outlier values are often the result of additive "noise" imposed on the image by the acquisition system or later processing errors. Median, Modal etc., are some of the examples of this type.

In this work a study is made on the spatial filtering techniques used to remove the speckle noise and to select best filter for a given image on the basis of statistical parameters. The filters required for speckle are obtained by the combination of the above mentioned filters for eg., In speckle removal both noise reduction filter characteristics and edge preservation filter characteristics are merged.

3.3 Speckle Noise

Speckle is not a noise in an image but noise-like variation in contrast. It arises from random variations in the strength of the backscattered waves from objects and is seen mostly in RADAR and US imaging.

Definition of speckle noise

Speckle noise is defined as multiplicative noise, having a granular pattern it is the inherent property of ultrasound image and SAR image.

Major causes of speckle noise

Due to incorrect assumption that the ultrasound pulse always travel in a straight line, to and fro from the reflecting interference. Another source of reverberations is that a small portion of the returning sound pulse may be reflected back into the tissues by the transducer surface itself, and generate a new echo at twice the depth.

Speckle is the result of the diffuse scattering, which occurs when an ultrasound pulse randomly interferes with the small particles or objects on a scale comparable to the sound wavelength.

The backscattered echoes from unresolvable random tissue inhomogenities in ultrasound imaging and from objects in Radar imaging undergo constructive and destructive interferences resulting in mottled b-scan image.

Need for filtering

Speckle degrades the quality of US and SAR images and therby reducing the ability of a human observer to discriminate the fine details of diagnostic examination

This artifact introduces fine-false structures whose apparent resolution is beyond the capabilities of imaging system, reducing image contrast and masking the real boundaries of the tissue leading to the decrease in the efficiency of further image processing such as edge detection, automatic segmentation, and registration techniques.

Another problem in Ultrasound data is that the received data from the structures lying parallel to the radial direction can be very weak, where as structures lying normal to the radial direction give stronger echo.

Filtering techniques can be classified as

- Incoherent processing techniques
- Image post processing

Incoherent processing techniques

These are based on the averaging of multiple images of the same scan plane, where the images are obtained by varying transducer frequency and/or view angle to achieve independent or partially uncorrelated speckle patterns.

These imaging techniques increase target-detection capability of phased array scanning at the expense of increased system complexity and loss of spatial resolution.

Image postprocessing:

Speckle Suppression schemes based on image postprocessing involve adaptive, anisotropic diffusion and wavelet based filtering techniques. These techniques do not require any hardware modification in the image reconstruction system, and hence have found a growing interest. In this the images are obtained as usual and the processing techniques are applied on the image obtained.

However, one of the chief difficulties of filtering methods proposed in literature is the understanding the nature of speckle.

Model of the speckle noise:

Literature survey shows that in speckle noise the ratio of variance and mean is constant over a wide region [13] which is also an inherent property of Rayleigh distribution. This implies that speckle could be modeled as multiplicative noise, it is also deterministic artifact. Deterministic artifact means that, two images acquired under exactly same circumstances, will experience exactly the same corruption [25**].** Being deterministic it differs from other types of noise. It can also be defined as destructive interference artifact and its severity depends on the relative phase between two overlapping returning echoes [25]. Other imaging techniques like laser or radar which use coherent sources of ultrasound acoustic waves suffer from speckle noise. The displayed images from the US device have properties like it is log compressed.

Many experiments are conducted in the literature [9] on the liver image, and phantom images to understand the speckle model. Results of the experiments show that displayed

US images have linear relationship between the local variance and mean of the speckle as shown in fig 1, hence it can be modeled as signal dependent noise [9] given by (1)

$$z_{ij} = x_{ij} + \sqrt{x_{ij}} \; . \; n_{ij} \qquad (1)$$

Where z_{ij} and x_{ij} denote the pixel gray levels of the observed and true images, respectively, and the n_{ij} are noise terms independent of x_{ij}.

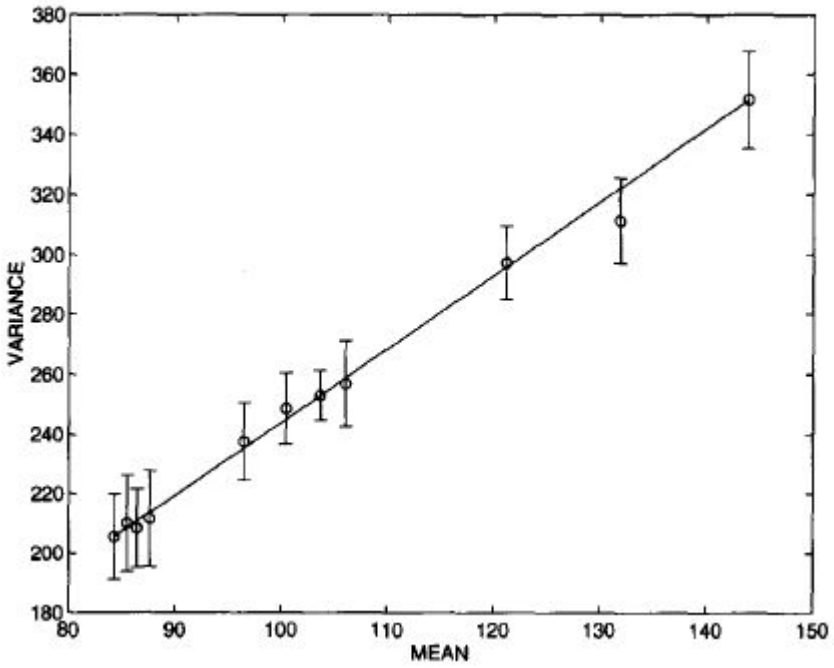

Fig 3.5(a)

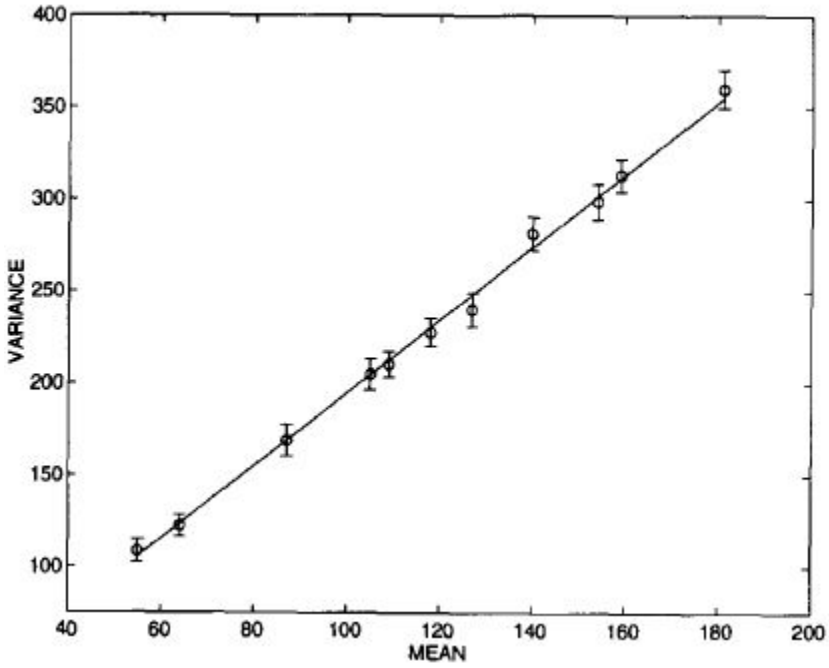

Fig 3.5(b)

Fig 3.5 The linear relation between the local variance and mean of the speckle [9]. (a) on phantom image (b) on liver image.

This signal dependent noise model helps us to smooth the image in the homogenous regions where the signal can be assumed to be constant. Using the parameter α, the local variance to mean ration given by (4), it is possible to decide whether the processed pixel is with in the homogenous region or not. Usually, if the local variance to the mean ratio is larger than the speckle, that corresponding pixel is considered as a resolvable object. Otherwise it is considered to be in homogenous region and is to be subjected to smoothening.

$$\mu_{i,j} = \frac{1}{W^2} \sum_{m=-W/2}^{W/2} \sum_{n=-W/2}^{W/2} x_{i-m,j-n} \qquad (2)$$

$$\sigma_{i,j}^2 = \frac{1}{W^2} \sum_{m=-W/2}^{W/2} \sum_{n=-W/2}^{W/2} (x_{i-m,j-n} - \mu_{i,j})^2 \qquad (3)$$

$$\alpha_{i,j} = \frac{\sigma_{i,j}^2}{\mu_{i,j}} \qquad (4)$$

Where $x_{i,j}$ is the pixel at the location (i,j), $\sigma_{i,j}^2$, $\mu_{i,j}$ are the local variance and local mean respectively. W is the moving window size and it should be selected, so that neither window size is too small leaving out speckle from being filtered out nor it is too large so that over smoothening will occur causing blurring of edges and also if the window size is large, processor takes long time for filtering and thus causing problem in real time application.

Images corrupted with speckle noise look like

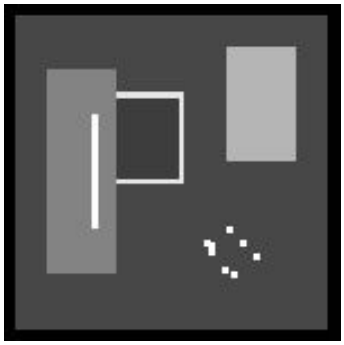

Fig 3.6(a)

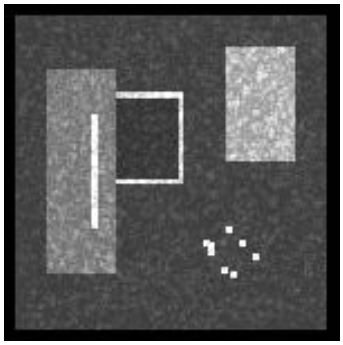

Fig 3.6(b)

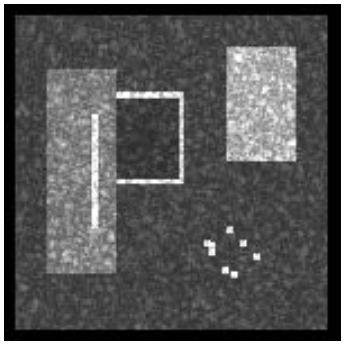

Fig 3.6(c)

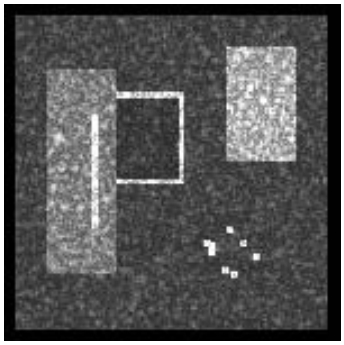

Fig 3.6(d)

Fig 3.6 Images corrupted with speckle noise having different standard deviations (σ) of noise (a) original synthetic image without noise (b) synthetic image having noise whose σ is 0.5 (c) synthetic image with noise whose standard deviation is 0.75 (d) noisy synthetic image where the standard deviation of the noise is 0.95.

Fig 3.7(a)

Fig 3.7(b)

Fig 3.7 Real US image (a) noise free image (b) image with standard deviation of noise as 0.7

3.4 Speckle Reduction Techniques

Speckle reduction techniques include adaptive filtering, anisotropic filtering, wavelet based filtering etc. This study is mainly based on adaptive filtering and anisotropic filtering.

3.4.1 Adaptive Filtering

Adaptive filter takes a moving filter window and calculates the statistical information of all pixels gray value, such as the local mean and the local variance. The central pixel's output value is dependent on this calculated statistical information. Lee filter, Kuan filter, and Frost filter are some of the e.g., of adaptive filters.

The overall procedure of the adaptive filtering [9] can be classified in to three steps as given below:

- Computation of local statistics.
- Region growing procedure
- Application of smoothening operator

3.4.1.1 Computation of local statistics

The local mean (μ) and variance (σ^2) obtained by using the equations (2) and (3) are used by equation (4) to calculate the parameter α. Depending on the values of μ and σ^2

the characteristic value of the local statistics of the speckle (α_0) is calculated for each of the image and is fixed for that particular image. $\alpha_{i.j}$ is calculated for all the pixel and tabulated in a look up table which has its use in region growing step.

3.4.1.2 Region Growing Procedure

Taking the homogeneity criteria which is a function of various image parameters, such as gray level, texture, local statistics, and color similarities homogeneous regions are developed by grouping the pixels satisfying certain homogeneity criteria. Each parameter characterizes homogeneity in a different manner.

In adaptive speckle suppression filter (ASSF), the local statistics $\alpha_{i,j}$ are used as homogeneity criteria to get homogeneous regions for every image pixel. In this procedure each pixel is considered as a seed point, any pixel with the local statistics close to the seed pixel's local statistics with in a certain bound is included in the region of seed pixel. This process is repeated for all the pixels in the image.

To test whether the pixel (m,n) belongs to homogeneous region of a seed pixel (i,j) the following conditions given by equations (5) and (7) must be satisfied

$$\alpha_{i,j} - \beta(\alpha_{i,j}) < \alpha_{m,n} \leq \alpha_{i,j} + \beta(\alpha_{i,j}) \qquad (5)$$

The statistical parameter β(.), is chosen as a function $\alpha_{i,j}$ given by

$$\beta(\alpha_{i,j}) = a + be^{-c\alpha_{i,j}} \qquad (6)$$

Where a, b and c are coefficients that depend on α_0 and on the desired smoothening level, 'a' is the biasing factor that controls both the smoothening of speckle and edges. Lower the value of 'a' lower will be the smoothening of both speckle and edges, 'b' is a scaling factor used for the adjustment of the statistical bound. Larger the value of 'b' increase smoothening as far as 'c' allows, 'c' directly depends on α_0 and hence controls the magnitude and sharpness of the statistical threshold. The pixels with local statistics below this statistical threshold undergo more smoothening and vice versa.

$$\sqrt{(m-i)^2 + (n-j)^2} \leq D_b \qquad (7)$$

Where, D_b is spatial bound locality parameter and depends on the kernel size used in the computation of local statistics, usually it is chosen in such a manner so that the number of pixel in homogenous region does not exceed W^2.

Since speckle statistics mostly depend up on the scanner specifications the coefficients in (6) are determined earlier and stored in a lookup table.

Using the equations (5) and (7) homogeneous regions are developed on the image
The developed homogeneous regions need not to be symmetric, also in the limiting case the grown region can have a single size that consists of only the seed pixel.

3.4.1.3 Application of Smoothening Operator

On each homogenous region smoothening operator like mean or median is applied. The result corresponding to each pixel is the mean or median of the pixels with in the grown region associated with the seed pixel. After filtering the whole image, the neighboring regions with similar intensity values are merged followed by updating the smoothening results on the newly developed regions in the lookup table.

3.4.2 Anisotropic Diffusion

In anisotropic diffusion [5] the main motto is to encourage smoothening with in the region in preference to the smoothening across the edges. This is achieved by setting the conduction coefficient as 1 with in the region and as 0 near edges, however the main problem involved in this is the detection of the presence and absence of edges. As a solution for this problem it is identified that conduction coefficient if chosen locally as a function of magnitude of the gradient of the brightness function of the image the edges can be determined.
A general expression [17] for anisotropic diffusion can be written as

$$I(x, 0) = I_0$$

$$\frac{\partial I}{\partial t} = \text{div}(F) + \beta(I_0 - I) \qquad (8)$$

Where, I is the input image, I_0 is the initial image, F is the diffusion flux and β is a data attachment coefficient. If β = 0, particular cases of equation are: 1) The heat diffusion equation $F=\nabla I$ which is equivalent to Gaussian convolution. 2) The non linear probability density function (PDF) with $F= c (|\nabla I |) .\nabla I$. where ∇ is the gradient operator, *div* is the divergence operator, || denotes the magnitude, and diffusion coefficient c (x) is given by:

$$C(x) = \frac{1}{1+(x/k^2)} \tag{9}$$

And

$$C(x) = \exp\left[-(x/k^2)\right] \tag{10}$$

Where, *k* is the edge magnitude parameter.

In this anisotropic diffusion method, for finding edges as a step discontinuity gradient magnitude is used. . If $|\nabla I| >> k$, then $c(|\nabla I|) \rightarrow 0$, an all pass filter is used; if $|\nabla I| << k$, then, $c(|\nabla I|) \rightarrow 1$, isotropic diffusion is achieved.

Discrete form of (8) is given by

$$I_d^{t+\nabla t} = I_d^t + \frac{\nabla t}{|\eta_s|} \sum_{q \in \eta_s} c(\nabla I_{d,q}^t) \nabla I_{d,q}^t \tag{11}$$

Where, I_d^t is discretely sampled image, s denotes the pixel position in a discrete (2-D) grid, and ∇t is the time step, $\overline{\eta_s}$ represents the spatial resolution of pixel d, $|\overline{\eta_s}|$ is the number of pixels in the window, and $\nabla I_{d,q}^t = I_q^t - I_d^t, \forall q \in \overline{\eta_s}$.

The above equations show that the anisotropic diffusion allows the smoothening of homogenous regions and prohibits smoothening near edges thus preserving edges.

3.4.2.1 Anisotropic Diffusion for Speckle Reduction

Casting the probability density function (PDE) approach and adaptive filtering approach Yongjian Yu et.al [17] developed a new model for speckle reduction called as speckle reducing anisotropic diffusion (SRAD) method.

Explanation of SRAD derivation is as follows

For an intensity image $I_0(x, y)$ which is having finite power and no zero values over the image support Ω, the output image *I(x, y; 0)* is given by the following PDE.

$$\begin{cases} \partial I(x,y;t)/\partial t = div[c(q)\nabla(x,y;t)] \\ I(x,y;0) = I_0(x,y), (\partial I(x,y;t)/\partial \overrightarrow{n})|_{\partial\Omega} = 0 \end{cases} \tag{12}$$

Where $\partial\Omega$ denotes the border of Ω, $\vec{n}$ is the outer normal to $\partial\Omega$, and

$$c(q) = \frac{1}{1+[q^2(x,y;t) - q_0^2(t)/[q_0^2(t)(1+q_0^2(t))]} \tag{13}$$

Or

$$c(q) = \exp\{-[q^2(x,y;t) - q_0^2(t)]/[q_0^2(t)(1+q_0^2(t))]\} \tag{14}$$

Where q is the instantaneous coefficient of variation and is given as

$$q(x,y;t) = \sqrt{\frac{(1/2)(|\nabla I|/I)^2 - (1/4^2)(\nabla^2 I/I)^2}{[1+(1/4)(\nabla^2 I/I)]^2}} \tag{15}$$

The above mentioned function, q which is the instantaneous coefficient of variation q(x, y; t) helps in detecting the edges present in the images corrupted by speckle. At edges and high contrast regions this function produces high values and at homogenous regions it gives low values, $q_0(t)$ is the speckle scale function and q(x, y; t) fluctuates around $q_0(t)$.

The parameters 'k' in the equations (9) and (10) and $q_0(t)$ used in equations (13) and (14) effectively controls the amount of smoothening applied to the image in filtering.

The function for $q_0(t)$ can be derived as follows

It is expected that in an uniform area the diffusion should be isotropic. Based on the discrete isotropic diffusion update, we have

$$I_{i,j}^{t+\nabla t} = I_{i,j}^{t} + \frac{\Delta t}{4}(I_{i+1,j}^{t} + I_{i-1,j}^{t} + I_{i,j+1}^{t} + I_{i,j-1}^{t} - 4I_{i,j}^{t}) \qquad (16)$$

If data regarding σ(t), the standard deviation of $I_{i,j}^{t}$ in a homogenous region is given then standard deviation of $I_{i,j}^{t+\nabla t}$ in the region can be calculated as follows

Assuming that in this region the pixel are statistically independent to each other and identically distributed, from the statistical formula for a variance of a sum of random variables and from the equation (16) we have

$$\sigma(t+\Delta t) = \sqrt{(1-\Delta t)^2 \sigma^2(t) + (\Delta t/4)^2 4\sigma^2(t)} \qquad (17)$$

Regarding the mean the local mean remains the same before and after the iteration hence we have

$$q_0(t+\Delta t) = q_0(t)\sqrt{(1-\Delta t)^2 + (\Delta t)^2 + (\Delta t)^2/4} \qquad (18)$$

For $\nabla t << 1$, the $(\nabla t)^2$ term can be neglected in (18) and we have

$$\sqrt{1-2\Delta t} \approx 1-\Delta t \qquad (19)$$

Expanding the above equation (17) using Taylor series expansion and neglecting higher order terms we have

$$q_0(t+\Delta t) - q_0(t) + q_0(t)\Delta t \approx 0 \qquad (20)$$

Dividing the above equation by ∇t on both sides and taking the limit as $\nabla t \to 0$, we have

$$\dot{q}_0(t) + q_0(t) \approx 0 \qquad (21)$$

Where $\dot{q}_0(t)$ is the first derivative of $q_0(t)$ with respect to t. Solution of (21) is given

$$q_0(t) \approx q_0 \exp[-t] \qquad (22)$$

Thus, $q_0(t)$ required by the equations (13), (14) (instantaneous coefficient of variation) is derived and given by the equation (22).

From the equation (22) it is understood that through a diffusion process, speckle would be reduced exponentially (with a delay factor of 1) in homogenous regions. However the

equation (22) is correctly valid only until the values of $I_{i,j}^{t}$ in the homogenous region are truly independent at any time.

Introducing a constant in the equation (22) to control the decay rate the resulting equation becomes

$$q_0(t) \approx q_0 \exp[-\rho t] \qquad (23)$$

Where ρ is a constant

Given the values of q_0 and ρ and using the equation (23) in implementing SRAD, the user does not have to choose a homogenous region.

The other way of finding q_0 is given by the equation (24)

$$q_0(t) = \frac{\sqrt{\text{var}[z(t)]}}{\overline{z(t)}} \qquad (24)$$

Where $\text{var}[z(t)]$ and $\overline{z(t)}$ are the intensity variance and mean over a homogenous area at t, respectively.

3.5 Estimation of Statistical Parameters

The parameters which are used in the filter performance evaluation are Signal to Noise Ratio (SNR), Root Mean Square Error (RMSE), Peak Signal to Noise Ratio (PSNR), Correlation Coefficient (COC), and Mean Structural Similarity Index Measure (MSSIM).

3.5.1 Estimation of SNR

SNR compares the level of desired signal to the level of background noise. The higher the ratio, the less obtrusive the background noise is.

SNR [22] in decibels is defined as

$$\text{SNR} = 10 \log \left(\sigma_g^2 / \sigma_e^2 \right) \qquad (25)$$

Where, σ_g^2 is the variance of the noise free image and σ_e^2 is the variance of error (between the original and denoised image).

Brighter regions have a stronger signal due to more light, resulting in higher overall SNR

3.5.2 Estimation of RMSE

Mean square error (MSE) is given by

$$MSE = \sum_{i=j=1}^{N} [f(i, j) - F(i, j)]^2 / N^2$$

$$RMSE = \sqrt{MSE} \qquad (26)$$

Where, f is the original image F is the filtered image and N is the size of image.

RMSE is an estimator in many ways to quantify the amount by which an filtered/noisy image differs from noiseless image

3.5.3 Estimation of PSNR

PSNR is the ratio between possible power of a signal and the power of corrupting noise that affects the fidelity of its representation.

PSNR in decibels is easily defined from RMSE as given below

$$PSNR = 20 \log_{10} (255/RMSE) \qquad (27)$$

Higher PSNR value provides higher image quality.

3.5.4 Estimation of COC

Correlation indicates the strength and direction of linear relationship between two signals and its value lie between +1 to -1. The correlation is 1 in the case of an increasing linear relationship, -1 in the case of a decreasing linear relationship, and some value in between for all the other cases, including the degree of linear dependence between the two signals. The closer the coefficient is to either -1 or +1, the stronger the correlation between the signals.

$$COC = \frac{\sum (g - \bar{g})(\hat{g} - \bar{g})}{\sqrt{\sum (g - \bar{g})^2 \sum (\hat{g} - \bar{\hat{g}})^2}} \qquad (28)$$

Where, g and $\hat{g}$ are original and denoised images respectively and $\bar{g}$ and $\bar{\hat{g}}$ are the mean's of the original image and denoised image respectively.

3.5.5 Estimation of MSSIM

MSSIM index is a novel method for measuring the similarity between two images. MSSIM values exhibit much better consistency with the qualitative appearance of the image. MSSIM [20] is given by

$$\text{MSSIM (X, Y)} = \frac{1}{M}\sum_{j=1}^{M} SSIM(x_j, y_j) \tag{29}$$

$$\text{SSIM(x,y)} = \frac{(2\mu_x\mu_y + C_1)(2\sigma_{xy} + C_2)}{(\mu_x^2 + \mu_y^2 + C_1)(\sigma_x^2 + \sigma_y^2 + C_2)} \tag{30}$$

$$\mu_x = \sum_{i=1}^{N} w_i x_i$$

$$\sigma_x = \left(\sum_{i=1}^{N} w_i (x_i - \mu_x)^2\right)^{\frac{1}{2}}$$

$$\sigma_{xy} = \sum_{i=1}^{N} w_i (x_i - \mu_x)(y_i - \mu_y)$$

$$C_1 = (K_1 L)^2$$

$$C_2 = (K_2 L)^2$$

Where, L is the dynamic range of pixel values (255 for 8-bit grayscale images). And $K_1 << 1$ is a small constant and also $K_2 << 1$.

Speckle is significant in Ultrasound and Synthetic Aperture Radar (SAR) imaging. Before the implementation of speckle reduction techniques it is necessary to understand the basics of these imaging modalities.

3.6 Ultrasound Imaging:

3.6.1 Introduction

It is a medical imaging technique that uses high frequency sound waves and their echoes. The technique is similar to the echolocation used by bats, whales and dolphins, as well as SONAR used by submarines. In ultrasound, the following events happen:

1. The ultrasound machine transmits high-frequency (1 to 5 megahertz) sound pulses into the human body using a probe.
2. The sound waves travel into the body and hit a boundary between tissues (e.g. between fluid and soft tissue, soft tissue and bone). Echoes are produced at any

tissue interface where a change in acoustical impedance occurs. On these images, the film density is proportional to the intensity of the echo (a more energetic echo would produce a darker or lighter dot on the film). The intensity of the returning echo, that is the energy returned to the transducer, is determined by,

- The magnitude of the change in the acoustical impedance at the echoing interface
- The characteristics of the intervening tissue, and
- The normality (perpendicularity) of the interface to the transducer.
- The appearance of the echo on the film is also determined by the degree of amplification (gain) applied after the echo has been received by the transducer.

3. Hence some of the sound waves get reflected back to the probe, while some travel on further until they reach another boundary and get reflected.
4. The reflected waves are picked up by the probe and relayed to the machine.
5. The machine calculates the distance from the probe to the tissue or organ (boundaries) using the speed of sound in tissue (1,540 m/s) and the time of the each echo's return (usually on the order of millionths of a second).
6. The machine displays the distances and intensities of the echoes on the screen, forming a two dimensional image.

3.6.2 Transducer Probe

The transducer probe is the main part of the ultrasound machine. The transducer probe makes and sends the sound waves and receives the echoes. The transducer probe generates and receives sound waves using a principle called the **piezoelectric (pressure electricity) effect**, which was discovered by Pierre and Jacques Curie in 1880. The probe also has a sound absorbing substance to eliminate back reflections from the probe itself, and an acoustic lens to focus the emitted sound waves. Transducer probes come in many shapes and sizes. The shape of the probe determines its field of view, and the frequency of emitted sound waves determines how deep the sound waves penetrate and the resolution of the image.

The piezoelectric effect also works in reverse. If the crystal is squeezed or stretched, an electric field is produced across it. So if ultrasound hits the crystal from outside, it will cause the crystal to vibrate in and out, and this will produce an alternating electric field. The resulting electrical signal can be amplified and processed in a number of ways. So a second crystal can be used to detect any returning ultrasound which has been reflected from an obstacle. Normally the transmitting and receiving crystals are built into the same hand-held unit, which is a called as ultrasonic transducer shown in fig 3.8 and the ultrasound machine is shown in fig 3.9

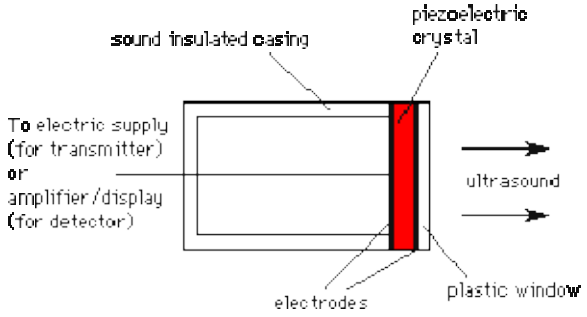

Fig 3.8 Ultrasonic transducer

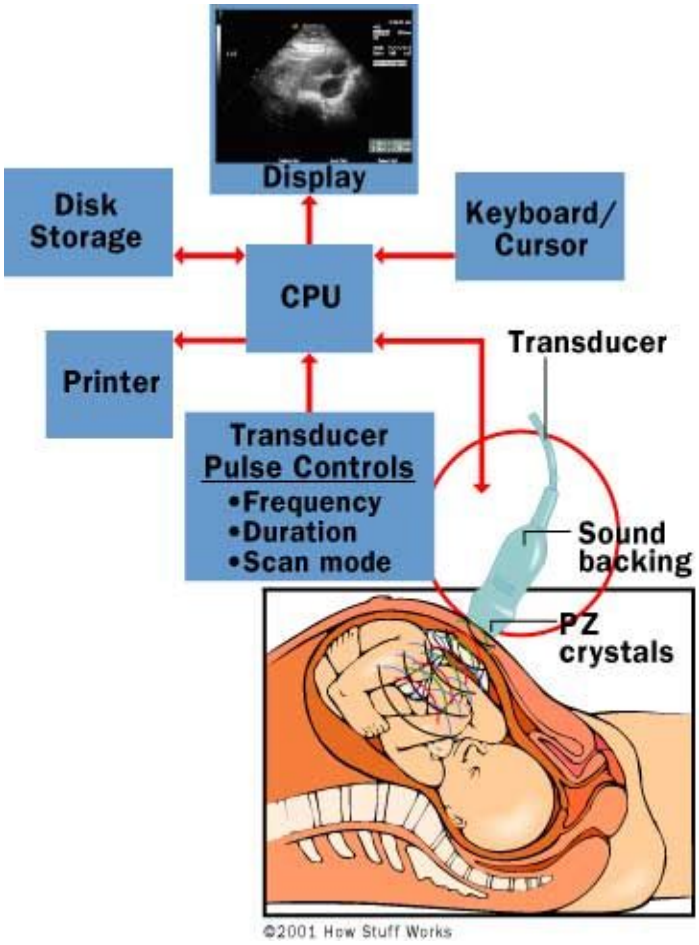

Fig 3.9 The parts of an ultrasound machine

3.6.3 Applications of Ultrasound Imaging

Ultrasound has been used in a variety of clinical settings, like obstetrics, gynecology, cardiology and in cancer detection. The main advantage of ultrasound is that certain structures can be observed without using radiation**.** Ultrasound can also be done much faster than X-rays or other radiographic techniques. Here is a short list of some applications of ultrasound:

1. **Obstetrics and Gynecology**
    - Measuring the size of the fetus to determine the due date
    - Determining the position of the fetus to see if it is in the normal head down position or breech
    - Checking the position of the placenta to see if it is improperly developing over the opening to the uterus (cervix)

- Checking the fetus's growth rate by making many measurements over time
- Detecting ectopic pregnancy, the life-threatening situation in which the baby is implanted in the mother's Fallopian tubes instead of in the uterus
- Determining whether there is an appropriate amount of amniotic fluid cushioning the baby
- Monitoring the baby during specialized procedures - ultrasound has been helpful in seeing and avoiding the baby during amniocentesis (sampling of the amniotic fluid with a needle for genetic testing). Years ago, doctors use to perform this procedure blindly; however, with accompanying use of ultrasound, the risks of this procedure have dropped dramatically.
- Seeing tumors of the ovary and breast

2. **Cardiology**

   Seeing the inside of the heart to identify abnormal structures or functions
   Measuring blood flow through the heart and major blood vessels

In addition to these areas, there is a growing use for ultrasound as a rapid imaging tool for diagnosis in emergency rooms.

3.7 Synthetic Aperture Radar Imaging

3.7.1 Introduction

Synthetic aperture radar (SAR) imaging is perpendicular to the aircraft velocity as shown in the figure below. SAR produces a two-dimensional (2-D) image. One dimension in the image is called range (or cross track) and is a measure of the "line-of-sight" distance from the radar to the target. Range measurement and resolution are achieved in synthetic aperture radar in the same manner as most other radars: Range is determined by precisely

measuring the time from transmission of a pulse to receiving the echo from a target and, in the simplest SAR, range resolution is determined by the transmitted pulse width, i.e. narrow pulses yield fine range resolution.

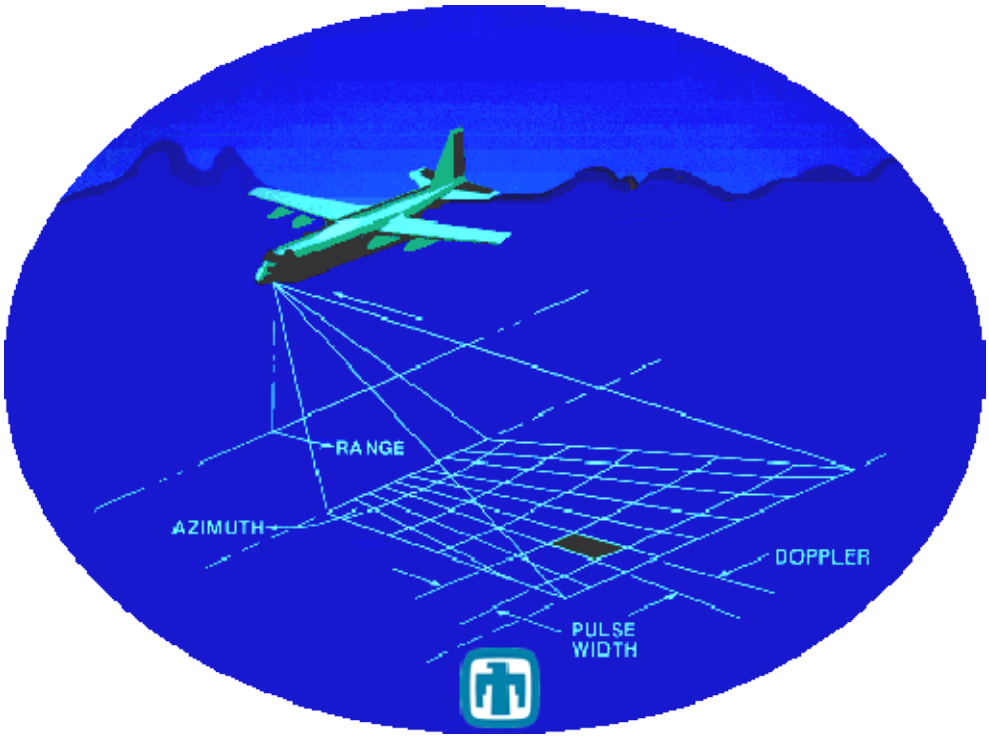

3.10 Synthetic Aperture Radar Imaging Concept (Sindia image lab)

The other dimension is called azimuth (or along track) this is perpendicular to range. It is the ability of SAR to produce relatively fine azimuth resolution that differentiates it from other radars. To obtain fine azimuth resolution, a physically large antenna is needed to focus the transmitted and received energy into a sharp beam. The sharpness of the beam defines the azimuth resolution. Similarly, optical systems, such as telescopes, require large apertures (mirrors or lenses which are analogous to the radar antenna) to obtain fine imaging resolution. Since SARs are much lower in frequency than optical systems, even moderate SAR resolutions require an antenna physically larger than the practical size carried by an airborne platform usually hundred meters long antenna lengths are often required. However, airborne radar could collect data while flying this distance and then process the data as if it came from a physically long antenna. The distance the aircraft flies in synthesizing the antenna is known as the synthetic aperture. A narrow synthetic

beam width resulting from the relatively long synthetic aperture, yields finer resolution than the resolution possible from a smaller physical antenna.

Achieving fine azimuth resolution may also be described from a doppler processing viewpoint. A target's position along the flight path determines the doppler frequency of its echoes. Targets ahead of the aircraft produce a positive doppler offset, targets behind the aircraft produce a negative offset. As the aircraft flies a distance (the synthetic aperture), echoes are resolved into a number of doppler frequencies. The target's doppler frequency determines its azimuth position.

While this section attempts to provide an intuitive understanding, SARs are not as simple as described above. Transmitting short pulses to provide range resolution is generally not practical. Typically, longer pulses with wide-bandwidth modulation are transmitted which complicates the range processing but decreases the peak power requirements on the transmitter. For even moderate azimuth resolutions, a target's range to each location on the synthetic aperture changes along the synthetic aperture. The energy reflected from the target must be "mathematically focused" to compensate for the range dependence across the aperture prior to image formation. Additionally, for fine-resolution systems, the range and azimuth processing are coupled (dependent on each other) these parameters greatly increases the computational processing.

3.7.2. Applications of Synthetic Aperture Radar Imaging:

Navigation and Guidance.

Synthetic aperture radar provides the capability for all-weather, autonomous navigation and guidance. By forming SAR reflectivity images of the terrain and then "correlating" the SAR image with a stored reference (obtained from optical photography or a previous SAR image), a navigation update can be obtained. Position accuracies of less than a SAR resolution cell can be obtained. SAR may also be used to guidance applications by pointing or "squinting" the antenna beam in the direction of motion of the airborne platform.

Foliage and Ground Penetration.

SAR imaging offers the capability for penetrating materials which are optically opaque, and thus not visible by optical or IR techniques. Low-frequency SARs may be used under certain conditions to penetrate foliage and even soil. This provides the capability for imaging targets normally hidden by trees, brush, and other ground cover. To obtain adequate foliage and soil penetration, SARs must operate at relatively low frequencies (10 MHz to 1 GHz).

Recent studies have shown that SAR may provide a limited capability for imaging selected underground targets, such as utility lines, arms caches, bunkers, mines, etc. Depth of penetration varies with soil conditions (moisture content, conductivity, etc.) and target size, but individual measurements have shown the capability for detecting 55-gallon drums and power lines at depths of several meters. In dry sand, penetration depths of 10's of meters are possible.

Moving Target Indication.

The motion of a ground-based moving target such as a car, truck, or military vehicle, causes the radar signature of the moving target to shift outside of the normal ground return of a radar image. One can even extract other target related information such as location, speed, size, and Radar Cross Section (RCS) from these target signatures.

Change Detection.

A technique known as coherent change detection offers the capability for detecting changes between imaging passes. To detect whether or not a change has occurred, two images are taken of the same scene, but at different times. These images are then geometrically registered so that the same target pixels in each image align. After the images are registered, they are cross correlated pixel by pixel. Where a change has not occurred between the imaging passes, the pixels remain correlated, whereas if a change has occurred, the pixels are uncorrelated. Of course, targets that are not fixed or rigid, such as trees blowing in the wind, will naturally decorrelate and show as having

"changed." While this technique is useful for detecting change, it does not measure direction or the magnitude of change.

Environmental Monitoring.

Synthetic aperture radar is used for a wide variety of environmental applications, such as monitoring crop characteristics, deforestation, ice flows, and oil spills. Oil spills can often be detected in SAR imagery because the oil changes the backscatter characteristics of the ocean. Radar backscatter from the ocean results primarily from capillary waves through what is known as Bragg scattering (constructive interference from the capillary waves being close to the same wavelength as the SAR). The presence of oil dampens the capillary waves, thereby decreasing the radar backscatter. Thus, oil slicks appear dark in SAR images relative to oil-free areas.

3.7.3. Radar Filters

Radar images have a distinctly grainy appearance that results from a characteristic image noise known as speckle. The signal received from a single ground-resolution cell is actually the sum of many signals generated by individual objects and surfaces within the cell. The strength of the aggregate return signal varies with direction and angle of view, in part due to varying degrees of constructive and destructive interference occurring among the individual signals. A minor change in direction of view can result in a great difference in the strength of the aggregate signal received by the sensor. As a result, image cells in areas with uniform ground materials and slope will exhibit random variations in image brightness, producing a speckled appearance. Speckle makes it difficult to assess the characteristics of the target materials from the measured radar response. In non-uniform areas, the presence of speckle also reduces the human interpreter's ability to resolve details in the image.

Speckle noise does not significantly alter the mean value in large, uniform areas of the image. For this reason, speckle in radar images can be reduced by simply averaging a number of values in a local neighborhood, but this process reduces the spatial resolution

of the image, and blurs edges. The filters in the Radar class utilize the specific properties of speckle noise to produce a more robust noise reduction.

For the purpose of processing radar images, it is useful to consider the aggregate return signal strength to be a function of a true signal (dependent on the properties of the objects in the individual cell). Unlike the additive image noise in many optical images, speckle is approximately multiplicative in nature. The brightness of a cell in the image is the product of the true signal and the random noise, so as target brightness increases, so does the amplitude of the noise. The radar filters included in this class are designed to account for this property of speckle noise. They are adaptive filters, varying the filter parameters spatially on the basis of the local statistical properties of the image.

Using the multiplicative model for speckle noise, it can be shown that the standard deviation of the speckle noise equals the ratio of the standard deviation of image brightness to the mean image brightness. Typically this ratio is nearly constant for areas of varying average brightness in a radar image. Some of the radar filters calculate the noise standard deviation for each filter window using local values, whereas others assume the constancy property, and calculate a single value for the entire image. The resulting value is then used along with the local statistics in each filter window to estimate the value of the true signal for the center cell of the filter window. The adaptive nature of these filters allows them to reduce speckle noise while minimizing loss of spatial resolution and preserving edge detail. With user-defined parameters chosen to produce optimum results for each filter, the output images from the different filters show only subtle visual differences. Standard filters that are used in speckle reduction in SAR images are

Frost

The Frost filter is an adaptive radar filter that incorporates the local image statistics in the filtering process, assuming a negative exponential distribution for the speckle noise. The filter performs a weighted average of the cell values in the filter window, with the weights for each cell being determined from the local statistics to minimize the mean

square error of the signal estimate. The filter weight for a cell is a negative exponential function of the noise standard deviation (calculated locally for each filter window), and also decrease with distance from the center cell. The center cells are weighted more heavily as the variance in the filter window increases. The filter therefore smoothes more in homogeneous areas, but provides a signal estimate closer to the observed value of the center cell in heterogeneous areas. The Frost filter has no user-defined parameters.

Lee

The Lee filter uses a least-squares approach to estimate the true signal strength of the center cell in the filter window from the measured value in that cell, the local mean brightness of all cells in the window, and a gain factor is calculated from the local variance and the noise standard deviation. The filter assumes a Gaussian (normal) distribution for the noise values, and calculates the local noise standard deviation for each filter window. The Lee filter calculation produces an output value close to the local mean for uniform areas, and a value close to the original input value in higher contrast regions. More smoothing occurs in the more uniform areas, while maintaining edges and other fine detail. The Lee filter has no user-defined parameters.

Kuan (MAP)

The Kuan Maximum A Posteriori filter uses a maximum likelihood probability approach to estimate the true signal value for the center cell in the filter window. The MAP filter assumes that speckle noise has a negative exponential distribution, and maximizes a probability function involving the center cell value, the local mean and standard deviation, and the noise standard deviation (assumed constant for the entire image). Parameter A is a multiplier applied to the noise standard deviation to modify the amount of smoothing. Parameter A can vary from 0.1 to 5.0, with a default value of 1.0. The Kuan (MAP) filter has not been implemented.

Kuan (Adaptive Noise Smoothing)

The Kuan Adaptive Noise Smoothing filter uses a minimum mean square error calculation to estimate the value of the true signal for the center cell in the filter window from the local statistics. It is similar in approach to the Lee filter, but makes simplifying assumptions in the calculations. The Adaptive Noise Filter calculates the signal estimate from the local mean and variance, and the noise standard deviation (assumed to be constant for the entire image); it assumes a Gaussian (normal) distribution for the speckle noise. Kuan filter has no user defined parameters.

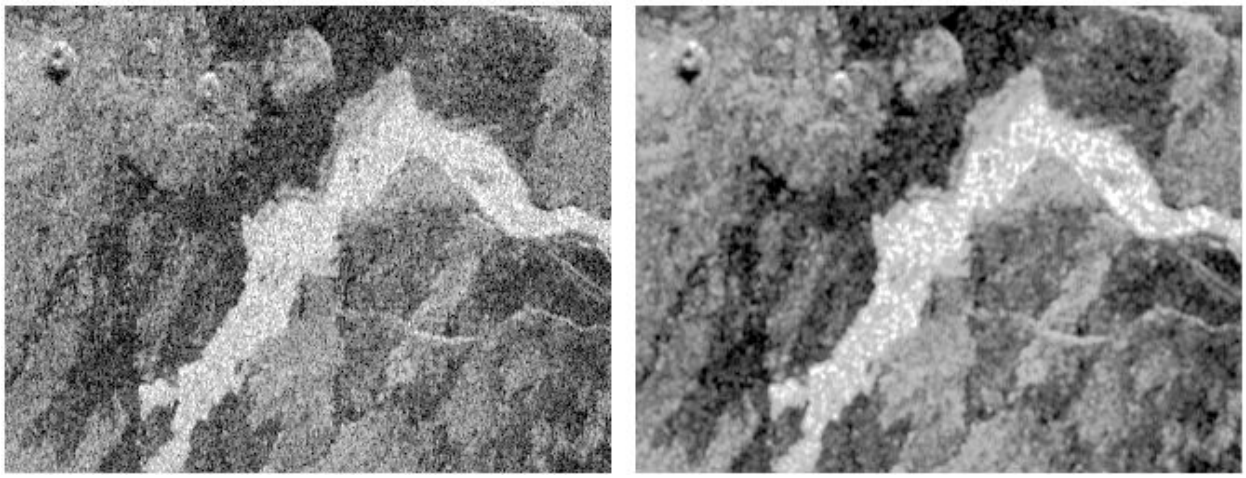

Fig 3.11 Radar image and result of Frost filter

In the proceeding work we have describe three different filtering techniques and evaluated results for six filters in terms of speckle removal.

Chapter 4
Methodology

4.1 Digital Image Processing

It is the process of using computer algorithms to perform image processing on digital images digital image processing field had evolved to be an important fileld. Digital image processing has many advantages over analog image processing; it allows a much wider range of algorithms to be applied to the input data, and can avoid problems such as the build-up of noise and signal distortion during processing. In this work image enhancement is done by removing the noise as a part of image processing. For removing the noise MATLAB software is used.

4.2 MATLAB Software

(**MAT**rix **LAB**oratory) is a programming language for technical computing from The Math Works, Natick, MA. Used for a wide variety of scientific and engineering calculations, especially for automatic control and signal, image processing, it also have extensive graphical capabilities.

MATLAB is a high-level language and interactive environment that enables us to perform computationally intensive tasks faster than with traditional programming languages such as C, C++, and FORTRAN.

4.3 Simulate Noise

Synthetic images have been taken from Dr. Alexandra Pizurica. She has many international publications and know for her contribution towards wavelet based speckle reduction filters. We used her synthetic images for testing of spatial filters . To generate speckle we have used the algorithm of Gent University, Belgium because it has been recognized by many researchers as the most real look speckle producing algorithm.
This algorithm is applied to synthetic image, photographic image, US and SAR image. These images are corrupted with uniformly distributed multiplicative noise having

different levels of standard deviation (σ) of the noise. With six different values of σ six synthetic images and six phtotgraphic images are produced, and from one value of σ one ultrasonic noisy image is produced. Similarly with four different values of σ four SAR noisy images are produced. σ values lie in the range [0.1 1], with σ=0.1 represents an almost noise-free image, σ=0.95 represents a very noise image.

4.4 Performance Evaluation of different Speckle Reducing Filters

In this work speckle reducing filters like Lee filter, Kuan filter, Frost filter, Perona Mallik [5] diffusion filter hereby referred as AD, SRAD [16] filter proposed by Y. Yu and S.T. Acton in which homogenous regions need not be selected by the user here by referred as SRAD1 and SRAD proposed by Y . Yu and S.T. Acton in which homogenous region selected by the user herby referred as SRAD2.

The performances of above mentioned filters are evaluated by applying these filters to noisy images produced by using the Aleksandra Pizurica [18] speckle simulation algorithm. The parameters of these filters are varied over a wide range and the optimal parameter combination is identified based on visual enhancement of the filtered images and also based upon the above mentioned statistical parameters, using these optimal parameters the filters are applied on an original US image and the performance of the filter is evaluated. Firstly resulting images with optimum values of the parameters are shown and corresponding statistical values are tabulated, followed with the discussion of pros and cons of each filter. Finally an algorithm for filter selection is developed in which the noisy image is filtered by all the 3 filters and the best of the 3 filtered images is given as output in terms of statistical parameters. This algorithm for filter selection is explained in section 4.5

4.4.1 Algorithm of SRAD1 [Yongjian Yu et.al.,]

Step 1- The image is read by using the command imread. This is an inbuilt command in MATLAB processing toolbox.

Syntax of image read function is I = imread(filename,fmt)

Definition: imread reads a grayscale or color image from the file specified by the string filename, the string fmt specifies the format of the file. I is a matrix each element of I is a pixel with the corresponding gray scale of the image.

Step 2 – Now the input image is converted in to double for the further operations like gradient.

Syntax of gradient function is $[F_x, F_y]$ = gradient(F)

Definition: The gradient of a function of two variables can be thought of as collection of vectors pointing in the direction of increasing values of gray levels. F_x corresponds to the differences in the column direction and F_y corresponds to the difference in the row direction. The spacing between the points is assumed to be one

Step 3 - Using the equation (23) the speckle scale function is determined

Step 4 – Substituting the result obtained in step 3 in the equation (15) instantaneous coefficient of variation is calculated q(x, y; t). From q(x, y; t) the presence and absence of edges are interpreted.

Step 5 - Using the equation (13) and (14) and with the help of q(x, y; t) obtained from step 4, two diffusion coefficients are obtained.

Step 6 - With the help PDE given by equation (12) and using the diffusion functions results obtained in step (4) the diffusion in the homogenous regions is enhanced and edges are preserved.

Step 7 - The performance of the filter is analyzed from the various statistical measures given by the equations (25), (26), (27), (28), and (29).

4.4.2 Algorithm of AD

Steps 1 & 2 are same as that of SRAD1,

Step 3- Edges are determined with the help of the gradient of the brightness function as given below.

$$E(x, y, t) = \nabla I(x, y, t)$$

Where, *E(x,y,t) = 0* in the interior of the region and *E(x,y,t) = ke(x,y,t)* at each point where *e* is a unit vector normal to the edge point and k is a local contrast(difference between the image intensities on the left and right) of the image.

Step 4- The conduction coefficient is chosen as the function of the edge estimate as given below

$$c(x, y, t) = g(\| \nabla I(x, y, t) \|)$$

Where, g(.) is a non negative monotonically decreasing function with g(0)=1. by this the diffusion process will take place mainly in the interior regions, and will not effect the region boundaries where magnitude of E is large.

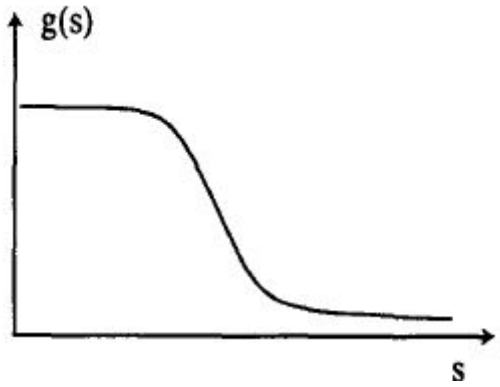

Fig 4.1 The quantitative shape of the nonlinearity g(.)

Step 5- Using the equation (12) and the above conduction coefficient the filter is developed.

Step 6- Input noisy image is filtered and the performance of the above filter is evaluated using the statistical parameters given by the equations (25), (26), (27), (28), and (29).

4.4.3 Algorithm of SRAD2 [17]

Step 1- An homogenous region is selected in the image using the function getrect

Syntax of getrect function is rect = getrect[]

This function returns an array of size 1*4 in the format as [x y width height] where (x, y) are the coordinates of minimum starting value of the rectangle selected by the user with the help of mouse. Width is the width of rectangle selected by the user same is the case with height.

Step 2- In this step firstly, the time and space coordinates are discretized so that the equation (12) can be solved numerically using an iterative Jacobi method. By taking Δt as small time step and h as small spatial step size in x and y directions equations become as follows:

$t = n\Delta t$, n=0,1,2,3……

$x = ih$, i= 0, 1, 2, …, M-1

$y = jh$, j=0, 1, 2,....., N-1

Where, $Mh \times Nh$ is the size of the input image

Assuming $I_{i,j}^{n} = I(ih, jh, n\Delta t)$, the derivative and Laplacian approximations are given as follows:

$$\nabla_R I_{i,j}^{n} = [\frac{I_{i+1,j}^{n} - I_{i,j}^{n}}{h}, \frac{I_{i,j+1}^{n} - I_{i,j}^{n}}{h}] \quad (31)$$

$$\nabla_L I_{i,j}^{n} = [\frac{I_{i,j}^{n} - I_{i-1,j}^{n}}{h} - \frac{I_{i,j}^{n} - I_{i,j-1}^{n}}{h}] \quad (32)$$

$$\nabla^2 I_{i,j}^{n} = \frac{I_{i+1,j}^{n} + I_{i-1,j}^{n} + I_{i,j+1}^{n} + I_{i,j-1}^{n} - 4I_{i,j}^{n}}{h^2} \quad (33)$$

Taking symmetry boundary conditions in to account

$$I_{-1,j}^{n} = I_{0,j}^{n},\ I_{M,j}^{n} = I_{M-1,j}^{n} \quad \text{for j=0, 1, 2, … ,N-1} \quad (34)$$

$$I_{i,-1}^{n} = I_{i,0}^{n},\ I_{i,N}^{n} = I_{i,N-1}^{n}, \quad \text{for i=0, 1, 2, … , M-1} \quad (35)$$

Step 3- The discretized diffusion coefficient c(q) is obtained with the help of the equations (13) and (14) as follows:

$$c_{i,j}^{n} = c[q(\frac{1}{I_{i,j}^{n}}\sqrt{|\nabla_R I_{i,j}^{n}|^2 + |\nabla_L I_{i,j}^{n}|^2}, \frac{1}{I_{i,j}^{n}}\nabla^2 I_{i,j}^{n})] \quad (36)$$

Step 4- In this step divergence $c(.)\nabla I$, which is required in equation (12) is calculated as follows

$$d_{i,j}^{n} = \frac{1}{h^2}[c_{i+1,j}^{n}(I_{i+1,j}^{n} - I_{i,j}^{n}) + c_{i,j}^{n}(I_{i-1,j}^{n} - I_{i,j}^{n}) + c_{i,j+1}^{n}(I_{i,j+1}^{n} - I_{i,j}^{n}) + c_{i,j}^{n}(I_{i,j-1}^{n} - I_{i,j}^{n})] \quad (37)$$

With symmetric boundary conditions

$$d_{-1}^{n} = d_{0,j}^{n},\ d_{M,j}^{n} = d_{M-1,j}^{n},\ \text{j=0, 1, 2, …., N-1} \quad (38)$$

$$d_{i,-1}^{n} = d_{i,0}^{n},\ d_{i,N}^{n} = d_{i,N-1}^{n},\ \text{i=0, 1, 2, ..., M-1} \quad (39)$$

Finally the numerical approximation to the differential equation with the help of approximating time derivative with forward difference, we have the equation as follows:

$$I_{i,j}^{n+1} = I_{i,j}^{n} + \frac{\Delta t}{4} d_{i,j}^{n} \quad (40)$$

The equation (40) is used finally for filtering the image, preserving homogenous region mean, reducing homogenous region variance, and preserving the edge positions.

Step 5- The performance of the above filter is evaluated using the statistical parameters given by the equations (25), (26), (27), (28), and (29).

4.4.4 Algorithm for Signal to Noise Ratio (SNR)

Step 1- standard deviation of the noise free image is calculated using the formula std2 and the value is squared in order to obtain the variance of noise free image.

Step 2- difference of the noise less image and noisy image is found using the function imsubtract

Syntax of imsubtract S = imsubtract(a,b)

This function imsubtract is an inbuilt command in MATLAB processing toolbox. It perform the subtraction image a from image b pixel wise and stored the difference matrix in S.

Step3- Standard deviation of S is caluculated and the value is squared.

Step4- Ratio of the value obtained in step 1 to the value obtained in step 3 is calculated.

Step5- log to base 10 is calculated for the value obtained in step 4 this gives SNR in decibels.

4.4.5 Algorithm for Correlation of Coefficient (Coc)

Step1- Mean of the noiseless image and noisy image are calculated.

Step2- Mean of the noiseless image is subtracted from each of the pixel in the noiseless image resulting in a matrix.

Step3- Similarly the mean of noisy image is subtracted from each of the pixels in the noise image resulting in a matrix.

Step 4- Values obtained in step 2 and step 3 are multiplied.

Step 5- Sum of all the elements in the matrix obtained in step 4 is calculated.

Step 6- Square of all the elements of the matrix obtained in step 2 is calculated and sum of this squared matrix is determined.

Step 7- Similarly square of all the elements of the matrix obtained in step 3 is calculated and sum of the elements of this squared matrix is also determined.

Step 8- Values obtained in step 6 and step 7 are multiplied and its square root is taken.

Step 9- Ratio of the value obtained in step 5 to the value obtained in step 8 is calculated.

4.4.6 Algorithm for Mean Structural Similarity Index Measure (MSSIM)

Step 1- Gaussian filter kernel is created by giving suitable parameters.

Step 2- Noise less image and noisy image both are converted in to double.

Step 3- Noisy image is filtered using the Gaussian kernel developed in step 1.

Steps 4- Also noiseless image is filtered using the Gaussian kernel developed in step1.

Step 5- Square the pixels of the matrix obtained in step 3.

Step 6- Square the pixels of the matrix obtained in step 4.

Step 7-Corresponding elements of the matrix obtained in step 5 and step 6 are multiplied.

Step 8- square of the pixels of the noiseless image is found, this is filtered with the Gaussian kernel.

Step 9- Similarly, square of the pixels of the noisy image is calculated and resultant is filtered by using the Gaussian kernel.

Step 10- corresponding elements of noiseless image and noisy image are multiplied and this is also filtered using Gaussian kernel.

Step 11- Matrix obtained in step 7 is multiplied by 2 and a constant c1 is added to it.

Step 12- Matrix obtained in step 10 is multiplied by 2 and a constant c2 is added to it.

Step 13- Matrix obtained in step 5 and step 6 are added and to the resultant matrix a constant c1 is added.

Step 14- Matrix obtained in step 8 and step 9 are added and to the resultant matrix a constant c2 is added

Step 16- Resultant of Steps 11 and 12 are multiplied in the array fashion means corresponding elements are multiplied

Step 17- Resultant of Steps 13 and 14 are multiplied in the array fashion means corresponding elements are multiplied

Step 18- Results obtained in step 16 is divided by the results obtained in step 17 giving rise to a matrix

Step 19- Mean of the matrix obtained in step18 gives the value of MSSIM.

4.4.7 Algorithm for Peak Signal to Noise Ratio (PSNR)

Step 1- Difference of noisy image and noiseless image is calculated using imsubract command.

Step 2- Size of the matrix obtain in step 1 is calculated.

Step 3- Each of the pixels in the matrix obtained in step is squared.

Step 4- Sum of all the pixels in the matrix obtained in step 3 is calculated.

Step 5- (MSE) is obtained by taking the ratio of value obtained in step 4 to the value obtained in the step 2

Step 6- (RMSE) is calculated by taking square root to the value obtained in step 5.

Step7- Dividing 255 with RMSE, taking 1og base 10 and multiplying with 20 gives the value of PSNR.

4.5 Algorithm for filter selection

Step 1- Noiseless and noisy images are given as input.

Step 2- Noisy image is filtered by all the six filters Lee, Kuan, Frost, SRAD1, AD and SRAD2.

Step 3- The statistical parameters are calculated for the filtered image obtained from Lee filter with respect to the noiseless image.

Step 4- Same action as that of Step 3 is performed on all the filtered images obtained. Finally we get six sets of statistical parameters each set corresponding to 1 filter.

Step 5- Giving some weightage to each of the parameter one result is calculated for each of the filtered output for eg., on the scale of 10 SNR is multiplied by 10, Coc is multiplied by 3 and MSSIM is multiplied by 2 and the result is divided by 10. this action results in six outputs, one output corresponding to each filter.

Step 6- Comparision is made among the six results and the best among the six results is obtained.

Step 7- The filtering technique used, filtered image and statistical parameters corresponding to this best result obtained in step 6 are given as the out put.

Chapter 5

Results & Discussions

5.1 Synthetic Image

Below are the results given for the synthetic image s7 is the noisy synthetic image with standard deviation of the noise as 0.7. Similar is the case with s75, s8, s85, s9, s95. Given below are the synthetic noisy images and noise free image.

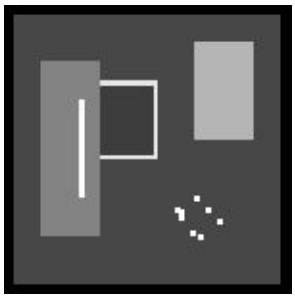

Fig 5.1(a)

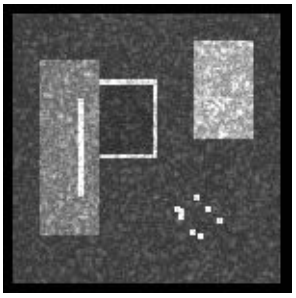

Fig 5.1(b)

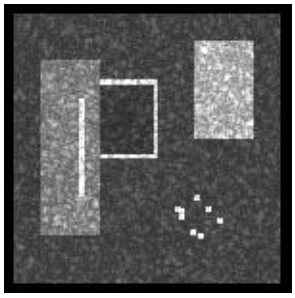

Fig 5.1(c)

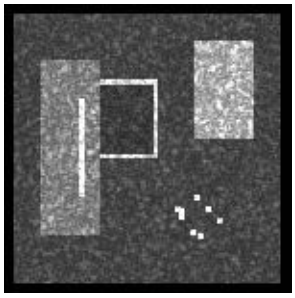

Fig 5.1(d)

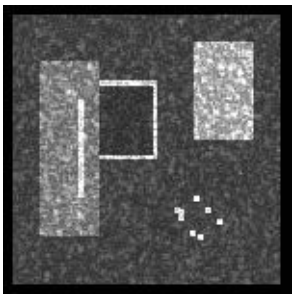

Fig 5.1(e)

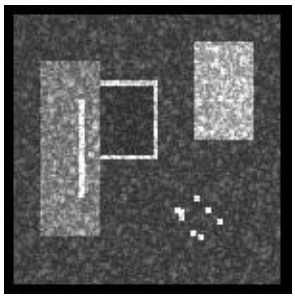

Fig 5.1(f)

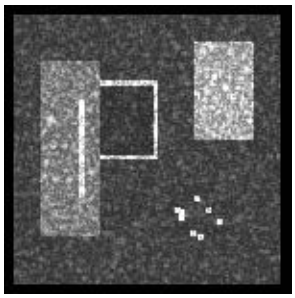

Fig 5.1(g)

Fig 5.1 Noise free image and noisy image with different levels of standard deviations of noise (a) noise free image (b) image with standard deviation of the noise as 0.7 (c) image with standard deviation of the noise as 0.75 (d) image with standard deviation of the noise as 0.8 (e) image with standard deviation of the noise as 0.85 (f) image with standard deviation of the noise as 0. 9 (g) image with standard deviation of the noise as 0.95.

5.1.1 Filtering Results of Lee, Kuan and Frost Filters on Synthetic Image

Table 5.1 Statistical Results of the images before filtering

Unfiltered Images					
image	SNR	Coc	MSSIM	RMSE	PSNR
s7	32.6284	0.9149	0.4571	6.9697	31.2665
s75	31.0854	0.9004	0.4408	7.2697	30.9005
s8	30.1644	0.8883	0.4286	7.4755	30.658
s85	28.6612	0.8794	0.4149	7.8801	30.2877
s9	27.8237	0.8712	0.4065	7.8887	30.1907
s95	27.1069	0.8629	0.3971	7.9804	30.0903

Table 5.2 Statistical Results of the images filtered by Lee filter

Lee Filter Results					
image	SNR	Coc	MSSIM	RMSE	PSNR
s7	28.3112	0.9376	0.5732	5.5932	33.1775
s75	27.5298	0.9308	0.5531	5.7666	32.9124
s8	27.0905	0.9257	0.5357	5.924	32.637
s85	27.3499	0.923	0.5201	6.2297	32.2414
s9	27.0099	0.9193	0.5139	6.2105	32.2682
s95	25.6733	0.917	0.9443	6.2971	32.148

Table 5.3 Statistical Results of the images filtered by Kuan filter

Kuan Filter Results					
image	SNR	Coc	MSSIM	RMSE	PSNR
s7	28.3112	0.9376	0.5732	5.5932	33.1775
s75	27.5298	0.9308	0.5531	5.7666	32.9124
s8	27.0905	0.9257	0.5357	5.9524	32.637
s85	27.3499	0.923	0.5201	6.2297	32.2414
s9	27.0099	0.9193	0.5139	6.2105	32.2682
s95	25.6733	0.917	0.4993	6.2971	32.148

Table 5.4 Statistical Results of the images filtered by Frost filter

Frost Filter Results					
image	SNR	Coc	MSSIM	RMSE	PSNR
s7	30.7965	0.9393	0.5601	5.7181	32.9858
s75	29.9803	0.9322	0.5404	5.9005	32.7131
s8	29.8816	0.926	0.5241	6.0826	32.449
s85	29.2594	0.9207	0.5078	6.3713	32.0462
s9	28.7994	0.917	0.5	6.4061	31.999
s95	28.5241	0.9146	0.4875	6.5034	31.868

These results show that Lee, Kuan and Frost increase the value of the parameters Coc, MSSIM, PSNR but there is not improvement in SNR. These results show us that after

filtering the similarity of the filtered image with the noiseless image is improved however, the signal strength decreased due to the smoothening applied to the image causing blurring effect.

5.1.2 Filtering Results of SRAD1 for Synthetic Image

T is the number of iterations.

Table 5.5 Statistical Results of the image s7 filtered by SRAD1 for different iterations

image	T	SNR	Coc	MSSIM	RMSE	PSNR
s7	1	30.3445	0.9411	0.4975	6.2884	32.16
s7	2	30.0937	0.9595	0.5477	4.6496	33.018
s7	3	33.7052	0.9665	0.6066	5.2186	33.7797
s7	5	34.712	0.9598	0.7205	5.6969	34.7824
s7	10	23.1239	0.9546	0.7929	4.1633	35.742
s7	12	20.648	0.9346	0.564	4.8474	34.4206
s7	15	17.4692	0.8932	0.3651	5.5823	33.1945

Graphical representation of the result obtained by applying SRAD1 on s7 is as follows

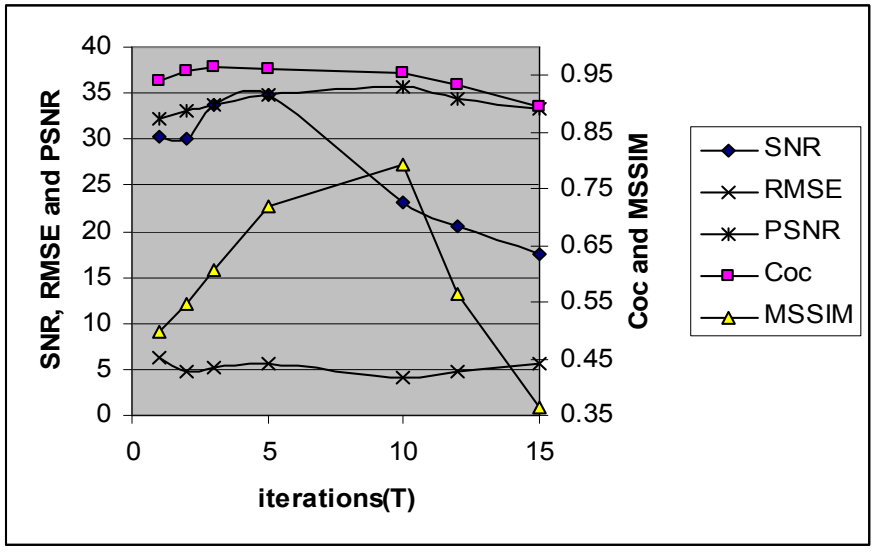

Graph 5.1 Representation of the result obtained by applying SRAD1 on s7

Table 5.6 Statistical Results of the image s75 filtered by SRAD1 for different iterations

image	T	SNR	Coc	MSSIM	RMSE	PSNR
s75	1	29.5667	0.9255	0.4787	6.5854	31.7592
s75	2	29.7666	0.9604	0.5259	4.7894	32.6415
s75	3	32.8222	0.9587	0.5825	5.4437	33.4129
s75	5	33.474	0.9465	0.7008	5.9493	34.5252
s75	10	22.744	0.95	0.7666	4.3514	35.3582
s75	12	19.9263	0.9263	0.5434	5.0126	34.1296
s75	15	17.9812	0.8891	0.3565	5.721	32.9814

Graphical representation of the result obtained by applying SRAD1 on s75 is as follows

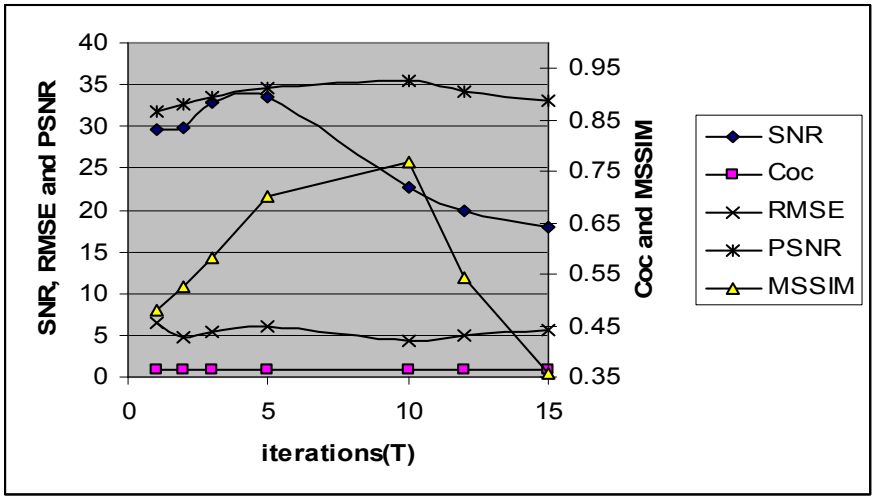

Graph 5.2 Representation of the result obtained by applying SRAD1 on s75

Table 5.7 Statistical Results of the image s8 filtered by SRAD1 for different iterations

image	T	SNR	Coc	MSSIM	RMSE	PSNR
s8	1	29.4321	0.9159	0.4651	6.8351	31.4359
s8	2	29.9691	0.9551	0.5112	4.8665	32.3157
s8	3	32.67	0.9526	0.5676	5.6195	33.1369
s8	5	33.0187	0.939	0.6903	6.1767	34.3865
s8	10	22.9314	0.9476	0.7672	4.4362	35.1906
s8	12	20.353	0.9253	0.5461	5.0975	33.9837
s8	15	17.8914	0.8868	0.3731	5.7809	32.8909

Graphical representation of the result obtained by applying SRAD1 on s8 is as follows

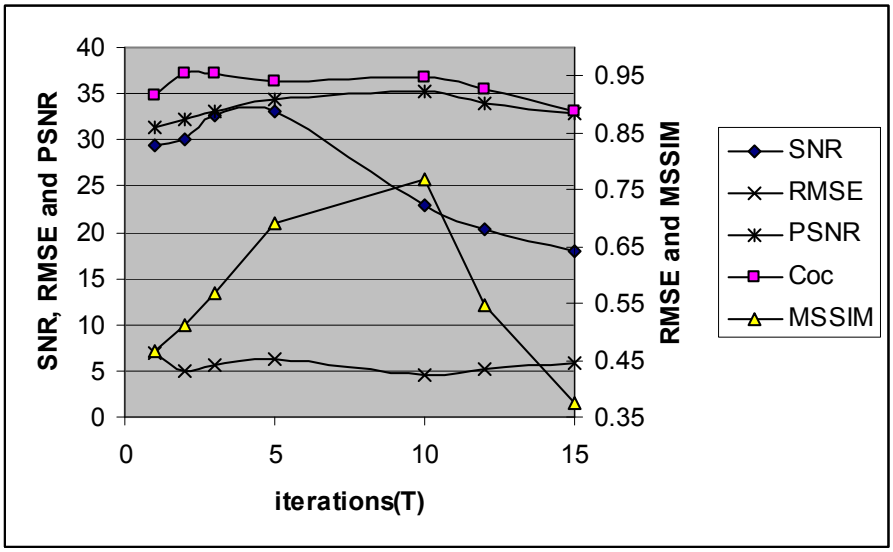

Graph 5.3 Representation of the result obtained by applying SRAD1 on s8

Table 5.8 Statistical Results of the image s85 filtered by SRAD1 for different iterations

image	T	SNR	Coc	MSSIM	RMSE	PSNR
s85	1	28.5689	0.9046	0.4494	7.189	30.9974
s85	2	29.1856	0.952	0.4921	5.0065	31.8542
s85	3	31.4867	0.9447	0.5444	5.9104	32.6984
s85	5	31.5915	0.9284	0.662	6.5137	34.14
s85	10	22.4396	0.9475	0.7513	4.327	35.4071
s85	12	19.8388	0.9195	0.5097	5.0869	34.0018
s85	15	17.3046	0.8821	0.3556	5.7673	32.9113

Graphical representation of the result obtained by applying SRAD1 on s85 is as follows

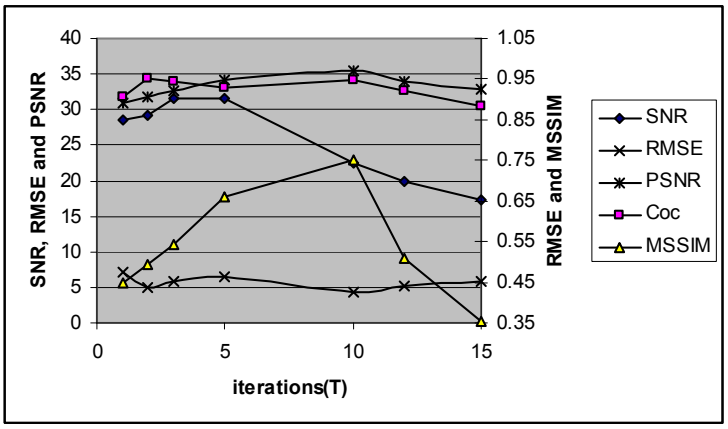

Graph 5.4 Representation of the result obtained by applying SRAD1 on s85

Table 5.9 Statistical Results of the image s9 filtered by SRAD1 for different iterations

image	T	SNR	Coc	MSSIM	RMSE	PSNR
s9	1	28.2332	0.8963	0.4397	7.2926	30.8732
s9	2	28.8322	0.923	0.4813	5.0461	31.735
s9	3	31.0171	0.9438	0.5331	5.9604	32.6253
s9	5	30.9871	0.9541	0.6537	6.6038	34.0717
s9	10	22.4876	0.95	0.7496	4.4961	35.0741
s9	12	19.93	0.9247	0.503	5.1455	33.9023
s9	15	17.6181	0.888	0.3586	5.8121	32.8441

Graphical representation of the result obtained by applying SRAD1 on s9 is as follows

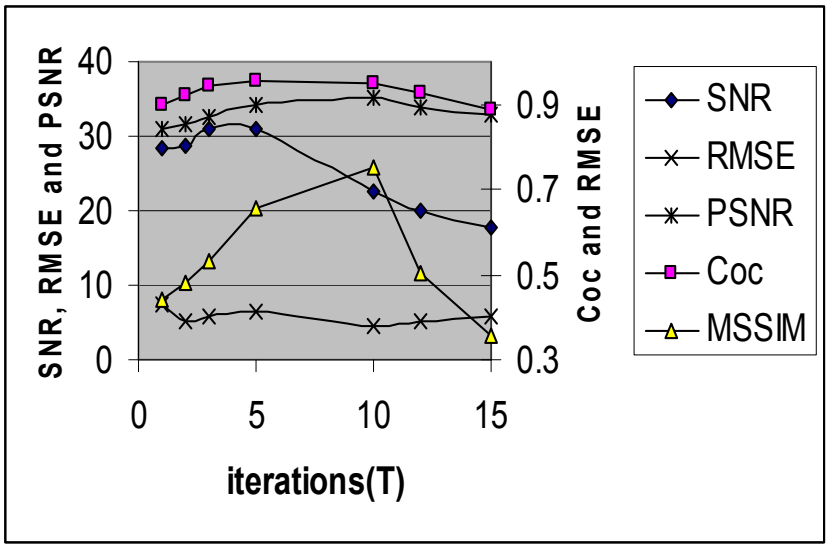

Graph 5.5 Representation of the result obtained by applying SRAD1 on s9

Table 5.10 Statistical Results of the image s95 filtered by SRAD1 for different iterations

image	T	SNR	Coc	MSSIM	RMSE	PSNR
s95	1	27.8992	0.8879	0.4289	7.3966	30.7502
s95	2	28.4636	0.9133	0.4688	5.1262	31.5965
s95	3	30.3635	0.934	0.519	6.0523	32.4923
s95	5	30.2298	0.95	0.6407	6.7099	33.935
s95	10	21.7852	0.9466	0.7255	4.5925	34.8998
s95	12	18.9554	0.9158	0.4689	5.3459	33.5704
s95	15	16.5586	0.8763	0.3354	5.9562	32.6314

Graphical representation of the result obtained by applying SRAD1 on s95 is as follows

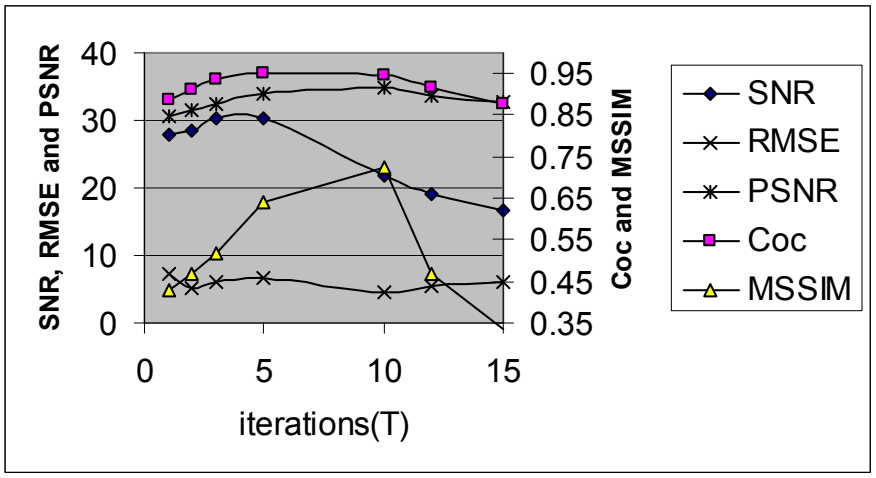

Graph 5.6 Representation of the result obtained by applying SRAD1 on s95

Imaging result of SRAD1 on s7 for T=3 is as follows

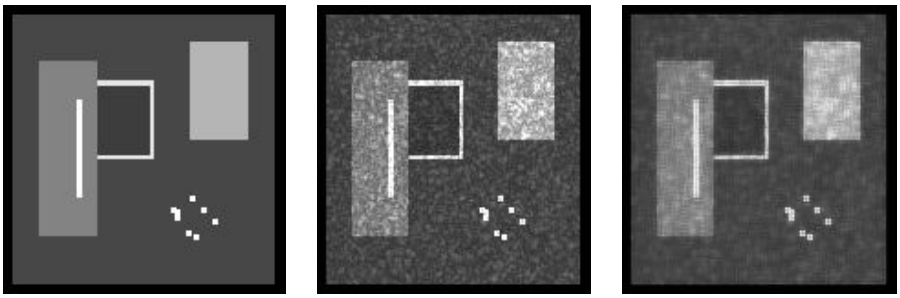

Fig 5.2(a) **Fig 5.2(b)** **Fig 5.2(c)**

Fig 5.2 Filtering Results of synthetic image obtained from SRAD1 with T=3 (a) Original Image (b) Unfiltered Image (c) Filtered Image

Imaging result of SRAD1 on s7 for T=5 is as follows

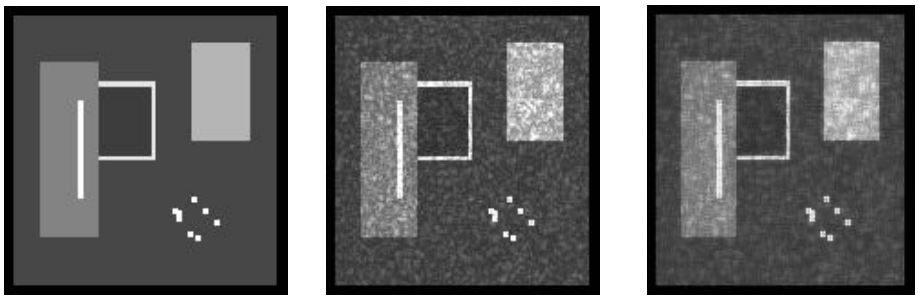

Fig 5.3(a) **Fig 5.3(b)** **Fig 5.3(c)**

Fig 5.3 Filtering Results of synthetic image obtained from SRAD1 with T=5 (a) Original Image (b) Unfiltered Image (c) Filtered Image

Imaging result of SRAD1 on s7 for T=10 is as follows

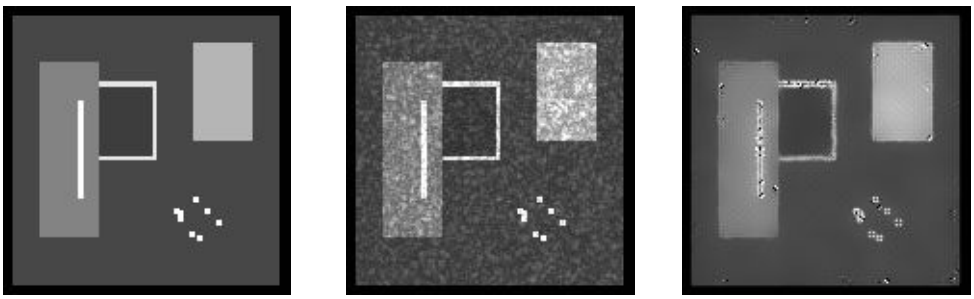

Fig 5.4(a) **Fig 5.4(b)** **Fig 5.4(c)**

Fig 5.4 Filtering Results of synthetic image obtained form SRAD1 with T=10 (a) Original Image (b) Unfiltered Image (c) Filtered Image

Imaging result of SRAD1 on s7 for T=15 is as follows

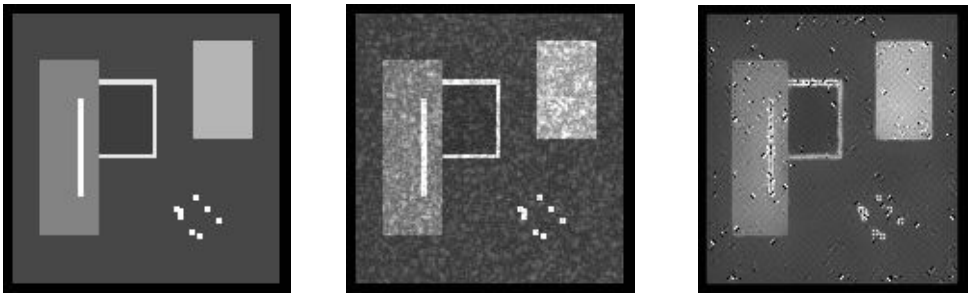

Fig 5.5(a) **Fig 5.5(a)** **Fig 5.5(a)**

Fig 5.5 Filtering Results of synthetic image obtained form SRAD1 with T=15 (a) Original Image (b) Unfiltered Image (c) Filtered Image

The above tables, graphs and images show that the filter results are good for $5 < T < 10$

5.1.3 Filtering Results of AD for Synthetic Image

5.1.3.1 Results of AD for different iterations

Table 5.11 Statistical Results of the image s7 filtered by AD for different iterations

image	noi	delta	kappa	option	snr	Coc	mmssi	RMSE	PSNR
s7	2	(1/7)	30	1	39.1371	0.9848	0.6388	4.895	34.3357
s7	4	(1/7)	30	1	42.9548	0.9974	0.7471	4.1328	35.8059
s7	5	(1/7)	30	1	44.359	0.9988	0.7808	3.8846	36.344
s7	10	(1/7)	30	1	48.2892	0.999	0.8712	3.2405	37.9185
s7	15	(1/7)	30	1	48.7508	0.9973	0.9061	3.0396	38.4745
s7	20	(1/7)	30	1	47.7953	0.9945	0.9208	3.0132	38.5502
s7	50	(1/7)	30	1	41.9568	0.975	0.9167	3.5337	37.1661

Graphical representation of the result obtained by applying AD on s7 is as follows

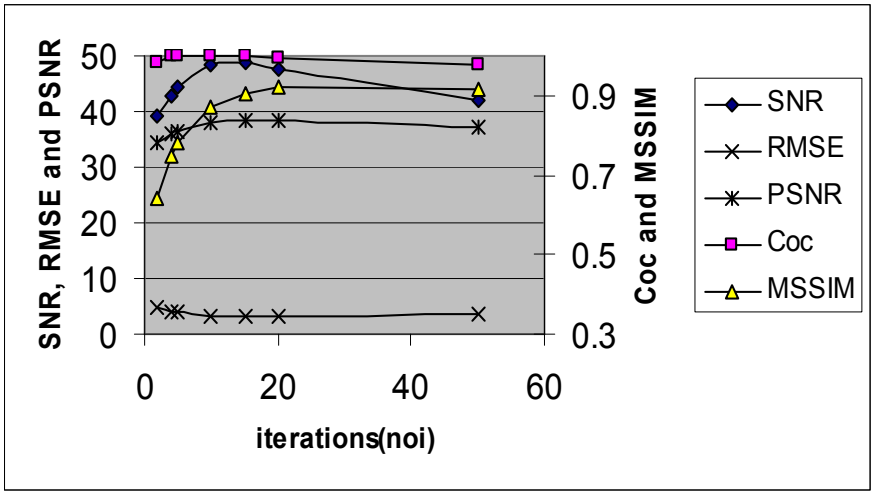

Graph 5.7 Representation of the result obtained by applying AD on s7

Table 5.12 Statistical Results of the image s75 filtered by AD for different iterations

image	noi	delta	kappa	option	snr	Coc	mmssi	RMSE	PSNR
s75	2	(1/7)	30	1	36.6856	0.9733	0.6073	5.2323	33.757
s75	4	(1/7)	30	1	40.0957	0.9925	0.7166	4.5142	0.0392
s75	5	(1/7)	30	1	41.3699	0.9957	0.77536	4.2662	35.53
s75	10	(1/7)	30	1	45.098	0.9991	0.8554	3.5538	37.1169
s75	15	(1/7)	30	1	46.3128	0.9983	0.8981	3.2763	37.8233
s75	20	(1/7)	30	1	46.338	0.996	0.9166	3.1822	38.0763
s75	50	(1/7)	30	1	42.0535	0.9749	0.9196	3.2123	37.9526

Graphical representation of the result obtained by applying AD on s75 is as follows

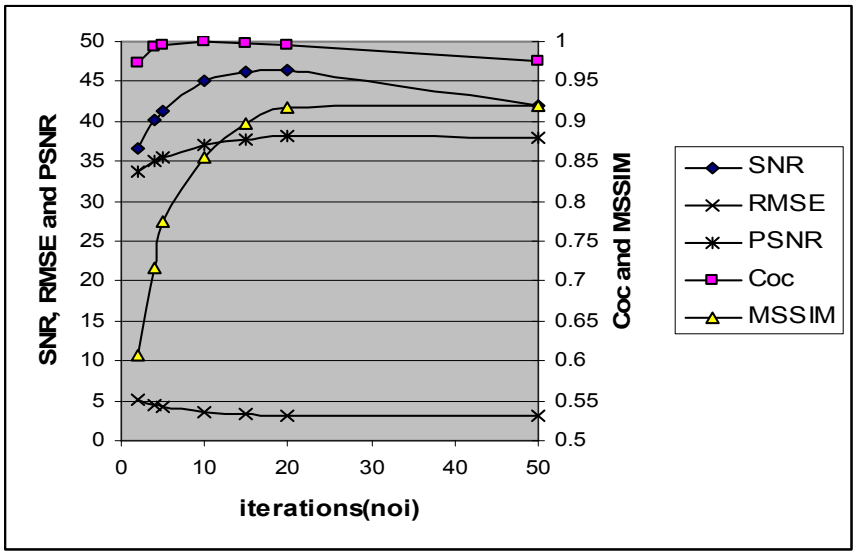

Graph 5.8 Representation of the result obtained by applying AD on s75

Table 5.13 Statistical Results of the image s8 filtered by AD for different iterations

image	noi	delta	kappa	option	snr	Coc	mmssi	RMSE	PSNR
s8	2	(1/7)	30	1	35.4975	0.9661	0.5821	5.466	33.3774
s8	4	(1/7)	30	1	38.7472	0.9902	0.6966	4.7213	34.6495
s8	5	(1/7)	30	1	39.9305	0.9942	0.735	4.4943	35.0776
s8	10	(1/7)	30	1	43.7	0.9976	0.8392	3.8111	36.5097
s8	15	(1/7)	30	1	45.7695	0.9959	0.883	3.4085	37.4794
s8	20	(1/7)	30	1	46.3976	0.9931	0.9052	3.2103	38
s8	50	(1/7)	30	1	42.6919	0.9699	0.9178	3.498	37.2545

Graphical representation of the result obtained by applying AD on s8 is as follows

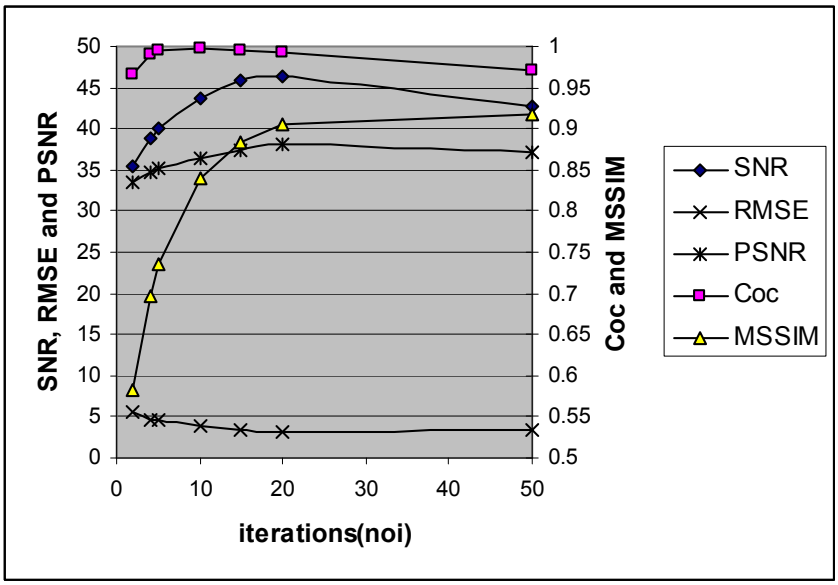

Graph 5.9 Representation of the result obtained by applying AD on s8

Table 5.14 Statistical Results of the image s85 filtered by AD for different iterations

image	noi	delta	kappa	option	snr	Coc	mmssi	RMSE	PSNR
s85	2	(1/7)	30	1	33.2984	0.9582	0.5566	5.88	32.7433
s85	4	(1/7)	30	1	35.9767	0.9874	0.665	5.1921	33.824
s85	5	(1/7)	30	1	37.018	0.9926	0.7022	4.9574	34.2257
s85	10	(1/7)	30	1	40.6037	0.9983	0.8097	4.2143	35.6364
s85	15	(1/7)	30	1	42.3554	0.9965	0.8571	3.7784	36.5846
s85	20	(1/7)	30	1	43.1513	0.9939	0.8847	3.514	37.2147
s85	50	(1/7)	30	1	41.0597	0.9716	0.9096	3.6228	36.95

Graphical representation of the result obtained by applying AD on s85 is as follows

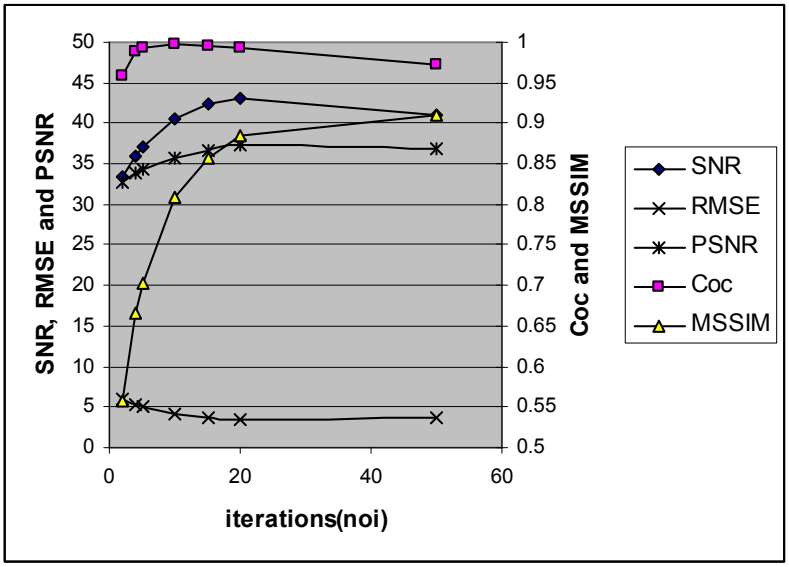

Graph 5.10 Representation of the result obtained by applying AD on s85

Table 5.15 Statistical Results of the image s9 filtered by AD for different iterations

image	noi	delta	kappa	option	snr	Coc	mmssi	RMSE	PSNR
s9	2	(1/7)	30	1	32.2747	0.9487	0.5385	5.9467	32.6453
s9	4	(1/7)	30	1	34.9878	0.9848	0.6536	5.1454	33.9024
s9	5	(1/7)	30	1	36.1033	0.9917	0.6934	4.8582	34.4014
s9	10	(1/7)	30	1	39.908	0.9987	0.8066	4.0342	36.0156
s9	15	(1/7)	30	1	41.843	0.9974	0.8603	3.662	36.8564
s9	20	(1/7)	30	1	42.3366	0.9937	0.8896	3.5257	37.186
s9	50	(1/7)	30	1	39.5393	0.9695	0.9019	3.9004	36.3087

Graphical representation of the result obtained by applying AD on s9 is as follows

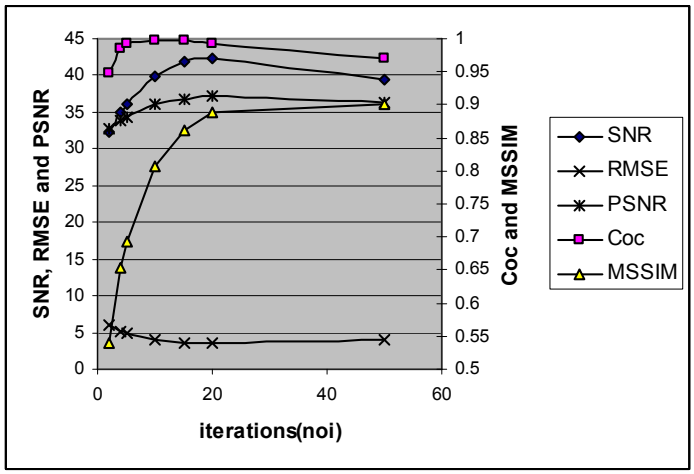

Graph 5.11 Representation of the result obtained by applying AD on s9

Table 5.16 Statistical Results of the image s95 filtered by AD for different iterations

image	noi	delta	kappa	option	snr	Coc	mmssi	RMSE	PSNR
s95	2	(1/7)	30	1	31.3404	0.9406	0.5191	6.066	32.4728
s95	4	(1/7)	30	1	33.9552	0.9784	0.6348	5.25	33.7276
s95	5	(1/7)	30	1	35.0091	0.9871	0.6772	4.9914	34.1664
s95	10	(1/7)	30	1	38.4459	0.9967	0.7989	4.2052	35.6551
s95	15	(1/7)	30	1	40.1392	0.9956	0.8542	3.7998	36.5356
s95	20	(1/7)	30	1	40.7291	0.9918	0.884	3.5898	37.0295
s95	50	(1/7)	30	1	38.7323	0.9678	0.8979	3.9168	36.2723

Graphical representation of the result obtained by applying AD on s95 is as follows

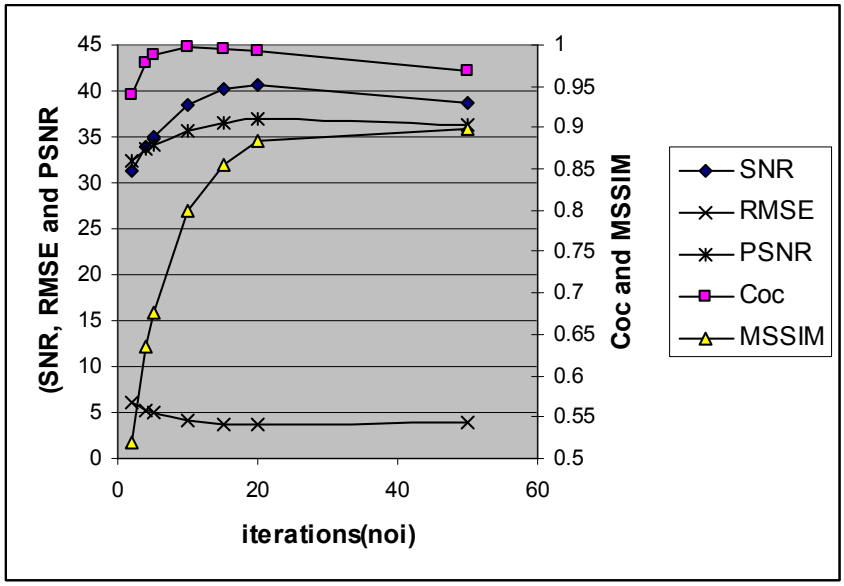

Graph 5.12 Representation of the result obtained by applying AD on s95

The above tables, graphs and images show that the filter results are good for noi = 15, when other parameters like kappa, delta and option are kept as constant.

Table 5.17 Statistical Results of the image s7 filtered by AD for different iterations and option = 2

image	noi	delta	kappa	option	snr	Coc	mmssi	RMSE	PSNR
s7	2	(1/7)	30	2	39.8586	0.9869	0.6507	4.8826	34.3577
s7	4	(1/7)	30	2	41.1489	0.9954	0.7485	4.5061	35.0548
s7	5	(1/7)	30	2	40.709	0.9953	0.7747	4.5134	35.0407
s7	10	(1/7)	30	2	35.8801	0.9853	0.8125	5.01	34.1341
s7	15	(1/7)	30	2	31.6575	0.9705	0.7918	5.5568	33.2343
s7	20	(1/7)	30	2	28.5224	0.9556	0.7589	6.003	32.5634
s7	50	(1/7)	30	2	17.3137	0.8616	0.5615	7.4965	30.6337

Table 5.18 Statistical Results of the image s75 filtered by AD for different iterations and option = 2

image	noi	delta	kappa	option	snr	Coc	mmssi	RMSE	PSNR
s75	2	(1/7)	30	2	37.7021	0.978	0.6224	5.1931	33.8222
s75	4	(1/7)	30	2	39.3078	0.9928	0.7244	4.7291	34.6352
s75	5	(1/7)	30	2	39.0866	0.9941	0.7543	4.6792	34.7274
s75	10	(1/7)	30	2	35.1458	0.985	0.8055	5.0242	34.1094
s75	15	(1/7)	30	2	31.165	0.9705	0.7904	5.5547	33.2376
s75	20	(1/7)	30	2	28.0598	0.9553	0.9667	5.9819	32.5941
s75	50	(1/7)	30	2	17.1163	0.8612	0.5629	7.4943	30.6361

Table 5.19 Statistical Results of the image s8 filtered by AD for different iterations and option = 2

image	noi	delta	kappa	option	snr	Coc	mmssi	RMSE	PSNR
s8	2	(1/7)	30	2	36.7157	0.9717	0.6006	5.3703	33.5309
s8	4	(1/7)	30	2	38.7705	0.9884	0.7071	4.8532	34.4102
s8	5	(1/7)	30	2	38.8385	0.9898	0.7397	4.7846	34.5339
s8	10	(1/7)	30	2	35.6991	0.9798	0.7998	5.104	33.9725
s8	15	(1/7)	30	2	31.7508	0.9639	0.7878	5.6168	33.141
s8	20	(1/7)	30	2	28.5861	0.9483	0.7588	6.0447	32.5034
s8	50	(1/7)	30	2	17.2665	0.8561	0.5626	7.5639	30.5559

Table 5.20 Statistical Results of the image s85 filtered by AD for different iterations and option = 2

image	noi	delta	kappa	option	snr	Coc	mmssi	RMSE	PSNR
s85	2	(1/7)	30	2	34.786	0.9659	0.5761	5.7846	32.8853
s85	4	(1/7)	30	2	36.9915	0.9882	0.6781	5.2056	33.8014
s85	5	(1/7)	30	2	37.231	0.9908	0.7105	5.0635	34.0418
s85	10	(1/7)	30	2	34.6714	0.9821	0.779	5.1323	33.9245
s85	15	(1/7)	30	2	30.9651	0.9651	0.7749	5.5811	33.1964
s85	20	(1/7)	30	2	27.8852	0.9498	0.7484	6.0028	32.5637
s85	50	(1/7)	30	2	17.0679	0.8541	0.5561	7.5185	30.6082

Table 5.21 Statistical Results of the image s9 filtered by AD for different iterations and option = 2

image	noi	delta	kappa	option	snr	Coc	mmssi	RMSE	PSNR
s9	2	(1/7)	30	2	33.9343	0.9583	0.5627	5.8058	32.8535
s9	4	(1/7)	30	2	36.4302	0.9846	0.6718	5.144	33.9047
s9	5	(1/7)	30	2	36.7294	0.9875	0.7062	5.0099	34.1342

s9	10	(1/7)	30	2	34.2354	0.9795	0.778	5.189	33.8292
s9	15	(1/7)	30	2	30.5717	0.9643	0.775	5.6542	33.0834
s9	20	(1/7)	30	2	27.5064	0.9479	0.7485	6.057	32.4857
s9	50	(1/7)	30	2	16.7551	0.8554	0.5561	7.532	30.5925

Table 5.22 Statistical Results of the image s95 filtered by AD for different iterations and option = 2

image	noi	delta	kappa	option	snr	Coc	mmssi	RMSE	PSNR
s95	2	(1/7)	30	2	33.0737	0.9513	0.5458	5.9116	32.6967
s95	4	(1/7)	30	2	35.4587	0.9818	0.6578	5.2223	33.7736
s95	5	(1/7)	30	2	35.7473	0.9859	0.6942	5.0818	34.0105
s95	10	(1/7)	30	2	33.2684	0.9787	0.7722	5.1868	33.8328
s95	15	(1/7)	30	2	29.6961	0.9633	0.7712	5.6303	33.1202
s95	20	(1/7)	30	2	26.7042	0.9471	0.7464	6.0437	32.5048
s95	50	(1/7)	30	2	16.7229	0.8591	0.562	7.5128	30.6148

From the above experiments conducted on 6 synthetic images with different standard deviation of the noise we can infer that the best result are given when **noi=15** with **option as 1** and noi=5 to 10 for option 2. However the option 1 is giving better results than option2 at their respective optimized parameters. Hence from now on wards parameters noi and option are fixed as 15 and 1 respectively and proceed to the next set of experiments.

5.1.3.2 Results of AD for different values of kappa

Table 5.23 Statistical Results of the image s7 filtered by AD for different values of kappa

image	noi	delta	kappa	option	SNR	Coc	MSSIM	RMSE	PSNR
s7	15	(1/7)	5	1	33.9664	0.9279	0.486	6.3202	32.1162
s7	15	(1/7)	10	1	37.3605	0.9793	0.7095	4.6505	34.7808
s7	15	(1/7)	12	1	39.0526	0.9926	0.7924	4.3441	35.3728
s7	15	(1/7)	13	1	39.9595	0.9955	0.8142	4.1568	35.7557
s7	15	(1/7)	26	1	49.8893	0.9995	0.9045	2.882	38.9369
s7	15	(1/7)	27	1	50.0872	0.9993	0.9064	2.8966	38.893
s7	15	(1/7)	28	1	49.9223	0.9989	0.9074	2.9366	38.7739

Table 5.24 Statistical Results of the image s75 filtered by AD for different values of kappa

image	noi	delta	kappa	option	SNR	Coc	MSSIM	RMSE	PSNR
s75	15	(1/7)	5	1	32.1807	0.9108	0.4625	6.7412	31.556
s75	15	(1/7)	10	1	35.0811	0.958	0.6446	4.9706	34.2026
s75	15	(1/7)	12	1	36.2417	0.9787	0.7335	4.643	34.7949
s75	15	(1/7)	13	1	36.9243	0.9861	0.7663	4.525	35.0185
s75	15	(1/7)	26	1	46.1562	0.9996	0.8914	3.2592	37.8686
s75	15	(1/7)	27	1	46.4714	0.9995	0.8948	3.2273	37.954
s75	15	(1/7)	28	1	46.5891	0.9993	0.8968	3.228	37.9521

Table 5.25 Statistical Results of the image s8 filtered by AD for different values of kappa

image	noi	delta	kappa	option	SNR	Coc	MSSIM	RMSE	PSNR
s8	15	(1/7)	5	1	31.0839	0.8982	0.4455	7.0659	31.1474
s8	15	(1/7)	10	1	33.9539	0.9457	0.5963	5.2405	33.7434
s8	15	(1/7)	12	1	35.0264	0.9704	0.6939	4.8475	34.4204
s8	15	(1/7)	13	1	35.6472	0.9816	0.732	4.714	34.663
s8	15	(1/7)	26	1	44.3634	0.9987	0.9915	3.6041	36.9949
s8	15	(1/7)	27	1	44.8921	0.9984	0.8768	3.5432	37.1428
s8	15	(1/7)	28	1	45.3052	0.9978	0.8799	3.485	37.2868

Table 5.26 Statistical Results of the image s85 filtered by AD for different values of kappa

image	noi	delta	kappa	option	SNR	Coc	MSSIM	RMSE	PSNR
s85	15	(1/7)	5	1	29.4162	0.8876	0.4288	7.5273	30.598
s85	15	(1/7)	10	1	31.9651	0.9357	0.5541	5.7186	32.985
s85	15	(1/7)	12	1	32.8028	0.9633	0.6453	5.3194	33.6136
s85	15	(1/7)	13	1	33.2305	0.9735	0.6851	5.1944	33.82
s85	15	(1/7)	26	1	40.9363	0.999	0.846	4.0503	35.981
s85	15	(1/7)	27	1	41.3902	0.9988	0.8497	3.9797	36.1338
s85	15	(1/7)	28	1	41.7816	0.9981	0.8523	3.8955	36.3195

Table 5.27 Statistical Results of the image s9 filtered by AD for different values of kappa

image	noi	delta	kappa	option	SNR	Coc	MSSIM	RMSE	PSNR
s9	15	(1/7)	5	1	28.436	0.8792	0.4172	7.6975	30.4038
s9	15	(1/7)	10	1	30.9151	0.9224	0.5187	5.8622	32.7696
s9	15	(1/7)	12	1	31.7319	0.9487	0.6042	5.3912	33.4971
s9	15	(1/7)	13	1	32.1558	0.9617	0.6459	5.257	33.7161

s9	15	(1/7)	26	1	40.116	0.9999	0.8461	3.7785	36.5844
s9	15	(1/7)	27	1	40.6794	0.9998	0.8504	3.7255	36.7072
s9	15	(1/7)	28	1	41.1735	0.9991	0.8539	3.6846	36.803

Table 5.28 Statistical Results of the image s95 filtered by AD for different values of kappa

image	noi	delta	kappa	option	SNR	Coc	MSSIM	RMSE	PSNR
s95	15	(1/7)	5	1	27.6432	0.8697	0.4059	7.8272	30.2586
s95	15	(1/7)	10	1	29.942	0.9069	0.488	6.0618	32.4788
s95	15	(1/7)	12	1	30.7135	0.9334	0.5584	5.4985	33.3259
s95	15	(1/7)	13	1	31.1285	0.949	0.5984	5.3287	33.5984
s95	15	(1/7)	26	1	38.6168	0.9981	0.8375	3.9606	36.1756
s95	15	(1/7)	27	1	39.1366	0.9978	0.843	3.9061	36.296
s95	15	(1/7)	28	1	39.5546	0.9973	0.847	3.8584	36.4026

Above results show that the filter gives optimum results when kappa = 27. Hence from now on wards we will fix the kappa value as 27 and proceed to the next set of experiments.

5.1.3.3 Results of AD for different values of delta

Table 5.29 Statistical Results of the image s7 filtered by AD for different values of delta

image	noi	delta	kappa	option	SNR	Coc	MSSIM	RMSE	PSNR
s7	15	(1/2)	27	1	36.1882	0.9612	0.4925	6.4357	31.9589
s7	15	(1/4)	27	1	50.7143	0.9976	0.9352	2.7083	39.4769
s7	15	(1/5)	27	1	51.0043	0.9987	0.9318	2.7376	39.3833
s7	15	(1/6)	27	1	50.6302	0.9991	0.919	2.8172	39.1345
s7	15	(1/7)	27	1	50.0872	0.9993	0.9064	2.8966	38.893

Table 5.30 Statistical Results of the image s75 filtered by AD for different values of delta

image	noi	delta	kappa	option	SNR	Coc	MSSIM	RMSE	PSNR
s75	15	(1/2)	27	1	35.6499	0.9425	0.482	6.6714	31.6465
s75	15	(1/4)	27	1	47.8551	0.9982	0.9298	2.9405	38.7623
s75	15	(1/5)	27	1	47.5774	0.999	0.9237	3.0094	38.5611
s75	15	(1/6)	27	1	47.0648	0.9994	0.9091	3.1185	38.2518
s75	15	(1/7)	27	1	46.4714	0.9995	0.8948	3.2273	37.954

Table 5.31 Statistical Results of the image s8 filtered by AD for different values of delta

image	noi	delta	kappa	option	SNR	Coc	MSSIM	RMSE	PSNR
s8	15	(1/2)	27	1	36.2582	0.9432	0.4902	6.4628	31.9224
s8	15	(1/4)	27	1	47.4999	0.9961	0.9152	3.0341	38.4902
s8	15	(1/5)	27	1	46.7434	0.9976	0.9058	3.2023	38.2023
s8	15	(1/6)	27	1	45.7738	0.9982	0.8913	3.3796	37.5536
s8	15	(1/7)	27	1	44.8921	0.9984	0.8768	3.5432	37.1428

Table 5.32 Statistical Results of the image s85 filtered by AD for different values of delta

image	noi	delta	kappa	option	SNR	Coc	MSSIM	RMSE	PSNR
s85	15	(1/2)	27	1	34.9096	0.9392	0.4796	6.7422	31.5548
s85	15	(1/4)	27	1	43.3643	0.9951	0.8916	3.4251	37.4373
s85	15	(1/5)	27	1	42.755	0.997	0.8804	3.6335	36.9243
s85	15	(1/6)	27	1	42.0634	0.9981	0.8648	3.8131	36.5051
s85	15	(1/7)	27	1	41.3902	0.9988	0.8497	3.9797	36.1338

Table 5.33 Statistical Results of the image s9 filtered by AD for different values of delta

image	noi	delta	kappa	option	SNR	Coc	MSSIM	RMSE	PSNR
s9	15	(1/2)	27	1	34.2781	0.9323	0.4741	6.823	31.4513
s9	15	(1/4)	27	1	42.4401	0.9961	0.8974	3.3737	37.5687
s9	15	(1/5)	27	1	42.0879	0.9982	0.8857	3.4552	37.3615
s9	15	(1/6)	27	1	41.4059	0.9992	0.8677	3.5821	37.048
s9	15	(1/7)	27	1	40.6794	0.9998	0.8504	3.7255	36.7072

Table 5.34 Statistical Results of the image s95 filtered by AD for different values of delta

image	noi	delta	kappa	option	SNR	Coc	MSSIM	RMSE	PSNR
s95	15	(1/2)	27	1	33.765	0.9306	0.4673	6.8465	31.4214
s95	15	(1/4)	27	1	40.7787	0.9936	0.8914	3.4454	37.3861
s95	15	(1/5)	27	1	40.381	0.9963	0.8787	3.5877	37.0344
s95	15	(1/6)	27	1	39.7797	0.9974	0.8606	3.7546	36.6395
s95	15	(1/7)	27	1	39.1366	0.9978	0.843	3.9061	36.296

Above results show that the filter gives optimum results when delta = 1/7.

By taking all the experiments of AD in to consideration the set of parameters to give optimum results comes out to be noi = 15, kappa = 27 delta = 1/6 and option = 1

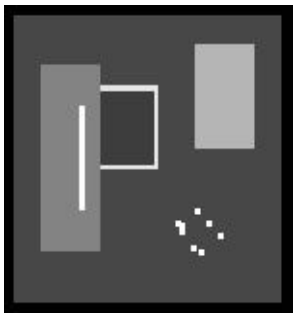

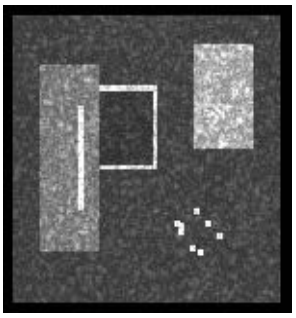

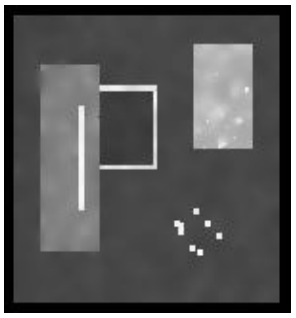

Fig 5.6(a) **Fig 5.6(b)** **Fig 5.6(c)**

Fig 5.6 Filtering Results for AD with noi = 15, kappa = 27, delta = 1/6 and option = 1 (a) Original Image (b) Unfiltered Image (c) Filtered Image

5.1.4 Filtering Results of SRAD2 for Synthetic Image

Here rect is variable which holds the coordinates of the selected rectangle homogenous region in the form of [x_{min} y_{min} width height].

Table 5.35 Statistical Results of the image s7 filtered by SRAD2 filter with the selection of different homogenous regions

image	rect	niter	lambda	NR	Coc	MSSIM	RMSE	PSNR
s7	10 10 10 10	200	0.5	40.6281	0.9808	0.8708	4.1675	35.7333
s7	10 10 20 10	200	0.5	40.6281	0.9808	0.8708	4.0424	35.9979
s7	10 10 30 10	200	0.5	41.3697	0.9826	0.8814	4.0691	35.9409
s7	10 10 40 10	200	0.5	42.5236	0.9857	0.9842	3.8735	36.3686
s7	10 10 50 10	200	0.5	42.5569	0.9858	0.8947	3.8969	36.3163
s7	10 10 60 10	200	0.5	42.3287	0.9851	0.8919	3.9504	36.198
s7	10 10 70 10	200	0.5	42.0542	0.9844	0.8886	4.0002	36.0892
s7	10 10 80 10	200	0.5	41.9381	0.9841	0.8874	4.0197	36.0468
s7	10 10 90 10	200	0.5	40.2979	0.9901	0.9182	3.4614	37.3457
s7	10 10 100 10	200	0.5	18.6887	0.8868	0.5036	6.6157	31.7193
s7	10 10 125 10	200	0.5	18.6887	0.8868	0.5036	7.0009	31.2277
s7	10 10 150 10	200	0.5	15.7578	0.8418	0.4544	7.0527	31.1637
s7	10 10 10 20	200	0.5	41.9427	0.9906	0.9205	3.5818	37.0488
s7	10 10 10 30	200	0.5	24.7243	0.9451	0.6292	5.0955	33.987
s7	10 10 10 40	200	0.5	21.4188	0.9171	0.5625	5.8321	32.8143
s7	10 10 10 50	200	0.5	19.8143	0.9005	0.5273	6.3152	32.1231
s7	10 10 10 60	200	0.5	19.5524	0.8975	0.5218	6.3624	32.0584
s7	10 10 10 70	200	0.5	19.6196	0.8982	0.5233	6.3376	32.0923
s7	10 10 10 80	200	0.5	19.3311	0.8948	0.517	6.4129	31.9897
s7	10 10 10 90	200	0.5	19.3158	0.8946	0.5169	6.4019	32.0046
s7	10 10 10 100	200	0.5	10.1836	0.893	0.5139	6.453	31.9356
s7	10 10 10 125	200	0.5	19.7378	0.8996	0.5258	6.3346	32.0965
s7	10 10 10 150	200	0.5	16.6167	0.856	0.4635	6.7879	31.4961

s7	20 20 10 10	200	0.5	24.9554	0.9457	0.6183	6.3538	32.0702
s7	20 20 10 20	200	0.5	15.7159	0.8406	0.4543	7.0764	31.1345
s7	20 20 10 30	200	0.5	15.6922	0.8401	0.4544	7.0746	31.1367
s7	20 20 10 40	200	0.5	15.7703	0.8415	0.4543	7.0553	31.1605
s7	20 20 10 50	200	0.5	15.9116	0.844	0.4549	7.0182	31.2063
s7	20 20 10 60	200	0.5	16.0989	0.8472	0.4566	6.9675	31.2693
s7	20 20 10 70	200	0.5	16.2794	0.8504	0.4587	6.9299	31.3162
s7	20 20 10 80	200	0.5	16.5612	0.8552	0.4628	6.8842	31.3737
s7	20 20 10 90	200	0.5	16.9296	0.8612	0.4691	6.8413	31.428
s7	20 20 10 100	200	0.5	17.3002	0.8672	0.4758	6.8052	31.474
s7	20 20 10 125	200	0.5	15.6462	0.8394	0.4549	7.0708	31.1414
s7	20 20 10 150	200	0.5	15.5295	0.8394	0.4554	7.1023	31.1028
s7	20 20 20 10	200	0.5	23.3273	0.9326	0.5933	6.4438	31.9479
s7	20 20 30 10	200	0.5	22.8252	0.928	0.5844	6.6377	31.6904
s7	20 20 40 10	200	0.5	23.2163	0.9316	0.5913	6.4818	31.8969
s7	20 20 50 10	200	0.5	23.7651	0.9365	0.6012	6.2628	32.1954
s7	20 20 60 10	200	0.5	24.6398	0.9438	0.6167	5.9998	32.5681
s7	20 20 70 10	200	0.5	25.51	0.9503	0.6327	5.752	32.9344
s7	20 20 80 10	200	0.5	18.5077	0.8844	0.4999	6.7437	31.5529
s7	20 20 90 10	200	0.5	15.4371	0.8355	0.4561	7.1184	31.0831
s7	20 20 100 10	200	0.5	15.4134	0.835	0.4566	7.1205	31.0806
s7	20 20 125 10	200	0.5	15.4101	0.835	0.4567	7.1205	31.0806
s7	20 20 150 10	200	0.5	15.4059	0.8349	0.4567	7.1207	31.0803
s7	10 10 50 50	200	0.5	15.4488	0.8357	0.4558	7.1175	31.0843
s7	10 10 50 100	200	0.5	15.4313	0.8354	0.4562	7.1195	31.0818
s7	10 10 80 15	200	0.5	41.4989	0.9829	0.8827	4.0664	35.9465

Table 5.36 Statistical Results of the image s75 filtered by SRAD2 filter with the selection of different homogenous regions

image	rect	niter	lambda	SNR	Coc	MSSIM	RMSE	PSNR
s75	10 10 10 10	200	0.5	38.3944	0.9778	0.8607	4.2748	35.5124
s75	10 10 20 10	200	0.5	38.1355	0.977	0.8557	4.3244	35.4122
s75	10 10 50 10	200	0.5	38.1355	0.977	0.8557	4.1313	35.8091
s75	10 10 80 10	200	0.5	39.4326	0.9809	0.8779	4.1229	35.8267
s75	10 10 90 10	200	0.5	40.757	0.989	0.9207	3.788	36.5627
s75	10 10 80 15	200	0.5	39.4663	0.9811	0.8784	4.1333	35.805
s75	10 10 90 15	200	0.5	29.3301	0.9763	0.7564	3.9776	36.1383
s75	120 100 20 25	200	0.5	38.3775	0.9777	0.86	4.3225	35.4161
s75	125 125 15 15	200	0.5	36.8441	0.9727	0.8101	4.6462	34.7888
s75	10 10 10 20	200	0.5	40.8958	0.9873	0.911	3.9484	36.2024
s75	10 10 10 30	200	0.5	23.9822	0.9423	0.6188	5.4261	33.441
s75	60 90 18 24	200	0.5	38.8539	0.9791	0.8676	4.2674	35.5276
s75	12 123 96 17	200	0.5	39.2306	0.9802	0.8739	4.2138	35.6373
s75	110 120 25 22	200	0.5	38.4878	0.978	0.8607	4.4127	35.2367
s75	134 11 7 129	200	0.5	38.3481	0.9775	0.8587	4.4127	35.2368
s75	84 40 11 39	200	0.5	37.2274	0.9741	0.8256	7.1052	31.0993

Table 5.37 Statistical Results of the image s8 filtered by SRAD2 filter with the selection of different homogenous regions

image	rect	niter	lambda	snr	COC	mssim	RMSE	PSNR
s8	10 10 5 5	200	0.5	34.4343	0.9629	0.6304	5.4755	33.3623
s8	10 10 10 10	200	0.5	35.6462	0.968	0.7638	4.936	34.2633
s8	10 10 70 10	200	0.5	37.8722	0.9755	0.8593	4.4574	35.1492
s8	10 10 80 10	200	0.5	38.0819	0.9762	0.8631	4.4316	35.1997
s8	10 10 90 10	200	0.5	39.5251	0.9887	0.9077	3.9554	36.1871
s8	10 10 100 10	200	0.5	20.0084	0.9838	0.5318	6.2398	32.2274
s8	10 10 10 70	200	0.5	18.7832	0.889	0.5052	6.5268	31.8368
s8	10 10 10 30	200	0.5	23.1971	0.9339	0.5982	5.593	33.1778
s8	10 10 10 90	200	0.5	18.4156	0.884	0.4979	6.5917	31.7508
s8	10 10 25 25	200	0.5	15.8277	0.844	0.4556	7.0623	31.1518
s8	20 20 5 5	200	0.5	34.0046	0.9616	0.5933	55,698	33.214
s8	20 20 10 10	200	0.5	22.0154	0.9222	0.5723	6.579	31.7676
s8	20 20 30 10	200	0.5	22.2741	0.9247	0.5768	6.5074	31.8626
s8	20 20 10 20	200	0.5	15.5472	0.8391	0.4562	7.121	31.0797
s8	20 20 50 10	200	0.5	24.2806	0.9427	0.6126	5.9733	32.6065
s8	20 20 50 20	200	0.5	15.4796	0.8378	0.4566	7.136	31.0617
s8	20 20 50 50	200	0.5	15.4064	0.8364	0.4576	7.1488	31.0461
s8	20 20 100 50	200	0.5	15.3852	0.836	0.4579	7.1513	31.0432
s8	20 20 125 50	200	0.5	15.3842	0.836	0.458	7.1517	31.0427
s8	20 20 75 75	200	0.5	15.3945	0.8362	0.4577	7.1504	31.0442
s8	20 20 100 100	200	0.5	15.3894	0.8361	0.4578	7.1507	31.0438
s8	30 30 10 10	200	0.5	38.1558	0.9884	0.9083	3.9714	36.152
s8	30 30 20 20	200	0.5	19.9947	0.9033	0.5297	6.6448	31.6812
s8	30 30 50 50	200	0.5	15.3816	0.8359	0.458	7.1518	31.0425
s8	30 30 5 5	200	0.5	39.7306	0.9892	0.916	3.7769	36.5881
s8	30 30 1 1	200	0.5	39.9346	0.9836	0.8965	3.969	36.1572
s8	10 10 40 10	200	0.5	36.7162	0.9718	0.8241	4.6824	34.7214
s8	10 10 50 10	200	0.5	37.1308	0.9731	0.8386	4.6565	34.7697
s8	20 20 1 1	200	0.5	33.9399	0.9617	0.5822	5.6333	33.1155
s8	10 10 1 1	200	0.5	33.5535	0.9602	0.558	5.9314	32.6676

Table 5.38 Statistical Results of the image s85 filtered by SRAD2 filter with the selection of different homogenous regions

image	rect	niter	lambda	SNR	Coc	MSSIM	RMSE	PSNR
s85	10 10 10 10	200	0.5	37.3752	0.9746	0.8653	4.4696	35.1255
s85	10 10 20 10	200	0.5	37.1116	0.9735	0.8608	4.5271	35.0144
s85	10 10 50 10	200	0.5	37.1795	0.9738	0.8618	4.5291	35.0106
s85	10 10 80 10	200	0.5	36.6083	0.9714	0.8525	438	34.7933
s85	10 10 90 10	200	0.5	38.3503	0.9798	0.8814	4.3946	35.2724
s85	10 10 80 15	200	0.5	36.8183	0.9722	0.8559	4.5935	34.8879
s85	10 10 90 15	200	0.5	28.3257	0.9704	0.7209	4.1497	35.7705
s85	120 100 20 25	200	0.5	36.355	0.9703	0.8485	4.6767	34.732
s85	125 125 15 15	200	0.5	34.8714	0.9645	0.8149	4.901	34.3251

s85	10 10 10 20	200	0.5	37.6241	0.9757	0.8682	4.5547	34.9615
s85	10 10 10 30	200	0.5	21.9207	0.924	0.5743	5.8567	32.7778
s85	60 90 18 24	200	0.5	36.8353	0.9723	0.8563	4.5677	34.9368
s85	12 123 96 17	200	0.5	37.2497	0.974	0.8631	4.52	35.028
s85	110 120 25 22	200	0.5	36.0947	0.9693	0.8433	4.7536	34.5904
s85	134 11 7 129	200	0.5	35.6698	0.9677	0.835	4.82	34.4699
s85	84 40 11 39	200	0.5	36.2232	0.9698	0.8461	7.1196	31.0817

Table 5.39 Statistical Results of the image s9 filtered by SRAD2 filter with the selection of different homogenous regions

image	rect	niter	lambda	SNR	Coc	mssim	RMSE	PSNR
s9	10 10 10 10	200	0.5	33.2125	0.9618	0.7726	5.018	34.1202
s9	10 10 20 10	200	0.5	33.3522	0.9626	0.7853	4.9831	34.1808
s9	10 10 50 10	200	0.5	34.9475	0.9698	0.8497	4.6813	34.7235
s9	10 10 80 10	200	0.5	34.845	0.9694	0.8475	4.6826	34.7211
s9	10 10 90 10	200	0.5	37.4072	0.984	0.8959	4.1928	35.6807
s9	10 10 80 15	200	0.5	34.9395	0.9698	0.8492	4.6978	34.6929
s9	10 10 90 15	200	0.5	25.7741	0.9562	0.6599	5.2447	33.7365
s9	120 100 20 25	200	0.5	35.3813	0.9716	0.8579	4.602	34.8718
s9	125 125 15 15	200	0.5	36.1929	0.9749	0.8684	4.3709	35.3195
s9	10 10 10 20	200	0.5	36.9314	0.9779	0.8784	4.4546	35.1546
s9	10 10 10 30	200	0.5	22.7155	0.9322	0.5977	5.6715	33.0568
s9	60 90 18 24	200	0.5	36.2263	0.975	0.8688	4.4491	35.1653
s9	12 123 96 17	200	0.5	35.6201	0.9725	0.861	4.5487	34.9731
s9	110 120 25 22	200	0.5	35.6296	0.9725	0.861	4.5855	34.903
s9	134 11 7 129	200	0.5	35.8838	0.9735	0.864	4.5652	34.9417
s9	84 40 11 39	200	0.5	34.8134	0.9693	0.847	7.098	31.108

Table 5.40 Statistical Results of the image s95 filtered by SRAD2 filter with the selection of different homogenous regions

image	rect	niter	lambda	SNR	Coc	MSSIM	RMSE	PSNR
s95	10 10 10 10	200	0.5	31.7784	0.9538	0.6742	5.3266	33.6018
s95	10 10 20 10	200	0.5	33.4238	0.9632	0.815	4.8006	34.5049
s95	10 10 50 10	200	0.5	33.2467	0.9623	0.8062	4.8586	34.4006
s95	10 10 80 10	200	0.5	34.5441	0.9685	0.847	4.6294	34.8203
s95	10 10 90 10	200	0.5	28.1986	0.9717	0.7616	4.2263	35.6116
s95	10 10 80 15	200	0.5	34.6728	0.9691	0.8504	4.5988	34.8779
s95	10 10 90 15	200	0.5	24.206	0.9457	0.6386	5.0427	34.0775
s95	120 100 20 25	200	0.5	33.7759	0.9649	0.8274	4.7005	34.6879
s95	125 125 15 15	200	0.5	34.3329	0.9676	0.8433	4.5147	35.0382
s95	10 10 10 20	200	0.5	36.0178	0.9791	0.8841	4.3961	35.2694
s95	10 10 10 30	200	0.5	23.8363	0.9427	0.634	4.9247	34.2831
s95	60 90 18 24	200	0.5	34.2979	0.9673	0.8414	4.6177	34.8422
s95	12 123 96 17	200	0.5	35.2049	0.9718	0.8608	4.478	35.1092
s95	110 120 25 22	200	0.5	33.7098	0.9646	0.8256	4.7271	34.6388

s95	134 11 7 129	200	0.5	34.8875	0.9702	0.8553	4.5089	35.0495
s95	84 40 11 39	200	0.5	35.1096	0.9712	0.859	7.0775	31.1332

Results of SRAD2 show that the filtering performance depends on the selection of the homogenous region on the image.

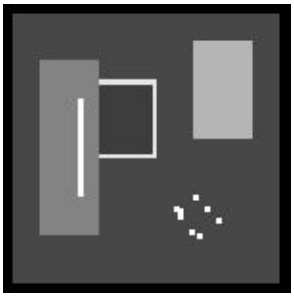

Fig 5.7(a)

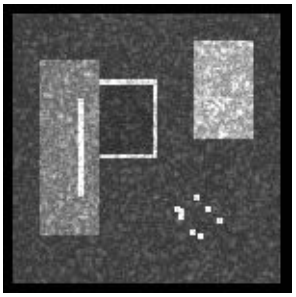

Fig 5.7(b)

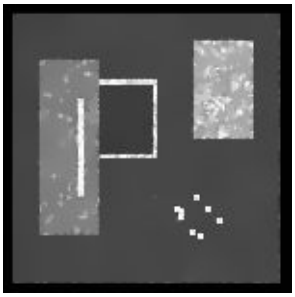

Fig 5.7(c)

Fig 5.7 Filtering results of SRAD2 with rect = [10 10 80 10]. (a) original noise less synthetic image (b) noise image with standard deviation 0.7 (c) filtered image

The above results given by different filters when applied on the synthetic image shows that AD filter is better than SRAD1 and SRAD2 filters when input image is an synthetic.

5.2 Photographic Image

Below are the results given for the synthetic image l7 is the noisy photographic image with standard deviation of the noise as 0.7. Similar is the case with l75, l8, l85, l9, l95. Given below are the photographic noise free and noisy images.

Fig 5.8(a)

Fig 5.8(b)

Fig 5.8(c)

Fig 5.8(d)

Fig 5.8(e)

Fig 5.8(f)

Fig 5.8(g)

Fig 5.8 Noise free image and noisy image with different levels of standard deviations of noise (a) noise free image (b) image with standard deviation of the noise as 0.7 (c) image with standard deviation of the noise as 0.75 (d) image with standard deviation of the noise as 0.8 (e) image with standard deviation of the noise as 0.85 (f) image with standard deviation of the noise as 0. 9 (g) image with standard deviation of the noise as 0.95.

5.2.1 Filtering Results of Lee, Kuan and Frost Filters on Photographic Image

Table 5.41 Statistical Results of the photographic images before filtering

Unfiltered Image Results					
image	SNR	Coc	MSSIM	RMSE	PSNR
I7	25.7157	0.9408	0.4033	8.6179	29.4228
I75	24.5757	0.9357	0.3836	8.8152	29.2262
I8	23.4721	0.9275	0.3682	8.9948	29.051
I85	22.4393	0.9194	0.3518	9.1578	28.895
I9	21.3815	0.9101	0.3382	9.3005	28.7607
I95	20.4174	0.9033	0.3224	9.4672	28.6064

Table 5.42 Statistical Results of the images filtered by Lee filter

Lee Filter Results					
image	SNR	Coc	MSSIM	RMSE	PSNR
I7	28.7482	0.9725	0.5237	7.0913	31.1163
I75	28.7482	0.9725	0.51	7.3241	30.8357
I8	28.6875	0.9699	0.51	7.3241	30.8357
I85	28.1038	0.9666	0.4942	7.5017	30.6276
I9	27.4763	0.9626	0.478	7.7024	30.3983
I95	26.997	0.9614	0.464	7.8996	30.1787

Table 5.43 Statistical Results of the images filtered by Kuan filter

Kuan Filter Results					
image	SNR	Coc	MSSIM	RMSE	PSNR
I7	30.032	0.9738	0.5423	6.902	31.3513
I75	28.7482	0.9725	0.5237	7.0913	31.1163
I8	28.6875	0.9699	0.51	7.3241	30.8357
I85	28.1038	0.9666	0.4942	7.5017	30.6276
I9	27.4763	0.9626	0.478	7.7024	30.3983
I95	26.997	0.9614	0.464	7.8996	30.1787

Table 5.44 Statistical Results of the images filtered by Frost filter

Frost Filter Results					
image	SNR	Coc	MSSIM	RMSE	PSNR
I7	33.355	0.9733	0.5205	7.0807	31.1293
I75	32.3686	0.9707	0.5012	7.2859	30.8812
I8	31.4115	0.9691	0.4864	7.5165	30.6105
I85	30.4237	0.9643	0.4704	7.6999	30.4011
I9	29.4013	0.9599	0.4544	7.8886	30.1908
I95	28.4785	0.9578	0.4391	8.0819	29.9806

Above results show that Lee, Kuan and Frost increase the value of the parameter SNR Coc, MSSIM and PSNR. These results show us that after filtering noise is reduced however reduction of noise is to a small extent.

5.2.2 Filtering Results of SRAD1 for Photographic Image

T is the number of iterations.

Table 5.45 Statistical Results of the image l7 filtered by SRAD1 for different iterations

image	T	SNR	Coc	MSSIM	RMSE	PSNR
l7	1	28.5718	0.9566	0.4442	8.1032	29.9577
l7	2	31.2863	0.9681	0.4883	7.5329	30.5915
l7	3	33.4382	0.975	0.5341	6.9437	31.299
l7	5	34.835	0.9802	0.6162	6.0604	32.4808
l7	10	31.8171	0.9777	0.646	58,541	32.7815
l7	12	24.3654	0.967	0.4252	6.6578	31.6641
l7	15	15.9445	0.9433	0.2359	7.2908	30.8753

Table 5.46 Statistical Results of the image l75 filtered by SRAD1 for different iterations

image	T	SNR	Coc	MSSIM	RMSE	PSNR
l75	1	27.4325	0.952	0.4235	8.3213	29.828
l75	2	30.1805	0.965	0.467	7.7549	30.3392
l75	3	32.4256	0.973	0.5125	7.1586	31.0343
l75	5	34.1517	0.979	0.597	6.2283	32.2434
l75	10	31.2478	0.9782	0.6321	5.9653	32.6182
l75	12	23.5414	0.9659	0.4067	6.7376	31.5606
l75	15	16.0217	0.9433	0.231	7.3704	30.781

Table 5.47 Statistical Results of the image l8 filtered by SRAD1 for different iterations

image	T	SNR	Coc	MSSIM	RMSE	PSNR
l8	1	26.3453	0.9454	0.4077	8.5215	29.5204
l8	2	29.1544	0.9601	0.4508	7.9759	30.0952
l8	3	31.5507	0.9695	0.4962	7.3943	30.7529
l8	5	33.7653	0.9772	0.5818	6.4248	31.9736
l8	10	30.9165	0.9766	0.6224	6.0141	32.5474
l8	12	23.0386	0.9625	0.3881	6.827	31.4463
l8	15	15.7818	0.94	0.2255	7.4284	30.7129

Table 5.48 Statistical Results of the image l85 filtered by SRAD1 for different iterations

image	T	SNR	Coc	MSSIM	RMSE	PSNR
l85	1	25.2889	0.9387	0.3905	8.7014	29.339
l85	2	28.0968	0.9544	0.4328	8.1756	29.8804

l85	3	30.5494	0.9657	0.4777	7.6018	30.5124
l85	5	33.0824	0.9757	0.5638	6.503	31.7527
l85	10	30.3318	0.9755	0.6128	6.0689	32.4686
l85	12	22.4419	0.9607	0.3802	6.8776	31.3821
l85	15	15.7934	0.9386	0.2239	7.4569	30.6796

Table 5.49 Statistical Results of the image l9 filtered by SRAD1 for different iterations

image	T	SNR	Coc	MSSIM	RMSE	PSNR
l9	1	24.2298	0.9312	0.3759	8.8648	29.1774
l9	2	27.0594	0.9484	0.4172	8.3599	29.6868
l9	3	29.5891	0.9609	0.461	7.8068	30.2814
l9	5	32.4372	0.9727	0.5464	6.8081	31.4702
l9	10	30.0131	0.9746	0.5965	6.2608	32.1983
l9	12	21.8766	0.9588	0.364	7.0207	31.2032
l9	15	15.1983	0.9367	0.2173	7.5817	30.5354

Table 5.50 Statistical Results of the image l95 filtered by SRAD1 for different iterations

image	T	SNR	Coc	MSSIM	RMSE	PSNR
l95	1	23.2422	0.9251	0.3595	9.0495	28.9984
l95	2	26.0666	0.9444	0.4003	8.5577	29.4837
l95	3	28.6238	0.9589	0.4437	8.0152	30.0525
l95	5	31.686	0.9729	0.5301	7.0317	31.1896
l95	10	28.9076	0.9753	0.5763	6.4274	31.9701
l95	12	20.6138	0.9588	0.3409	7.1531	31.0409
l95	15	14.3124	0.9312	0.2012	7.6423	30.4663

Imaging result of SRAD1 on l7 for T=3 is as follows

Fig 5.9(a) **Fig 5.9(b)** **Fig 5.9(c)**

Fig 5.9 Filtering Results of SRAD1 on l7 image with T=3 (a) Original Image (b) Unfiltered Image (c) Filtered Image

Imaging result of SRAD1 on l7 for T=5 is as follows

Fig 5.10(a) **Fig 5.10(b)** **Fig 5.10(c)**

Fig 5.10 Filtering Results of SRAD1 on l7 image with T=5 (a) Original Image (b) Unfiltered Image (c) Filtered Image

Imaging result of SRAD1 on l7 for T=10 is as follows

Fig 5.11(a) Fig 5.11(b) Fig 5.11(c)

Fig 5.11 Filtering Results of SRAD1 on l7 image with T=10 (a) Original Image (b) Unfiltered Image (c) Filtered Image

Imaging result of SRAD1 on l7 for T=15 is as follows

Fig 5.12(a) **Fig 5.12(b)** **Fig 5.12(c)**

Fig 5.12 Filtering Results of SRAD1 on l7 image with T=15 (a) Original Image (b) Unfiltered Image (c) Filtered Image

The above tables and images show that the filter results are good for $5 < T < 10$.

5.2.3 Filtering Results of AD for photographic Image

From the experiments conducted on the synthetic image we got the best result when, noi=15, kappa = 27, delta = 1/6 and option = 1. Hence the results of the filtering of the photographic image by AD around these optimized parameters are tabulated as given below

Table 5.51 Statistical Results of the image l7 filtered by AD for

image	noi	delta	kappa	option	SNR	Coc	MSSIM	RMSE	PSNR
l7	15	(1/7)	30	1	34.9947	0.9834	0.6749	5.649	33.0914
l7	15	(1/7)	27	1	35.0954	0.984	0.653	5.77	32.0954
l7	15	(1/6)	27	1	34.804	0.9835	0.6638	5.6989	33.015
l7	4	(1/7)	30	1	28.1932	0.9571	0.4483	8.1493	29.9084
l7	4	(1/7)	15	1	26.3169	0.9449	0.4184	8.4747	29.5683
l7	4	(1/7)	17	1	26.519	0.9464	0.4222	8.4364	29.6076

Table 5.52 Statistical Results of the image l75 filtered by AD

image	noi	delta	kappa	option	SNR	Coc	MSSIM	RMSE	PSNR
l75	15	(1/7)	30	1	34.2262	0.9835	0.6511	5.8329	32.8131
l75	15	(1/7)	27	1	34.0901	0.9836	0.6208	6.028	32.5274
l75	15	(1/6)	27	1	33.9269	0.9834	0.6338	5.9257	32.6759
l75	4	(1/7)	30	1	26.8009	0.9508	0.4255	8.397	29.6484
l75	4	(1/7)	15	1	25.0934	0.9392	0.3975	8.6885	29.3519
l75	4	(1/7)	17	1	25.2723	0.9405	0..4010	8.6551	29.3854

Table 5.53 Statistical Results of the image l8 filtered by AD

image	noi	delta	kappa	option	SNR	Coc	MSSIM	RMSE	PSNR
l8	15	(1/7)	30	1	33.6613	0.9819	0.6259	6.0819	32.4501
l8	15	(1/7)	27	1	33.1951	0.9824	0.5906	6.3607	32.0607
l8	15	(1/6)	27	1	33.1778	0.9819	0.6045	6.2157	32.361
l8	4	(1/7)	30	1	25.5043	0.9424	0.4075	8.6249	29.4157
l8	4	(1/7)	15	1	23.923	0.9308	0.3809	8.8797	29.1628
l8	4	(1/7)	17	1	24.0806	0.932	0.3842	8.8507	29.1913

Table 5.54 Statistical Results of the image l85 filtered by AD

image	noi	delta	kappa	option	SNR	Coc	MSSIM	RMSE	PSNR
l85	15	(1/7)	30	1	32.8202	0.9816	0.5926	6.3147	32.1237
l85	15	(1/7)	27	1	32.0405	0.9817	0.5533	6.6624	31.6582
l85	15	(1/6)	27	1	32.1756	0.9817	0.5671	6.4901	31.8858
l85	4	(1/7)	30	1	24.2707	0.9338	0.3887	8.8212	29.2203
l85	4	(1/7)	15	1	22.8361	0.9225	0.3635	9.052	28.996
l85	4	(1/7)	17	1	22.9777	0.9236	0.3666	9.025	29.0218

Table 5.55 Statistical Results of the image l9 filtered by AD

image	noi	delta	kappa	option	SNR	Coc	MSSIM	RMSE	PSNR
l9	15	(1/7)	30	1	31.7866	0.9793	0.5596	6.6986	31.6111
l9	15	(1/7)	27	1	30.6738	0.9792	0.5209	7.0768	31.134
l9	15	(1/6)	27	1	30.956	0.9795	0.5335	6.9076	31.3443
l9	4	(1/7)	30	1	23.0135	0.9239	0.3728	8.9933	29.0524
l9	4	(1/7)	15	1	21.721	0.9126	0.349	9.2039	28.8514
l9	4	(1/7)	17	1	21.8431	0.9137	0.3519	9.1795	28.8745

The above tables show that the best results are produced when noi = 15, kappa = 27, delta = 1/7 and option = 2 which is slightly different from the optimized parameter set obtained for synthetic image.



Fig 5.13(a) **Fig 5.13(b)** **Fig 5.13(c)**

Fig 5.13 Filtering Results of AD on l7 with noi = 15, kappa = 27, delta = 1/7 and option = 1 (a) Original Image (b) Unfiltered Image (c) Filtered Image

5.2.4 Filtering Results of SRAD2 for Photographic Image

Here rect is variable which holds the coordinates of the selected rectangle homogenous region in the form of [x_{min} y_{min} width height].

Table 5.56 Statistical Results of the image l7 filtered by SRAD2 filter with the selection of different homogenous regions

image	rect	niter	lambda	SNR	Coc	MSSIM	RMSE	PSNR
l7	75 14 34 227	200	0.5	31.3095	0.9796	0.6607	6.6356	31.693
l7	88 8 229 20	200	0.5	28.305	0.9691	0.6046	7.1003	31.105
l7	79 28 55 55	200	0.5	28.0537	0.968	0.6	7.1295	31.07
l7	2 109 17 218	200	0.5	27.7584	0.9666	0.5948	7.1566	31.037
l7	445 197 46 58	200	0.5	28.9814	0.9722	0.6177	6.9925	31.238
l7	445 8 26 22	200	0.5	30.8248	0.9786	0.652	6.6976	31.612
l7	90 35 64 32	200	0.5	27.9064	0.9673	0.5973	7.1471	31.048

Table 5.57 Statistical Results of the image l75 filtered by SRAD2 filter with the selection of different homogenous regions

image	rect	niter	lambda	SNR	Coc	MSSIM	RMSE	PSNR
l75	75 14 34 227	200	0.5	32.087	0.9782	0.6557	6.0016	32.566
l75	88 8 229 20	200	0.5	24.5232	0.9428	0.5312	6.9662	31.271
l75	79 28 55 55	200	0.5	28.7713	0.9677	0.5997	6.5369	31.823
l75	2 109 17 218	200	0.5	27.6294	0.9623	0.5813	6.6675	31.652
l75	445 197 46 58	200	0.5	29.1867	0.9697	0.6085	6.4569	31.93
l75	445 8 26 22	200	0.5	32.8686	0.977	0.651	5.963	32.622
l75	90 35 64 32	200	0.5	28.1251	0.9645	0.5889	6.6271	31.704

Table 5.58 Statistical Results of the image l8 filtered by SRAD2 filter with the selection of different homogenous regions

image	rect	niter	lambda	SNR	Coc	MSSIM	RMSE	PSNR
l8	75 14 34 227	200	0.5	31.194	0.9772	0.6497	6.4001	32.007
l8	88 8 229 20	200	0.5	27.8487	0.9659	0.5948	6.9187	31.33
l8	79 28 55 55	200	0.5	27.1001	0.9619	0.5814	7.0131	31.213
l8	2 109 17 218	200	0.5	27.6589	0.9647	0.5912	6.9388	31.305
l8	445 197 46 58	200	0.5	28.972	0.9712	0.6175	6.7071	31.6
l8	445 8 26 22	200	0.5	32.8301	0.9659	0.602	6.7271	31.574
l8	90 35 64 32	200	0.5	27.314	0.963	0.5851	6.988	31.244

Table 5.59 Statistical Results of the image l85 filtered by SRAD2 filter with the selection of different homogenous regions

image	rect	niter	lambda	SNR	Coc	MSSIM	RMSE	PSNR
l85	75 14 34 227	200	0.5	29.8132	0.9762	0.6436	6.8598	31.405
l85	88 8 229 20	200	0.5	27.1355	0.9648	0.5924	7.242	30.934
l85	79 28 55 55	200	0.5	27.4077	0.9662	0.5974	7.2016	30.982
l85	2 109 17 218	200	0.5	26.7005	0.9626	0.5843	7.2865	30.88
l85	445 197 46 58	200	0.5	27.5796	0.967	0.6008	7.1826	31.005
l85	445 8 26 22	200	0.5	31.4893	0.9697	0.6161	6.9682	31.268
l85	90 35 64 32	200	0.5	26.6888	0.9625	0.5841	7.2955	30.87

Table 5.60 Statistical Results of the image l9 filtered by SRAD2 filter with the selection of different homogenous regions

image	rect	niter	lambda	SNR	Coc	MSSIM	RMSE	PSNR
l9	75 14 34 227	200	0.5	31.4172	0.975	0.637	5.7811	32.891
l9	88 8 229 20	200	0.5	28.3913	0.9641	0.5854	6.2842	32.166
l9	79 28 55 55	200	0.5	26.9368	0.9569	0.562	6.4652	31.919
l9	2 109 17 218	200	0.5	28.4153	0.9641	0.5858	6.2705	32.185
s9	445 197 46 58	200	0.5	29.8941	0.9709	0.6146	6.0019	32.565
s9	445 8 26 22	200	0.5	31.5001	0.9752	0.6363	5.7396	32.953

s9	90 35 64 32	200	0.5	27.2516	0.9584	0.9369	6.4329	31.963

Table 5.61 Statistical Results of the image l95 filtered by SRAD2 filter with the selection of different homogenous regions

image	rect	niter	lambda	SNR	Coc	MSSIM	RMSE	PSNR
l95	75 14 34 227	200	0.5	30.8352	0.9736	0.6295	5.8647	32.766
l95	88 8 229 20	200	0.5	28.5658	0.9651	0.5914	6.2424	32.224
l95	79 28 55 55	200	0.5	27.4391	0.9595	0.5725	6.387	32.025
l95	2 109 17 218	200	0.5	27.8647	0.9616	0.5794	6.3261	32.108
l95	445 197 46 58	200	0.5	28.5812	0.9654	0.5931	6.2214	32.353
l95	445 8 26 22	200	0.5	32.3979	0.9681	0.6075	5.8079	32.85
l95	90 35 64 32	200	0.5	26.9891	0.9571	0.5652	6.4438	31.948

Results of SRAD2 show that the filter performance depends on the selection of the homogenous region on the image.

Fig 5.14(a)

Fig 5.14(b)

Fig 5.14(c)

Fig 5.14 Filtering results of SRAD2 on l7 with rect = [75 14 34 227]. (a) original noise less synthetic image (b) noise image with standard deviation 0.7 (c) filtered image

For photographic image SRAD1, AD and SRAD2 filters show almost same performance in removing the speckle at the same time gave significant results.

5.3 Ultrasonic Image

Below are the results given for the ultrasonic image us3.7 is the noisy photographic image with standard deviation of the noise as 0.7. Given below are the ultrasonic real image and noise induced image.

Fig 5.15(a)

Fig 5.15(b)

Fig 5.15 Real ultrasonic image and noise induced ultrasonic image (a) real image (b) noise induced image with standard deviation of the noise as 0.7.

5.3.1 Filtering Results of Ultrasound Image by Lee, Kuan, Frost, SRAD1, AD and SRAD2

Table 5.62 Statistical Results of the ultrasonic images for unfiltered images, Lee filtered images, Kuan filtered images and Frost filtered images

Filtering Results of us3.7					
filter	SNR	Coc	MSSIM	RMSE	PSNR
unfiltered	31.9417	0.96	0.7359	5.6325	33.1168
Lee	25.8927	0.9507	0.7488	5.3543	33.5567
Kuan	25.8927	0.9507	0.7488	5.3543	33.5567
Frost	30.9191	0.9558	0.7625	5.0681	34.0339

Table 5.63 Best results obtained from different filters for ultrasonic image

filter	parameters	SNR	Coc	MSSIM	RMSE	PSNR
SRAD1	T=2	33.3773	0.9722	0.8011	4.815	34.4788
AD	noi = 15, kappa = 4, delta = 1/7 option = 1	32.1469	0.9553	0.7802	5.3466	33.5693
SRAD2	rect = [224 239 6 3]	26.3295	0.9642	0.7456	14.1841	25.0947

Fig 5.16(a) **Fig 5.16(b)** **Fig 5.16(c)**

Fig 5.16 Filtering Results of us3.7 image from SRAD1 with T=2 (a) Original Image (b) Unfiltered Image with the standard deviation of the noise as 0.7 (c) Filtered Image

Fig 5.17(a) **Fig 5.17(a)** **Fig 5.17(a)**

Fig 5.17 Filtering Results of us3.7 image from AD for l7 with noi = 15, kappa = 4, delta = 1/7 and option = 1 (a) Original Image (b) Unfiltered Image (c) Filtered Image.

Fig 5.18(a) **Fig 5.18(b)** **Fig 5.18(c)**

Fig 5.18 Filtering results of us3.7 image from SRAD2 with rect = [224 239 6 3]. (a) original noise less synthetic image (b) noise image with standard deviation 0.7 (c) filtered image.

The results show that for ultrasonic image SRAD1 is giving comparatively good results.

5.4 Synthetic Aperture Radar (SAR) image

Below are the results given for the SAR image sar2 is the noisy radar image with standard deviation of the noise as 0.2. Similar is the case with sar4, sar6, sar8. Given below are the Radar real image and noise induced images.

Fig 5.19(a)

Fig 5.19(b)

Fig 5.19 Real Synthetic Aperture Radar Image and noise induced image (a) Real SAR image (b) noise induced image with standard deviation of noise as 0.7

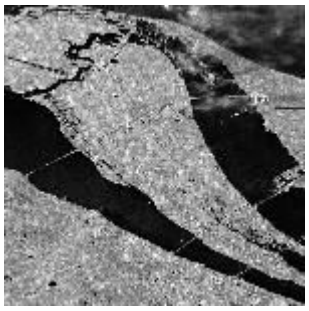

Fig 5.20(c)

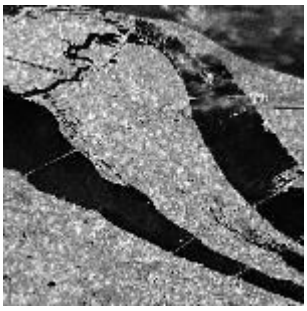

Fig 5.20(d)

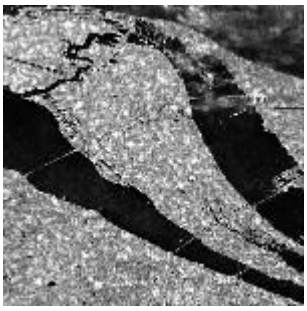

Fig 5.20(e)

Fig 5.20 Real image and noisy induced images with different levels of standard deviations of noise (a) real image (b) image with standard deviation of the noise as 0.2 (c) image with standard deviation of the noise as 0.4 (d) image with standard deviation of the noise as 0.6 (e) image with standard deviation of the noise as 0.8.

5.4.1 Filtering Results of Lee, Kuan and Frost Filters on Synthetic Image

Table 5.64 Statistical Results of SAR images before filtering

Unfiltered Image Results					
image	SNR	Coc	MSSIM	RMSE	PSNR
sar2	43.3583	0.9953	0.945	5.8338	32.8118
sar4	36.578	0.992	0.8867	7.3007	30.8635
sar6	31.7024	0.9848	0.8228	8.1455	29.9124
sar8	29.3712	0.9781	0.7636	8.6693	29.3712

Table 5.65 Statistical Results of the SAR images filtered by Lee filter

Lee Filter Results					
image	SNR	Coc	MSSIM	RMSE	PSNR
sar2	20.7805	0.9538	0.5304	8.607	29.4338
sar4	20.7222	0.9528	0.5259	8.6465	29.394
sar6	20.2772	0.9528	0.5144	8.7734	29.2675
sar8	20.1471	0.9534	0.5037	8.8558	29.1862

Table 5.66 Statistical Results of the SAR images filtered by Kuan filter

Kuan Filter Results					
image	snr	coc	mssim	rmse	psnr
sar2	20.7805	0.9538	0.5304	8.607	29.4338
sar4	20.7222	0.9528	0.5259	8.6465	29.394
sar6	20.2772	0.9528	0.5144	8.7734	29.2675
sar8	20.1471	0.9534	0.5037	8.8558	29.1862

Table 5.67 Statistical Results of the images filtered by Frost filter

Frost Filter Result					
image	snr	coc	mssim	rmse	psnr
sar2	21.318	0.9562	0.4336	8.5684	29.4728
sar4	21.2081	0.9559	0.4376	8.6271	29.4135
sar6	20.9487	0.9551	0.4345	8.7724	29.2685
sar8	20.491	0.9531	0.4304	8.891	29.1518

Above results show that Lee and Kuan gave same results. However the experiments show that Lee, Kuan and Frost doesnot give significant result on Radar images.

5.4.2 Filtering Results of SRAD1 for SAR Image

T is the number of iterations.

Table 5.68 Statistical Results of the image SAR2 filtered by SRAD1 for different iterations

image	T	snr	coc(mine)	MSSIM	RMSE	PSNR
sar2	1	41.5314	0.9942	0.9355	6.1213	32.3939
sar2	2	37.4521	0.9902	0.8576	6.8477	31.4199
sar2	3	33.4547	0.9854	0.8292	7.4816	30.6509
sar2	5	27.9623	0.9778	0.6526	8.2318	29.821
sar2	10	20.9572	0.9582	0.4371	8.7284	29.3121

Table 5.69 Statistical Results of the image SAR4 filtered by AD for different iterations

image	T	snr	coc(mine)	MSSIM	RMSE	PSNR
sar4	1	36.5939	0.9932	0.8862	7.1641	31.0276
sar4	2	34.8429	0.9902	0.8606	7.3645	30.788
sar4	3	32.3831	0.9854	0.8061	7.6937	30.4081
sar4	5	27.995	0.9779	0.6469	8.2405	29.8118
sar4	10	20.6971	0.9564	0.4391	8.7277	29.3128

Table 5.70 Statistical Results of the image SAR6 filtered by SRAD1 for different iterations

image	T	snr	coc(mine)	MSSIM	RMSE	PSNR
sar6	1	32.4035	0.9871	0.8296	7.8732	30.2078
sar6	2	31.924	0.9866	0.8154	7.8188	30.268
sar6	3	30.4963	0.9833	0.7739	7.949	30.1246
sar6	5	27.3095	0.9756	0.633	8.3343	29.7135
sar6	10	20.8884	0.9568	0.425	8.7667	29.274

Table 5.71 Statistical Results of the image SAR8 filtered by SRAD1 for different iterations

image	T	snr	coc(mine)	MSSIM	RMSE	PSNR
sar8	1	29.1332	0.9854	0.7777	8.3699	39.6764
sar8	2	29.3615	0.9862	0.7735	8.1882	29.867
sar8	3	28.7511	0.9841	0.7457	8.1775	29.8784
sar8	5	26.5512	0.9759	0.6221	8.4224	29.622
sar8	10	19.7171	0.9592	0.4141	8.8442	29.1977

Results show that SRAD1 is not appropriate for SAR images.

Imaging result of SRAD1 on sar2 for T=1 is as follows

Fig 5.21(a)

Fig 5.21(b)

Fig 5.21(c)

Fig 5.21 Filtering Results for SRAD1 on sar2 image with T=1 (a) Original Image (b) Unfiltered Image (c) Filtered Image

5.4.3 Filtering Results of AD for SAR Image

Table 5.72 Statistical Results of the image SAR2 filtered by AD

image	noi	delta	kappa	option	SNR	Coc	MSSIM	RMSE	PSNR
sar2	15	(1/7)	30	1	29.9122	0.9855	0.6499	8.2819	29.7682
sar2	15	(1/7)	27	1	30.8579	0.9879	0.6824	8.181	29.8747
sar2	15	(1/6)	27	1	30.3215	0.9869	0.6646	8.2457	29.8063
sar2	1	(1/7)	30	1	43.2119	0.9956	0.9346	5.9387	32.657
sar2	1	(1/7)	15	1	43.4837	0.9953	0.9435	5.8221	32.8292
sar2	1	(1/7)	17	1	43.4984	0.9953	0.9428	5.825	32.8249

Table 5.73 Statistical Results of the image SAR4 filtered by AD

image	noi	delta	kappa	option	SNR	Coc	MSSIM	RMSE	PSNR
sar4	15	(1/7)	30	1	29.6255	0.9855	0.6614	8.2821	39.768
sar4	15	(1/6)	27	1	30.0531	0.9864	0.678	8	29.8014
sar4	15	(1/7)	27	1	30.5157	0.987	0.6954	8.1777	29.8782
sar4	1	(1/7)	30	1	37.0881	0.9933	0.8847	7.1998	30.9844
sar4	1	(1/7)	15	1	36.7267	0.9923	0.8875	7.2585	30.9139
sar4	1	(1/7)	17	1	36.783	0.9923	0.8874	7.2469	30.9278

Table 5.74 Statistical Results of the image SAR6 filtered by AD

image	noi	delta	kappa	option	SNR	Coc	MSSIM	RMSE	PSNR
sar6	15	(1/7)	30	1	28.9947	0.9836	0.6676	8.3808	29.6651
sar6	15	(1/7)	27	1	29.6783	0.9857	0.7001	8.3318	29.716
sar6	15	(1/6)	27	1	29.3395	0.9851	0.6838	8.3782	29.6678
sar6	1	(1/7)	30	1	32.3127	0.9865	0.8278	8.018	30.0495
sar6	1	(1/7)	15	1	31.8288	0.9849	0.8261	8.1003	29.9608
sar6	1	(1/7)	17	1	31.88	0.9851	0.8265	8.0866	29.9755

Table 5.75 Statistical Results of the image SAR8 filtered by AD

image	noi	delta	kappa	option	SNR	Coc	MSSIM	RMSE	PSNR
sar8	15	(1/7)	30	1	27.6737	0.9815	0.668	8.5503	29.4912
sar8	15	(1/7)	27	1	27.9432	0.9829	0.6916	8.5652	29.4761
sar8	15	(1/6)	27	1	27.7466	0.9825	0.6794	8.5751	29.7466
sar8	1	(1/7)	30	1	28.434	0.9817	0.7721	8.5582	28.434
sar8	1	(1/7)	15	1	27.9622	0.9788	0.7685	8.6194	29.4213
sar8	1	(1/7)	17	1	28.0066	0.9791	0.769	8.6101	29.4306

Results show that the filter gives good results at noi = 1, delta = 1/7, kappa = 17 and option = 1 for SAR image.

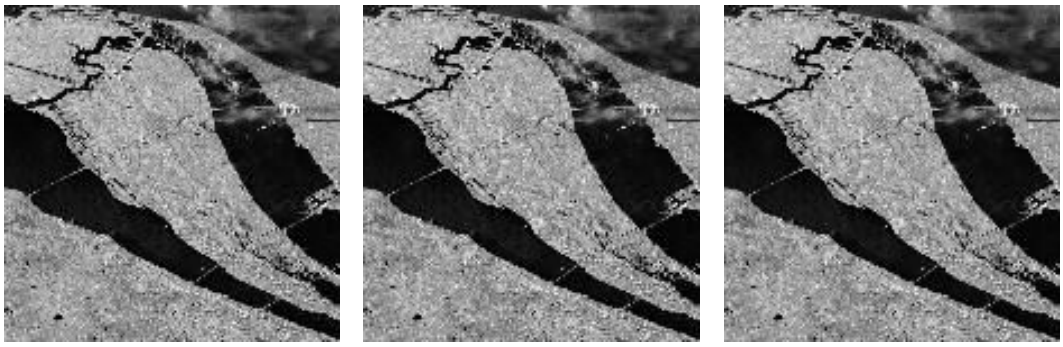

Fig 5.22(a) **Fig 5.22(b)** **Fig 5.22(c)**

Fig 5.21 Filtering Results for AD on sar2 image with noi = 1, delta = 1/7, kappa = 17 and option = 1 (a) Original Image (b) Unfiltered Image (c) Filtered Image

5.4.4 Filtering Results of SRAD2 for SAR Image

Table 5.76 Statistical Results of the image SAR2 filtered by SRAD2

image	rect	niter	lambda	SNR	Coc	MSSIM	RMSE	PSNR
sar2	87 69 3 6	200	0.5	34.5648	0.9465	0.7325	7.4973	30.6327
sar2	11 59 7 9	200	0.5	43.658	0.9815	0.9329	5.8067	32.8523
sar2	110 63 17 11	200	0.5	43.6336	0.9816	0.9272	5.8345	32.8108
sar2	140 96 5 7	200	0.5	43.6541	0.9816	0.9303	5.82	32.8323
sar2	137 99 8 9	200	0.5	43.5352	0.9813	0.941	5.8024	32.8586

Table 5.77 Statistical Results of the image SAR4 filtered by SRAD2

image	rect	niter	lambda	SNR	Coc	MSSIM	RMSE	PSNR
sar4	87 69 3 6	200	0.5	31.2853	0.9224	0.6468	7.8465	30.2373
sar4	11 59 7 9	200	0.5	36.9022	0.9553	0.879	7.2358	30.9411
sar4	110 63 17 11	200	0.5	36.9922	0.9556	0.876	7.2298	30.9483
sar4	140 96 5 7	200	0.5	36.7616	0.9547	0.8826	7.2573	30.9154

sar4	137 99 8 9	200	0.5	36.7219	0.9546	0.8837	7.2645	20.9067

Table 5.78 Statistical Results of the image SAR6 filtered by SRAD2

image	rect	niter	lambda	SNR	Coc	MSSIM	RMSE	PSNR
sar6	87 69 3 6	200	0.5	30.2506	0.9125	0.6508	7.8977	30.1808
sar6	11 59 7 9	200	0.5	32.1373	0.9241	0.819	8.0432	30.0222
sar6	110 63 17 11	200	0.5	32.0655	0.9237	0.8201	8.0523	30.0124
sar6	140 96 5 7	200	0.5	31.8877	0.9229	0.8225	8.0865	29.9756
sar6	137 99 8 9	200	0.5	31.8025	0.9225	0.8229	8.1085	29.952

Table 5.78 Statistical Results of the image SAR8 filtered by SRAD2

image	rect	niter	lambda	SNR	Coc	MSSIM	RMSE	PSNR
sar8	87 69 3 6	200	0.5	30.2506	0.9125	0.6508	7.8977	30.1808
sar8	11 59 7 9	200	0.5	32.1373	0.9241	0.819	8.0432	30.0222
sar8	110 63 17 11	200	0.5	32.0655	0.9237	0.8201	8.0523	30.0124
sar8	140 96 5 7	200	0.5	31.8877	0.9229	0.8225	8.0865	29.9756
sar8	137 99 8 9	200	0.5	31.8025	0.9225	0.8229	8.1085	29.952

Results of SRAD2 show that the filter performance depends on the selection of the homogenous region on the image

Fig 5.23(a) **Fig 5.23(b)** **Fig 5.23(c)**

Fig 5.23 Filtering results of SRAD2 with rect = [140 96 5 7]. (a) real SAR image (b) noise induced image with standard deviation of noise as 0.7 (c) filtered image

Considering the above results we can infer that AD and SRAD2 give significant result for SAR images.

Based on the above experiments, the optimum parameters for which the filter gives the best result for a particular type of image is inferred.

Conclusion

The use of filter in Digital Image Processing improves the image to a great extent. Mainly in the case of presence of Speckle noise, filtering is very much required in order to improve the diagnostic examination and also to improve the efficiency of post processing techniques like segmentation. Out of the six filters used, Anisotropic Diffusion (AD) filter did the best job as far as synthetic image is concerned. SRAD1 and AD gives the best result for photographic image also SRAD1 has given the best result in ultrasonic image and in case of SAR images the SRAD2 and AD are showing better performance however there is no significant improvement in the results of SAR images and also SRAD2 filter removes the speckle but its efficiency is based on the selection of homogenous region. This homogenous region is selected by the user and the user has to be careful while selecting the homogenous region. Hence SRAD2 algorithm is not user friendly. The developed algorithm selects the best filter for a given image on the basis of statistical parameters. This algorithm reduces the burden of the user in selecting the filter for the removal of the speckle in different types of images.

Scope for Future Work

In this thesis initially all the filters are run and the best output is selected by comparing the statistical values of the images obtained from the different filters. However in future the best filter can automatically selected using a lookup-table or by applying fuzzy rules after studying and using the image properties. Metrics like edges in the image, Neural network can also be implemented to increase the filter optimization.

References

[1] Christoph B. Burckhardt, "Speckle in Ultrasound B-Mode Scans", IEEE TRANSACTIONS ON SONICS AND ULTRASONICS, 1978, VOL.25, pages: 1 - 6

[2] Kiyo Tomiyas, "Computer Simulation of Speckle in a Synthetic Aperture Radar Image Pixel", IEEE TRANSACTIONS ON GEOSCIENCE AND REMOTE SENSING, 1983, VOL.21, pages: 357 - 363,

[3] Matthew O 'Donnell and Seth D. Silverstein "Optimum Displacement for Compound Image Generation in Medical Ultrasound", IEEE TRANSACTIONS ON ULTRASONICS, FERROELECTRICS, AND FREQUENCY CONTROL, 1988, VOL. 35, pages: 470-476

[4] Armand Lopes, Ridha Touzi. and E. Nezry "Adaptive Speckle Filters and Scene Heterogeneity", IEEE TRANSACTIONS ON GEOSCIENCE AND REMOTE SENSING, 1990, VOL. 28, pages: 992-1000

[5] Pietro Perona AND Jitendra Malik, "Scale-Space and Edge Detection Using Anisotropic Diffusion", IEEE TRANSACTIONS ON PATTERN ANALYSIS AND MACHINE INTELLIGENCE, 1990, VOL. 12, page(s): 629-639

[6] A. J. Healey, F. Forsberg, and S. Leeman., "Processing techniques for speckle reduction in medical ultrasound images", IEE Colloquium on Image Processing in Medicine, 1991, pages: 6/1-6/4

[7] Erik Steen and B. Olstad, "Volume Rendering in Medical Ultrasound Imaging based on Nonlinear Filtering", IEEE winter workshop on Nonlinear Digital Signal Processing, 1993, pages: P_6.1-P_6.6

[8] Richard N. Czerwinska**,** Douglas L. Jones and William D. O'Brien, Jr*,* "Ultrasound Speckle Reduction by Directional Median Filtering", IEEE International Conference on Image processing 1995, VOL. 1, pages: 358-361

[9] Mustafa Karaman, M. Alper Kutay, and Gozde Bozdagi, **"**An Adaptive Speckle Suppression Filter for Medical Ultrasonic Imaging", IEEE TRASACTIONS ON MEDICAL IMAGING, 1995, VOL. 14, pages: 283-292

[10] Sofia Ben Jebara, Zied Bel Hadj, and He'di Maatar "Combined Predictive and Multiresolution Schemes for Speckle Reduction in Radar Images", 6th IEEE International Conference on Electronics, Circuits and Systems, 1999, VOL. 2, pages: 965-968

[11] Mark P. Wachowiak and Renata Smolikova , "Classification and Estimation of Ultrasound Speckle Noise with Neural Networks", IEEE International Symposium on Bio-Informatics and Biomedical Engineering, 2000, pages: 245-252

[12] Chedsada Chinrungrueng and Aimamorn Suvichakorn, "Fast Edge-Preserving Noise Reduction for Ultrasound Images", IEEE TRANSACTIONS ON NUCLEAR SCIENCE, 2001, VOL.48, pages: 849-854

[13] Alin Achim, Anastasios Bezerianos and Panagiotis Tsakalides, "Novel Bayesian Multiscale Method for Speckle Removal in Medical Ultrasound Images", IEEE TRANSACTIONS ON MEDICAL IMAGING, 2001, VOL.20, pages: 772-783

[14] Debasis Mazumdar, Sudipta Chatterjee, Dibyendu Roy and Soma Mitra, **"**Analysis and Statistical Characterization of Signal and Noise in Ultrasonography Images".http://www.kolkatacdac.in/downloads/technical%20papers/Ana_noise_filter_usg.pdf

[15] C. Loizou, C. Christodoulou, C. S. Pattichis, R. Istepanian, M. Pantziaris and A. Nicolaides, "Speckle Reduction In Ultrasound Images Of Atherosclerotic Carotid Plaque", IEEE 14th International Conference on Digital Signal Processing, 2002, Vol.2, On pages: 525- 528

[16] Yongjian Yu and Scott T. Acton, "Speckle Reducing Anisotropic Diffusion", IEEE TRANSACTIONS ON IMAGE PROCESSING, 2002, VOL.11, pages: 1260- 1270

[17] Scott T. Acton, Janelle A. Molloy and Yongjian Yu, "Three-Dimensional Speckle Reducing Anisotropic Diffusion", IEEE Conference Record of the 37th Asilomar Conference on Signals, Systems and Computers, 2003, Vol.2, pages: 1987- 1991

[18] Aleksandra Pizurica, Wilfried Philips, Member, and Marc Acheroy "A Versatile Wavelet Domain Noise Filtration Technique for Medical Imaging", IEEE TRANSACTIONS ON MEDICAL IMAGING, 2003, VOL.22, pages: 323-331

[19] Yongjian Yu, Janelle A. Molloy and Scott T. Acton "Generalized Speckle Reducing Anisotropic Diffusion for Ultrasound Imagery", 17th IEEE Symposium on Computer-Based Medical Systems, 2004, pages: 279- 284

[20] Zhou Wang, Alan Conrad Bovik, Hamid Rahim Sheikh and Eero P. Simoncelli, "Image Quality Assessment: From Error Visibility to Structural Similarity", IEEE TRANSACTIONS ON IMAGE PROCESSING, 2004, VOL.13, pages: 600-612

[21] M. Mastriani, A. E.Giraldez, "Enhanced Directional Smoothing Algorithm for Edge-Preserving Smoothing of Synthetic-Aperture Radar Images", Measurement Science Review, 2004, Vol. 4, pages: 600-612

[22] Scott T. Acton, "De-convolution speckle reducing anisotropic diffusion", IEEE International Conference on Image Processing, 2005, Vol.1, pages: I- 5-8

[23] Yong Yue, Mihai M. Croitoru, Akhil Bidani, Joseph B. Zwischenberger and John W Clark, Jr., "Ultrasound Speckle Suppression and Edge Enhancement Using Multiscale Nonlinear Wavelet Diffusion", IEEE 27th Annual International Conference of the Engineering in Medicine and Biology Society, 2005, pages: 6429-6432

[24] Khalifa Djemal, "Speckle Reduction in Ultrasound Images by Minimization of Total Variation", IEEE International Conference on Image Processing, 2005, Vol.3, pages: III- 357-60

[25] Fan Zhang, Yang Mo Yoo, Lichen Zhang, Liang Mong Koh and Yongmin Kim, "Multiscale Nonlinear Diffusion and Shock Filter for Ultrasound Image Enhancement", IEEE Computer Society Conference on Computer Vision and Pattern Recognition, 2006, Volume: 2, pages: 1972- 1977

[26] Ahmed M. Badawi, and Muhammad A. Rushdi, "Speckle Reduction in Medical Ultrasound: A Novel Scatterer Density Weighted Nonlinear Diffusion Algorithm Implemented as a Neural-Network Filter", IEEE 28th Annual International Conference on Engineering in Medicine and Biology, 2006, pages: 2776-2782

[27] Yong Yue, Mihai M. Croitoru, Akhil Bidani, Joseph B. Zwischenberger and John W. Clark, "Nonlinear Multiscale Wavelet Diffusion for Speckle Suppression and Edge Enhancement in Ultrasound Images", IEEE TRANSACTIONS ON MEDICAL IMAGING, 2006, VOL.25, pages: 297-311

[28] Peter C. Tay, Scott T Acton, and John A. Hossack, "Ultrasound Despeckling using an Adaptive Window Stochastic Approach", IEEE International Conference On Image Processing, 2006, pages: 2549-2552

[29] Alla Aksel, Andrew D. Gilliam, John A. Hossack, Scott T. Acton, "SPECKLE REDUCING ANISOTROPIC DIFFUSION FOR ECHOCARDIOGRAPHY", ACSSC 40th Asilomar Conference on Signals, Systems and Computers, 2007, pages: 1988-1992

[30] Yang Mo Yoo, Fan Zhang, Liang Mong Koh, and Yongmin Kim, "Nonlinear Diffusion in Laplacian Pyramid Domain for Ultrasonic Speckle Reduction", IEEE TRANSACTIONS ON MEDICAL IMAGING, 2007, VOL.26, pages: 200-211

[31] Ricardo G. Dantas and Eduardo T. Costa, "Ultrasound Speckle Reduction Using Modified Gabor Filters", IEEE TRANSACTIONS ON ULTRASONICS, FERROELECTRICS AND FREQUENCY CONTROL, 2007, VOL.54, pages: 530-538

[32] www.dwp.gov.uk/medical/med_conditions/malignancies/imaging_malignancy.asp consists of different medical images

[33] http://health.howstuffworks.com/ultrasound2.htm consists the image of the ultrasound machine

Bibliography

1. Rafael C. Gonzalez, Richard E. Woods [2002]. Digital Image Processing, 2nd ed, Prentice Hall, Upper Saddle River, NJ
2. Chris Oliver, Shaun Quegan [2004]. Understanding Synthetic Aperture Radar Images, SciTech Publishing